MAGNETIC-METAMATERIAL BASED FREQUENCY, POLARIZATION AND PATTERN RECONFIGURABLE ANTENNA

BY

MOUSA AHMAD AL-OMARI

A Thesis Presented to the

DEANSHIP OF GRADUATE STUDIES

KING FAHD UNIVERSITY OF PETROLEUM & MINERALS

DHAHRAN, SAUDI ARABIA

In Partial Fulfillment of the
Requirements for the Degree of

MASTER OF SCIENCE

In

ELECTRICAL ENGINEERING

January 2017

KING FAHD UNIVERSITY OF PETROLEUM & MINERALS

DHAHRAN- 31261, SAUDI ARABIA

DEANSHIP OF GRADUATE STUDIES

This thesis, written by **Mousa Ahmad Al-Omari** under the direction his thesis advisor and approved by his thesis committee, has been presented and accepted by the Dean of Graduate Studies, in partial fulfillment of the requirements for the degree of **MASTER OF SCIENCE IN ELECTRICAL ENGINEERING.**

Dr. Sharif Iqbal Mitu Sheikh
(Advisor)

Dr. Ali Ahmad Al-Shaikhi
Department Chairman

Dr. Mohammad Said Sharawi
(Member)

Dr. Salam A. Zummo
Dean of Graduate Studies

Dr. Essam Eldin Hassan
(Member)

25/1/17
Date

To my esteemed parents, lovely wife and son.

ACKNOWLEDGMENTS

I would like first to give my special thanks to my supervisor Dr. Sharif Iqbal for his support, time and effort during my research. His door was always open to me and didn't hesitate at any point to provide his help in his tight schedule even by phone or by visiting me in the lab. My sincere appreciation is extended to committee members Prof. Mohammad Sharawi and Prof. Essam Hassan for their valuable suggestions and evaluation for this thesis.

I would like to express my very deep gratitude to my parents, who covered me along the journey with their support and motivation. They allowed me to be ambitious and pushed me to continue the road along my objectives.

Finally, I would like to thank my wife who I am deeply indebted to her for her continued support, encouragement and quiet patience and tolerance to provide me the needed time to attain my study

TABLE OF CONTENTS

LIST OF TABLES

LIST OF FIGURES

ABSTRACT

Full Name : Mousa Ahmad Al-Omari

Thesis Title : Magnetic-Meta material based frequency, polarization and pattern reconfigurable antenna

Major Field : Electrical Engineering

Date of Degree : January, 2017.

Recent indoor wireless sensors and communication devices require simple reconfigurable antennas, capable of handling dynamic system parameters. RF switches are widely used in tuning antenna parameters, but require complex control mechanism. In this research work, a novel ferrite-dielectric 4-GHz operating antenna is proposed with 870 GHz frequency tuning capability and left-handed and right-handed elliptical polarization reconfigurability. This is achieved by utilizing the gyromagnetic interaction of magnetized ferrite-dielectric composite. In addition, ferrimagnetic-metamaterial with embedded metallic split ring resonators (SRR's) structure will be integrated within the substrate to considerably reduce the external magnetizing requirement of the antenna and propose an enhanced frequency tuning range of 1.44 GHz and 25^{o} of beam steering properties. In addition, a simple 2x1 array of the antenna can demonstrate 3D scanning capability. This novel magnetic-metamaterial based patch antenna will be optimized using EM commercial simulator (HFSS) to achieve the required reconfigurable coverage. The optimized antenna will be fabricated and tested to validate simulated results.

By fabricating the antenna using low temperature co-fired ceramic (LTCC) technology, the biasing requirements can be further reduced.

ملخص الرسالة

الاسم الكامل: موسى احمد العمري

عنوان الرسالة: هوائي مصنوع باستخدام مواد هندسية ومغناطيسية ذا قدرة على اعادة ضبط وتشكيل خصائص التردد والاستقطاب ونمط الاشعاع.

التخصص: الهندسة الكهربائية

تاريخ الدرجة العلمية: يناير 2017

تتطلب اجهزة الاستشعار اللاسلكية الحديثة واجهزة الاتصالات وجود هوائيات بسيطة ذات قدرة على اعادة تشكيل وضبط خصائصها والتعامل بديناميكية مع عوامل الانظمة المختلفة. ورغم ان النظم الكهروميكانيكية المصغرة تستخدم بشكل شائع لضبط خصائص الهوائيات, الا انها تتطلب انظمة معقدة للتحكم بها.

في هذا العمل البحثي سوف يتم تقديم دراسة وتصميم جديد لهوائي مطبوع باستخدام مواد هندسية وكهرومغناطيسية يعمل على تردد 4 جيجاهيرتز ذا قدرة على اعادة ضبط التردد لمدى 870 ميجاهيرتز وقدرة تغيير الاستقطاب للعمل على الاستقطاب البيضاوي اليساري واليميني وذلك باستغلال التفاعل بين تركيبة المادة العازلة والمغناطيسية .

دمج مواد هندسية ومغناطيسية تحتوي على حلقة الانقسام الرنانة ضمن المادة التي يتم تصميم الهوائي عليها حيث سيتم خفض كمية المجال المغناطيسي المطلوبة وزيادة مدى قدرة الهوائي على اعادة ضبط التردد لمدى 1.44 جيجاهيرتز و توجيه الطيف الاشعاعي لمدى 25 درجة. كما سيتم تصميم مصفوفة من هوائيين ذات قدرة على المسح ثلاثي الابعاد. تنفيذ التصميم وتحسين الهوائي الجديد المطبوع سيتم باستخدام برنامج المحاكاة الاحترافي (HFSS) للحصول على المقدار اللازم من قدرة اعادة الضبط والتشكيل. كما سيتم تصنيع الهوائي واختباره لمقارنته بنتائج المحاكاة والنتائج النظرية.

كما انه عن طريق تصنيع الهوائي باستخدام تقنية (LTCC) في درجة حرارة منخفضة، فان كمية المجال المغناطيسي المطلوبة سوف تتقلص ايضاً.

CHAPTER 1

INTRODUCTION

1.1 Introduction

In modern wireless communication systems, like communications satellites, electronic intelligent aircraft, cognitive radio and sensing applications, it is desired to increase functionality (e.g., frequency tuning, beam steering, radar, multi-polarization) within confined radio frequency (RF) devices. Reconfigurable antennas with single radiating elements that have the capability to perform different functions with additional degrees of freedom are required to meet these requirements.

Reconfiguring an antenna is achieved by dynamically changing its characteristics like frequency, polarization, or radiation on demand to maintain ease of adapting to the system requirements. This change is achieved by redistributing the antenna currents and thus alter the electromagnetic fields or other electrical properties without the need for physical reconstruction.

Reconfigurable antennas can be categorized according to tunable factors into three main categories:

- ***Frequency reconfigurable antennas***, which can change its operating frequency to different bands.

- ***Pattern reconfigurable antennas***, where the radiation pattern of the antenna can be altered and changed in terms of direction, gain…etc.
- ***Polarization reconfigurable antennas*** that have the ability to change its polarization (horizontal, vertical, left-handed circular, right-handed circular, etc.)

The degree of reconfigurability can be achieved in many ways and techniques including Electrical, optical, material or physical change. These techniques are summarized in Figure 1.1

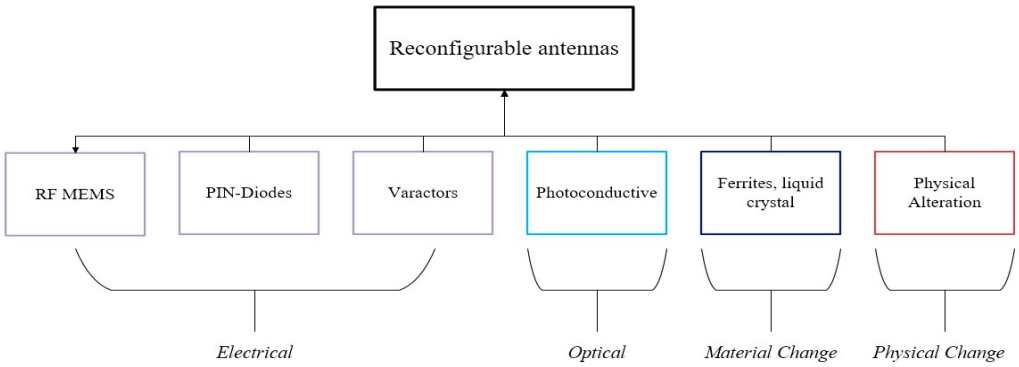

Figure 1.1: Techniques of reconfiguring antennas.

Using any of these techniques depends on how much it has more desired performance characteristics to the constraints in the application for which the antenna is designed. Next subsections will give an introduction to every method [1-4].

1.1.1 RF Microelectromechanical Systems (MEMS)

RF MEMS are devices used to change the electrical properties of the antenna by means of mechanical movements to provide the change of the surface current path along radiating part of the antenna. They can be integrated within antenna structure to provide an open or

short circuits. The mechanical movements of MEMS are gained from providing electrostatic or magnetostatic designs. MEMs can provide good isolation and low loss configuration with a relatively slow response [5,6].

1.1.2 PIN diodes

PIN diodes are current controlled switching devices that operate in two modes; “ON” mode when the diode is biased or “OFF” mode when the diode is not biased. The controlling current is excited using external biasing network. PIN diodes are easy to integrate and have a faster response than MEMs which can be in nanoseconds [1-3], but it has a nonlinear effect on the circuit.

1.1.3 Varactors

Varactors are devices excited by external voltage to provide tuning capability to the antenna. By biasing the varactors, the capacitance is changed and switching states can also be changed. Varactors are like PIN diodes that have a fast response, but controlling varactors require biasing lines that may negatively affect the antenna radiation pattern and add more losses [5,6].

1.1.4 Photoconductive switches

Photoconductive switche is an optical switch that is formed when laser light is incident on a semiconductor material (silicon, gallium arsenide). This results in exciting electrons from the valence to the conduction band and thus creating a conductive connection [4].

1.1.5 Ferrite materials

Ferrite materials which will be used in this thesis, have the advantage of providing continues tuning of the antenna by changing its effective permeability using external magnetic bias. On the other hand, due to their high permittivity they can noticeably decrease the electrical size of the antenna. By proper use of these materials with enhanced biasing mechanisms, many controllable and tunable characteristics can be achieved [5, 6].

1.2 Thesis motivation

In recent wireless sensors and communication systems, frequency, polarization and pattern reconfigurable antennas are of great interest to achieve multitasking capabilties within one antenna [6]. RF diodes acting as switches are widely used to tune the antenna frequency, polarization and radiation patterns at the cost of complex control mechanism [8-10]. In addition, the narrow half power beam width (HPBW) of phased array antenna can be a limiting factor for the beam scan-able sector-antennas or sensors used in many indoor applications like GPS, RFID and WLAN. Although Microstrip patch antennas (MPA) have a wider HPBW and are more suited for the above mentioned applications, in its simple structure they lack the reconfigurable capability in terms of frequency, pattern and polarization [11].

Ferrite materials are popular in reconfiguring the radiation properties of microwave antennas [12-18]. In the literature, the gyrotropic properties of externally magnetized ferrite substrate or superstrates are widely used to introduce frequency tuning [19-22], antenna miniaturization [29,30], widening the impedance bandwidth [31,32], beam steering [33-

38] and polarization tuning [39-41]. But the magnetic field required to magnetize the ferrite material often increase the size and limit their application in planar devices.

Metamaterials or engineered materials are also widely used to improve antennas properties including gain, directivity, insertion loss and beam forming [42-57]. Split ring resonators (SRR's) are artificial structures common in metamaterials [59-65]. Typically, they consist of two enclosed wire loops with splits in them at the opposite ends. SRR responds to incident magnetic field component of a microwave signal and induces rotating currents in the loops. These, in turn, produces its own flux to strengthen or weaken the incident magnetic field.

In this proposed research work, SRR's will be integrated into the ferrite material to constructively couple their magnetic resonances. Theoretically, this magnetic-metamaterial should reduce the required magnetizing fields needed by microwave ferrite control devices. In addition, this material will be integrated into the dielectric substrate of a microstrip patch antenna to demonstrate externally reconfigurable properties, like beam steering, tuning the resonant frequency or polarization. A professional software will be used to optimize the theoretically predicted antenna parameters. Rigours parametric analysis will be carried out to find the best dimensions and locations to integrate the magnetic-meta material. Simulated S-parameter results and radiation responses of the patch antenna will be used to demonstrate a frequency tuning of about 40% of the resonance frequency, beam scanning of 25^{o} and switching between left-hand (LHCP) and right-handed (RHCP) circular or elliptical polarizations in addition to an average gain 5 dB. A simple 2x1 array will be designed to demonstrate three-dimensional (3D) scan

capabilities. In-house facilities will be used to fabricate a prototype of the patch antenna on dielectric-ferrite substrate to verify the simulated responses.

These easily integrated antenna or array with frequency, polarization and pattern reconfigurable properties will be very useful in the applications like RFID and WLAN. The requirement of magnetic biasing can be further reduced using LTCC technology, where biasing coils are embedded within the ferrite superstrate [66].

1.3 Thesis objectives

1. Conduct thorough literature survey to know the existing designs of the ferrite and mate-material based reconfigurable patch antennas. Extensively search available reference literature on SRR integrated ferrite devices, particularly for microwave planar antenna application.
2. Study the properties of microwave ferrites and determine the best-suited ferrite material for this project, based on saturation magnetizing, resonance line width, gyromagnetic ratio, dielectric constant, hysteresis curve, etc.
3. Design 4-GHz rectangular patch and integrate the ferrite slabs within the dielectric substrate to introduce frequency tuning of 870 MHz which is forming 20% tuning from the center frequency and polarization reconfigurable between left-hand (LHCP) and right-handed (RHCP) elliptical polarizations antenna. Professional software is used to optimize the structure in terms number, size, location and magnetizing requirement of the ferrite slabs.

4. Design SRR based metamaterial to resonate at 4-GHz. Optimally integrate the SRR's within the ferrite slabs to introduce antenna beam scanning of 25° in addition to low-bias frequency tuning of about 40% with an average gain of 5 dB.
5. Design a 2x1 array from microstrip designed antenna with SRR integrated to demonstrate 3D beam scanning.
6. Fabricate the patch antenna based on dielectric-ferrite substrate composite. Validate the simulated results with experimentally observed antenna responses.

CHAPTER 2

THEORETICAL BACKGROUND

2.1 Antennas fundamentals

Antennas are the front-end elements and one of the most critical components of wireless communication systems, they play a significant role through interfacing transmitting and receiving terminals. Antennas are defined as a transducer that converts the electrical power into electromagnetic waves and vice versa [7]. It acts as the interface between the waveguide and the medium. Depending on the application, popular antennas include wire antennas, aperture antennas, patch antennas, reflector antennas, and traveling wave antennas, etc. In recent communication devices, microstrip patch antennas are widely used due to its low profile, good efficiency and easy fabrication and integration properties. In this section, basic parameters that govern the design and performance of antennas are briefly reviewed.

2.1.1 Reflection coefficient and impedance bandwidth

In Antennas, reflection coefficient (S11) is a parameter that describes the reflected portion of the antenna excitation signals. It measures the mismatch between the antenna and the feeder transmission line, mostly measured in dB. Smaller reflection often indicates that majority of the excitation signal is radiated through the low loss antenna. Figure 2.1 shows a typical S11 versus frequency curve of a single band antenna. Note that this antenna radiates EM signal with a center frequency around the 3 GHz, where |S11| = -25 dB. EM

signal for other frequencies with S11 values close to 0 dB is considered to be reflected back to the source.

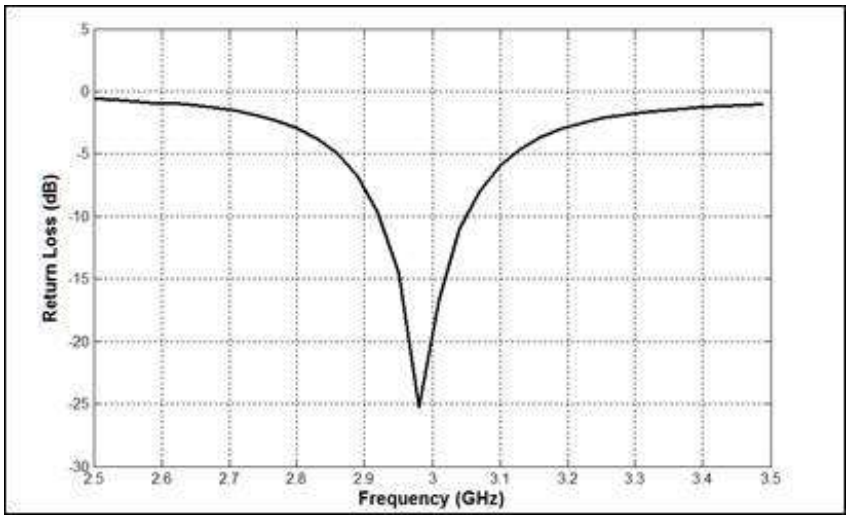

Figure 2.1 Reflection coefficient of printed antenna.

Another fundamental parameter of the antenna is the impedance bandwidth (B/W), which describes the range of frequencies that antenna radiates in addition to center frequency. Usually, for directional antennas, it is measured by the range of frequencies that has a reflection coefficient (S11) less than -10 dB. Bandwidth is often expressed as a fractional bandwidth between its impedance bandwidth and the center frequency. For multi-band antennas, the B/W consist of a range of frequencies with S11 values less than -6 dB.

2.1.2 Radiation pattern

Antennas are energy radiating devices, the graphical distribution of the radiated signal constitutes the radiation pattern. The radiation pattern is typically expressed in a suitable coordinate system to represent spherically radiated symmetrical patterns, and often measured in the far field [7].

Antennas that radiate their power equally in one plane are called omnidirectional antennas. Dipoles are good example of the omnidirectional antennas. Antennas that radiate the RF power in a particular direction are referred to as directional antennas like microstrip patch and dish antennas. The 3-D radiation pattern of a typical dipole antenna, formed with two thin wires oriented vertically along the z-axis, is shown in Figure 2.2. Note that the radiated power is equally distributed in the x-y plane (called the azimuth plane).

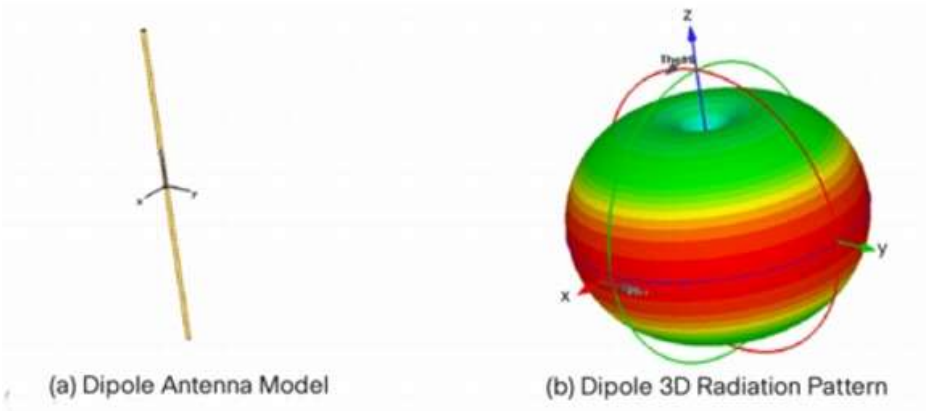

Figure 2.2: (a) Dipole antenna, (b) Three-dimensional radiation pattern.[67]

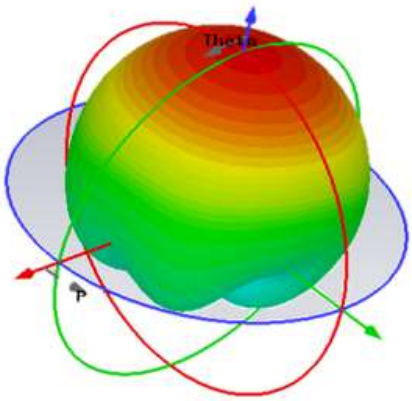

Figure 2.3: Directional radiation pattern of a microstrip patch antenna.

Figure 2.3, shows a directional radiation pattern of a simple patch antenna. Note that the radiated power is consternated in one direction (z direction), which makes it a directional type of antennas.

2.1.3 Directivity

Directivity is a figure of merit that measures the direction of the strongest signal radiated from the antenna with respect to the radiated signal from an isotropic source. An isotropic antenna is an ideal device that radiates equally in all directions with a perfect efficiency. Mathematically Directivity can be defined as:

$$D = \frac{4\pi U}{P_{rad}} \tag{2.1}$$

Where, P_{rad} is the radiated power in watts, U is the radiation intensity in watts per steradian [7].

2.1.4 Efficiency

In radiating devices, the percentage of radiated power is important to measure the performance of the device. Antenna efficiency is a measure of how much power is radiated with respect to the input power of the antenna. It is a key performance factor of the antenna which is given by equation (2.2).

$$Efficiency = \frac{P_{rad}}{P_{in}} \tag{2.2}$$

The radiated power of antennas is affected by different types of losses that decrease their efficiencies, such as conduction, dielectric and reflection losses. Hence, the total efficiency of the antenna can be expressed by:

$$\epsilon = \epsilon_r \epsilon_c \epsilon_d (1 - \Gamma) \quad (2.3)$$

Where, ϵ_r is the reflection efficiency, ϵ_c is the conduction efficiency, ϵ_d is the dielectric efficiency and Γ is the reflection coefficient. Efficiency of antenna can be high for dish, the horn, or half-wavelength dipole antennas. Whereas it becomes lower in microstrip antennas, because of high losses in the substrates due to the excitation of surface waves.

2.1.5 Gain

Gain is a dimensionless parameter that measures the radiated energy concertation in a particular direction with respect to the radiation energy from an ideal isotropic source. The gain of the antenna is given by:

$$G = \frac{4\pi\, U}{P_{in}\,(Isotropic\,)} \quad (2.4)$$

Where U is the radiation intensity in watts per steradian in the direction specified and P_{in} is the radiated power in watts from an ideal isotropic radiator. Gain can be related to the directivity with respect to the efficiency of the antenna [7], by the following equation:

$$G = \epsilon\, D \quad (2.5)$$

Where ϵ the total efficiency and D is the directivity of the antenna.

2.2 Microstrip antennas

Microstrip antennas are one of the most popular antennas and since this research work aims to design a novel tunable patch antenna, the theoretical background related to this class of antenna is briefly described in this section. Microstrip antenna consists of a conducting metal patch radiator and a ground plane below a dielectric substrate. Figure 2.4 shows a basic microstrip antenna configuration.

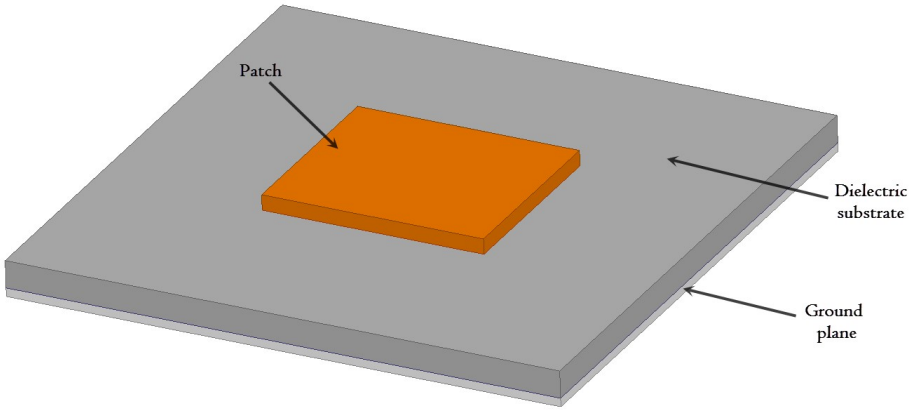

Figure 2.4: Configuration of the microstrip antenna.

Deschanps [73] introduced the idea of using microstrip radiators in 1953, and about 20 years later the first microstrip antenna was fabricated by Howell [74] and Munson [75]. During the 1970s, the development of microstrip antennas was accelerated because of the availability of good substrates with decent thermal and mechanical properties [23]. The early use of microstrip antenna was in radar applications, where lower bandwidth was required. Then it was used in military, aircraft and finally in mobile communication devices due to its low profile, good efficiency, and easily integrable properties. According to the geometry, microstrip antennas can be categorized into four basic configurations [23];

Microstrip patch antennas, microstrip dipoles and monopoles, microstrip printed slots, microstrip traveling-wave antenna, planar Inverted-F antenna (PIFA).

Shapes of the patch could vary depending on the application, and the features required. It can be rectangular, circular, triangular, semicircular, sectorial and annular, etc. In microstrip patch antenna, the dielectric material - called substrate – which is sandwiched between the two conductors (patch and ground plane) is used to provide a suitable space and mechanical support between the patch and the ground. The substrate height is usually chosen in the range of 0.01–0.05 free-space wavelength (λ_0) [24] and depends on the required performance of the antenna. Typical ranges of dielectric constants of the substrate are ($2 \leq \epsilon_r \leq 10$) [7], where higher dielectric constant substrates are being used in antenna miniaturization. The substrate affects the bandwidth, efficiency insertion loss and size of the antenna. For example, higher dielectric constant substrate provides antenna miniaturization at the cost of lower radiation-efficiency and lower impedance-bandwidth.

2.2.1 Design and analysis

In the literature, many models are being used in analyzing and designing microstrip patch antennas. The primary analysis approaches that are being used to design patch antennas are:

1. Transmission line model.
2. Cavity model.
3. Full wave method.

Transmission line model is considered to be the simplest and least accurate model, but it can provide a calculation of the initial design parameters of the antenna. For the rectangular

patch, transmission line model considers the antenna to be a collection of lumped circuit elements, and the patch as a transmission line with a length of λ\2, where the two radiating slots are on the two sides as shown in Figure 2.5 [24].

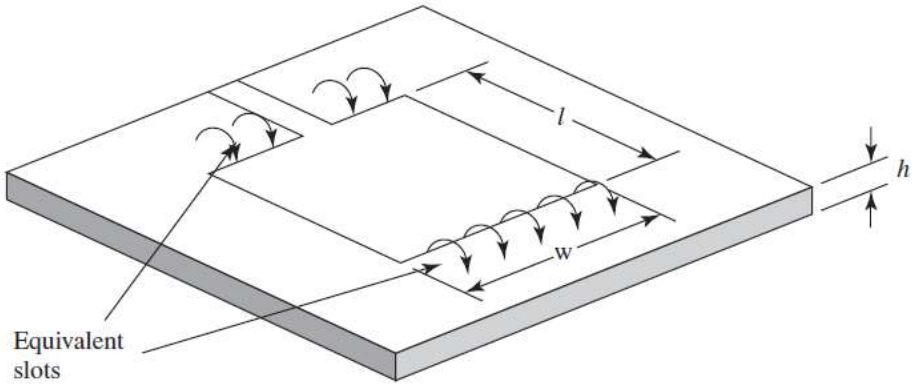

Figure 2.5: Transmission line model of the rectangular patch antenna.

Full wave method depends on modelling the design in computer-aided design software (CAD) that use many analysis techniques to solve Maxwell's equation in the 3D space like, finite element method (FEM), a method of moment (MOM) and finite difference time domain (FDTD), which provides more accurate results.

Cavity model [7] gives an approximation of current densities in microstrip antennas, which describes the radiation mechanism of the patch. In this modeling approach, the antenna is considered as a resonating cavity with two radiating slots having a distance of half-wavelength.

Initially, in the design of microstrip patch antenna, transmission line model is often used to calculate the design parameters, which are then optimized using CAD packages to generate the required antenna responses. In the upcoming subsections, we will introduce the main equations that govern the design considerations using transmission line model.

Resonance frequency, electrical length and effective dielectric constant

Microstrip patch antenna resonates at the fundamental mode (TM_{01}), which is the mode where the electrical length of the patch is half-wavelength [7]. Hence, the resonance frequency of the patch can be expressed by [7]:

$$f_c = \frac{v_o}{2(L + 2\Delta L)\sqrt{\varepsilon_{reff}}} \qquad (2.6)$$

Where v_o is the speed of light in free space and [12]

$$\frac{\Delta L}{h} = 0.412\frac{(\epsilon_{reff} + 0.3)(\frac{W}{h} + 0.264)}{(\epsilon_{reff} - 0.258)(\frac{W}{h} + 0.8)} \qquad (2.7)$$

$$\epsilon_{reff} = \frac{\epsilon_r + 1}{2} + \frac{\epsilon_r - 1}{2}\left[1 + 12\frac{h}{e}\right]^{-1/2} \qquad (2.8)$$

ϵ_{eff}: Effective dielectric constant.

ΔL: Effective dielectric constant.

ϵ_r: Dielectric constant of substrate.

Width and input resistance.

The width of the antenna has a minor effect on its resonance frequency, whereas it affects the input impedance of the patch. Thus, it has an effect on the radiated power of the antenna. To reach a good radiator the width of the patch is approximated by [24]:

$$W = \frac{v_o}{2f_r}\sqrt{\frac{2}{\varepsilon_r + 1}} \qquad (2.9)$$

Finally, the input resistance of the patch can be obtained by transmission line equivalent and given by the following equation [24]:

$$R_{in}(y=0)=\frac{1}{2(G_1+G_{12})} \tag{2.10}$$

Where G is the conductance and G_{12} is the mutual conductance, which depends on the current density of the patch and other factors. Input resistance is an important parameter to maximize power transfer by improving the impedance matching between the feed line and the patch antenna.

From the previous background, it can be shown that microstrip antennas are low profile antennas that have many vital properties in many communication systems. In the process of designing the antenna, the substrate of patch antennas can affect the performance and the size of the antenna. Accordingly, choosing the appropriate material is critical in achieving the specific performance of the antenna. Ferrites are one of the materials that have high dielectric constant and used in microstrip antennas design to provide tuning capabilities. Next section discusses ferrite materials structure, properties, magnetic response and theoretical analysis of the main tunable factor in these materials which is its permeability.

2.3 Microwave ferrites

Ferrite materials are anisotropic materials which have different values of property that depend on the direction. They often used in microwave controlled devices, like circulators and phase shifters. Due to their non-reciprocal behavior and tuning capabilities, they can introduce tunable characteristics. Ferrites are metallic oxide based materials and according to material structures they can be categorized into two types:

1. Spinel ferrites are composed by $MgAl_2O_4$ components and are one of the first discovered ferrites.
2. Garnets have more complex structures and are mainly composed of $Ca_3Fe_2(SiO_4)_3$ components. The most well-known material of garnets is yttrium-iron-garnet (YIG), which is used extensively because of its low absorption loss and good behavior at microwave frequencies.

The detailed chemical compositions of different ferrites are not the main interest in this thesis and can be found in resources [25- 27]. Furthermore, the physical behavior of these materials and their response in microwave frequencies are of interest, because their understanding is essential before employing them to control antenna responses.

In antenna design, it is critical to have good radiation efficiency, and using ferrites to tune the antenna properties needs to have materials with low absorption loss. This absorption is characterized by a quantity known as the resonance linewidth (ΔH), and because garnets have lower absorption loss compared to spinel ferrites, we will select them in this thesis. Next subsection discusses ferrite physical structure and their response to external subjected magnetic fields.

2.3.1 Ferrite material interaction at microwave frequencies

Most materials interact with an external magnetic field. The degree of interaction depends on the existence of magnetic dipole moments within the material. Ferrite materials have highly dense magnetic dipoles within its structure and demonstrate considerably higher interaction. By applying external DC magnetic field (H_{dc}) ferrite materials magnetic dipoles are aligned, the material is initially biased, and controller interaction is achieved [28]. This applied field aligns the magnetic dipoles due to two main factors [15]; spin and orbital motions of the electrons. This physical interpretation is forming the main basis of deriving the behavior of ferrites in RF frequencies.

The magnetic properties resulting from the spin motions of electrons are dominant and can be explained using quantum mechanical approach [13], assuming that the electron is a rotating sphere with a magnetic moment along its axis. The intrinsic unit magnetic moment due to spin motion is given by [27, 13]:

$$m_s = \frac{q\bar{h}}{2m_e} = 9.27 \times 10^{-27} A - m^2 \tag{2.11}$$

Where q is electron charge, $h^{-}$is Planck's constant divided by 2π and $m_e$is the mass of electron. The orbital motion of electron gives rise of tiny current loop [14] and results in an insignificant magnetic moment expressed as:

$$m_o = Ia \tag{2.12}$$

Where, I is the current in ampere, and a is the area of the orbit trace of motion in meters. The magnetic moment in ferrite materials is the sum of moments due to the spin or orbital

motion of the electron. The coupling between different moments can be measured by a metric parameter called ***Land´e g-factor*** [15]. This factor measures the contribution of spin moments and orbital moments relative to total magnetic moment. It has a value of 1 when the orbital moment is dominant and has the largest contribution, and 2 when magnetic moment due to electron spin is dominant. At microwave frequencies ferrites generally takes values between "1.98 – 2", indicating that the spin magnetic moment is dominant.

2.3.2 Effect of external magnetic field on ferrites

Without any existence of the external magnetic field, magnetic moments in ferrite materials are randomly oriented with a total vector magnetic moment of zero. When a DC magnetic field is applied to ferrite material, the electrons of the material start precessing to align themselves with the direction of the field (magnetic moment parallel to the magnetic field), forming an angular momentum ($\overline{m}$) along their axis as shown in Figure 2.6.

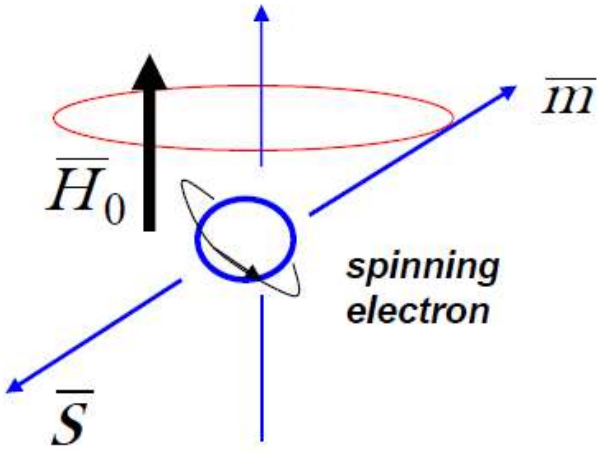

Figure 2.6: Electron spin in ferrite materials.

While precessing, electron traces a gyroscopic motion, and follows a circular track around the applied magnetic field forming a spinning angle of $\theta = \sin^{-1}\frac{\sqrt{m_x^2+m_y^2}}{|\bar{m}|}$, where m_x is the

moment vector in x direction and m_y is the moment vector in y direction. This motion will not continue in an infinite manner, because of what is like a friction force called ***Damping force***. This force will affect the electron and make them slowly spiral to its equilibrium position and finally to be aligned in the direction of the magnetic field, in this case the material is said to be ***magnetized***.

The magnetization of ferrite materials is analogous to polarization in dielectric materials under an electric field influence. The difference in ferrites is that the relationship between the magnetization and magnetic field is not linear. In dielectrics, the polarization is related to the field using ***Electric Susceptibility***, and it is linear relationship expressed by $\bar{P} = \chi\bar{E}$. In ferrites, the magnetization is related to the magnetic field using tensor ***Magnetic Susceptibility*** **(χ)** which depends on the direction of magnetic field. Thus, the nonlinear relationship between magnetization $\bar{M}$ and the magnetic field $\bar{H}$ given by well-known constitutive relationship $\overline{M} = \chi\bar{H}$, this makes these materials anisotropic. The physical interaction between ferrites and subjected magnetic field, leads the analytical insight of ferrite materials. Before going further into the analysis of ferrite, it is important to discuss some main properties that characterize these materials.

2.3.3 General properties of ferrites

- **Saturation Magnetization:** When all electrons respond to external magnetic field and align on a regular basis, we can say that the material has reached ***Saturation Magnetization*** **(M_s).** Saturation magnetization is a property of magnetic material that is provided by the manufacturer, it is generally measured by changing the magnetic flux applied on the material using Helmholtz bobbins [16]. It is good to mention that the frequency of magnetization is the frequency where

the material is saturated and it is linearly proportional to applied magnetic field, given by:

$$w_m = \mu_0 \gamma M_s \tag{2.13}$$

Where w_m is the magnetization frequency, μ_0 is permeability in free space, γ gyromagnetic ratio which is equal to 1.759×10^{11} (C/kg) and M_s is the saturation magnetization of the material.

Figure.2.7 shows the relationship between increasing magnetic field applied and the magnetization of typical magnetic materials.

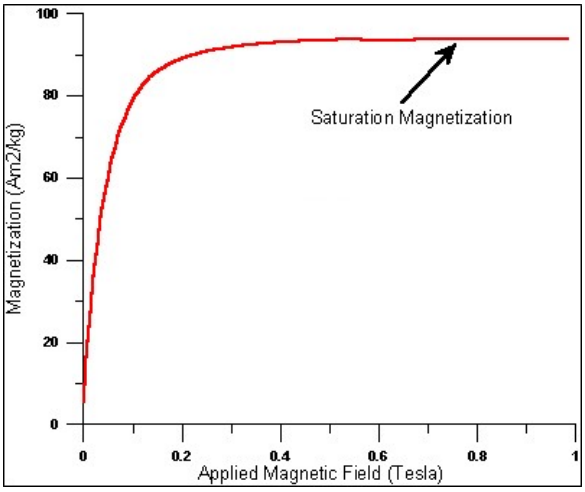

Figure 2.7: Relationship between magnetization and applied magnetic field.

- **Ferromagnetic Resonance (FMR) and Resonance Linewidth:** When an RF signal is applied in a perpendicular plane to that of the biasing field, the magnetic field components of the RF signal restarts the precessing of the magnetic dipoles. When the RF signal frequency with the same ferrite pressing frequency, maximum energy transfer from the RF signal to the ferrite material occurs. The maximum transfer is due to the need of higher damping force to reach the alignment. This phenomenon is called Ferromagnetic resonance (FMR). FMR can be derived from

the quantum mechanical approach of the spinning electron, by relating the angular momentum with the torque generated from the precessing of the electron. Equation (2.14) gives the expression of ferromagnetic resonance [15]:

$$\omega_0 = \mu_0 \gamma H_0 \tag{2.14}$$

Where H_0 is the applied field and $\mu_{0,}\gamma$ are the permeability in free space and gyromagnetic ratio, respectively. A point of interest is that precession frequency is proportional to the external magnetic bias applied on ferrite material, which means that the frequency of spinning will increase by increasing the applied bias. ***Linewidth*** ($\boldsymbol{\Delta H}$) which was mentioned before can be measured by the frequency bandwidth where the susceptibility (permeability) curve falls 3 dB below the peak of the susceptibility (permeability) curve. Wider linewidth means that ferrite material can be lossy for larger region, which makes ferrites with lower linewidth is preferable for antenna applications.

2.3.4 Polder tensor permeability

As shown earlier, magnetized ferrite materials respond to an external EM field, applied in a direction perpendicular to DC magnetization field. The field causes the dipoles inside the material to re-starts pressing, which causes an axis dependent anisotropic interaction and the ferrite material to have tensor permeability, which is an important characterization to achieve ferrite control devices. Permeability of the materials is defined as the ratio of magnetic flux, ($\bar{B}$) and the magnetic field ($\bar{H}$), which can be expressed mathematically by [5]:

$$\bar{B} = \mu_0 \mu_r \bar{H} \tag{2.15}$$

Where μ_0 and μ_r are permeability in free space and the relative permeability of the material, respectively. In ferrite materials, μ_r is not a scalar quantity, and the permeability depends directly on the external applied field. When the external DC bias is increased, the magnetization of the materials increases till it reaches the saturation magnetization. In this case the macroscopic magnetization of material can be expressed by the microscopic magnetization multiplied by the unit volume [5]:

$$\bar{M} = N\bar{m} \tag{2.16}$$

Where N represents the number of magnetic dipoles per unit volume. This makes the relationship between magnetic flux and magnetic field intensity in equation (2.16) is also nonlinear as shown in equation (2.17):

$$B = \mu (\bar{H} + \bar{M}) \tag{2.17}$$

Where the permeability $\mu = 1 + \chi$, B = magnetic flux density (Tesla), B is magnetic flux density (Tesla), μ_0 is permeability of free space which is equal to $4\pi \times$ 10-7(H/m), H is the applied magnetic bias field (A/m), and M is magnetization (A/m). To derive relationship of tensor permeability of ferrite materials, we will consider RF signal propagating in ferrite medium with an applied magnetic bias that is in $+\hat{z}$ and expressed by [5]:

$$H_{rf} = H_{rfx} + H_{rfy} + H_{rfz} \tag{2.18}$$

The total magnetic field is given by [5]:

$$H = H_{rf} + H_{dc} \tag{2.19}$$

And H_0, is the external applied DC magnetic field. Again, using quantum mechanical model and by using equations of motions that models the electron motions, the equations can be yielded:

$$\frac{d\bar{M}}{dt} = -\mu_0 \gamma \bar{M} \times \bar{H} \tag{2.20}$$

Which can give three equations with respect to every direction of magnetization:

$$\frac{dM_x}{dt} = -\mu_0 \gamma M_y (H_{dc} + H_z) + \mu_0 \gamma (M_s + M_z) H_y \tag{2.21}$$

$$\frac{dM_y}{dt} = \mu_0 \gamma M_x (H_{dc} + H_z) - \mu_0 \gamma (M_s + M_z) H_x \tag{2.22}$$

$$\frac{dM_z}{dt} = -\mu_0 \gamma M_x H_y + \mu_0 \gamma M_y H_x \tag{2.23}$$

The fact that the AC magnetic field is smaller than the applied field makes equations 2.21, 2.22 and 2.23 above to be:

$$\frac{dM_x}{dt} = -\omega_o M_y + \omega_m H_y \tag{2.24}$$

$$\frac{dM_y}{dt} = -\omega_o M_x - \omega_m H_x \tag{2.25}$$

$$\frac{dM_z}{dt} = 0 \tag{2.26}$$

Solving the above equations, we can get the relationship between magnetization and applied field in terms of tensor susceptibility and in matrix form as [5]:

$$\bar{M} = [\chi]\bar{H} = \begin{bmatrix} \chi_{xx} & \chi_{xy} & 0 \\ \chi_{yx} & \chi_{yy} & 0 \\ 0 & 0 & 0 \end{bmatrix} \bar{H} \tag{2.27}$$

Where

$$\chi_{xx} = \chi_{xy} = \frac{\omega_0 \omega_m}{\omega_0^2 - \omega}$$
$$\chi_{xy} = -\chi_{yx} = \frac{j\omega\omega_m}{\omega_0^2 - \omega} \tag{2.28}$$

In accordance with above analysis, the tensor permeability of ferrite materials assuming a positive z-directed H bias is given by:

$$[\mu] = \begin{bmatrix} \mu & jk & 0 \\ -jk & \mu & 0 \\ 0 & 0 & \mu_0 \end{bmatrix} \tag{2.29}$$

Where

$$\mu = \mu_0 \left(1 + \frac{\omega_o \omega_m}{\omega_o^2 - \omega^2}\right)$$
$$\kappa = \frac{\omega\omega_m}{\omega_0^2 - \omega^2} \tag{2.30}$$

And

$$\omega_0 = \mu_0 \gamma H_{dc}$$
$$\omega_m = \mu_0 \gamma M_s \tag{2.31}$$

Where, μ_0 is permeability of free space (Henry), M_s is the saturation magnetization of ferrite material, γ gyromagnetic ratio which is equal to 1.759×10^{11} (C/kg), H_0 is the applied field and ω_0 is precessing frequency (rad/s).

In this section, ferrite materials were briefly discussed theoretically, and it was shown that by applying the external magnetic field they respond by changing their magnetic permeability. In the next section, resonating structures which that will be used in our antenna design will be discussed to provide a constructing magnetic field to interact with ferrites; these materials are called "Metamaterials."

2.4 Metamaterials

2.4.1 Introduction

In 1890 Maxwell showed that both varying electric and magnetic fields can generate electromagnetic waves that travel at speed relative to free space speed, and depends on both permittivity and permeability of the medium. Maxwell equations described the relationship between electric and magnetic fields and how the EM wave propagation dependent on the properties of the media. These equations in their differential forms are:

$$\nabla . \epsilon E = \rho_v$$

$$\nabla . B = 0$$

$$\nabla \times E = \frac{d}{dt}(\mu H) \tag{2.32}$$

$$\nabla \times H = \sigma E + \frac{d}{dt}(\epsilon E)$$

Maxwell equations show that the electric and magnetic field components of EM wave can be defined for known boundary conditions and the permittivity (ϵ), conductivity (σ) and permeability (μ) of the media. These parameters are also used to define wave impedance, refractive index and the wave number of the EM wave, as given by the following equations:

$$\eta = \sqrt{\frac{\mu}{\epsilon}} \tag{2.33}$$

$$n = \sqrt{\mu\epsilon} \tag{2.34}$$

$$k = \alpha + j\beta = \alpha + \omega\sqrt{\mu\epsilon} \tag{2.35}$$

Where ω the frequency of operation, α is the attenuation constant, β is the propagation constant, η is intrinsic impedance and n is the refractive index. Thus, knowing the constitutive parameters of the media in addition to boundary conditions is essential to define the electrical and magnetic field components of the propagating EM wave.

Naturally, both permittivity and permeability take positive values in microwave frequencies for most materials. A few materials exist in nature that follows the Drude model [42] show negative permittivity at high frequency [41], such as plasma. Drude model can be expressed mathematically by [41]:

$$\epsilon = \epsilon_o(1 - \frac{\omega_p}{\omega^2}) \tag{2.36}$$

Where $\epsilon_o$the permittivity in free space, ω_p is the plasma frequency and ω is the angular frequency. It can be shown from equation (2.36) that below plasma frequency, materials

show a negative permittivity and no propagation occurs. On the other hand, ferrite magnetic materials often display negative permeability for certain conditions [44]. Since for most materials, these parameters are positive in microwave frequencies, extensive research towards artificially engineered materials with negative values of permittivity was conducted.

2.4.2 Metamaterial concept

Metamaterials are artificially engineered materials that are not existing in nature. These materials in contrary of natural materials have unusual properties like negative permittivity and permeability that can give these materials interesting responses in microwave frequencies. Victor Veselago first introduced metamaterials [47] in 1968, he studied the wave propagation in mediums have both negative permittivity and permeability, and showed that the phase velocity and group velocity of electromagnetic energy in such a medium are anti-parallel [48].

Rodger M. Walse [34] has defined metamaterials to be “Macroscopic composites having a synthetic, three-dimensional, periodic cellular architecture designed to produce an optimized combination, not available in nature, of two or more responses to specific excitation “. David Smith [46] defines metamaterials as “a macroscopic composite of periodic or non-periodic structure, whose function is due to both the cellular architecture and the chemical composition”.

Sir John Pendry and David R. Smith then proposed artificial media, similar to “Metamaterials”, where conductor geometries are used to form a medium with a negative permittivity [49] and negative permeability [50]. In his research work, Smith has

experimented and verified the non-typical and negative refraction of this class of media [48]. Metamaterials are constructed in pattern configurations. Properties of ordinary materials can be described by macroscopic permittivity and permeability, whereas in metamaterials it is derived from the structure and configuration of metamaterials, rather than the properties of the materials itself.

Materials and mediums can be classified depending on their macroscopic parameters into four categories: materials that have both positive permittivity and permeability which are called Double Positive materials (DPS), and most dielectric materials have this property. Other materials that have negative epsilon and positive permeability, and called Epsilon Negative materials (ENG), some Nobel metals like gold and silver at some frequencies acting like a plasma, and have a negative value of permittivity. The medium with negative permeability and positive permittivity is called Mu negative materials (MNG). Some magnetic materials have negative permeability and at this region and no propagation happens due to cutoff. In Double Negative materials (DNG) both permittivity and permeability are having negative values; metamaterials are a good example of this type which is artificially made and fabricated. Figure 2.8 shows materials classifications.

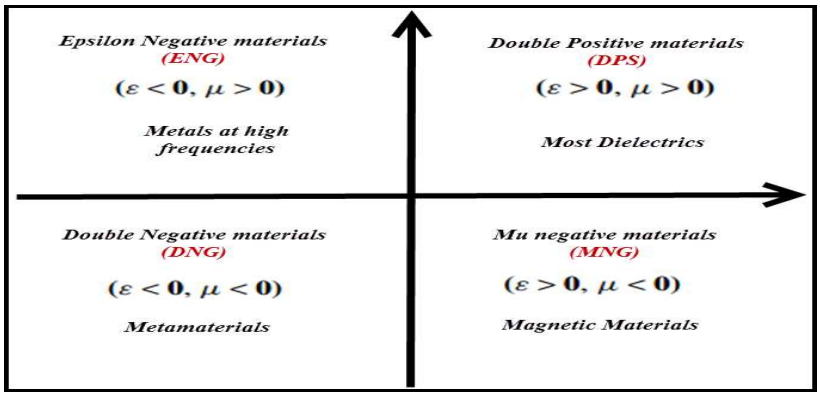

Figure 2.8: Classifications of materials depending on its permittivity and permeability.

Since permittivity and permeability are results of electric and magnetic dipoles, respectively, metamaterials are designed to construct resonating dipoles acting like dipoles in material molecules, but with an engineered electromagnetic parameter. These altered parameters can be achieved using different configurations which can be divided into two different operation categories: Magnetic dipoles metamaterials, including Single Split Resonator (SRR) and slot lines and Electric dipoles metamaterials, which includes Complimentary Single Split Resonator (CSRR) and metal wire lines. Figure.2.9 shows simple structures of both SRRs and CSRRs.

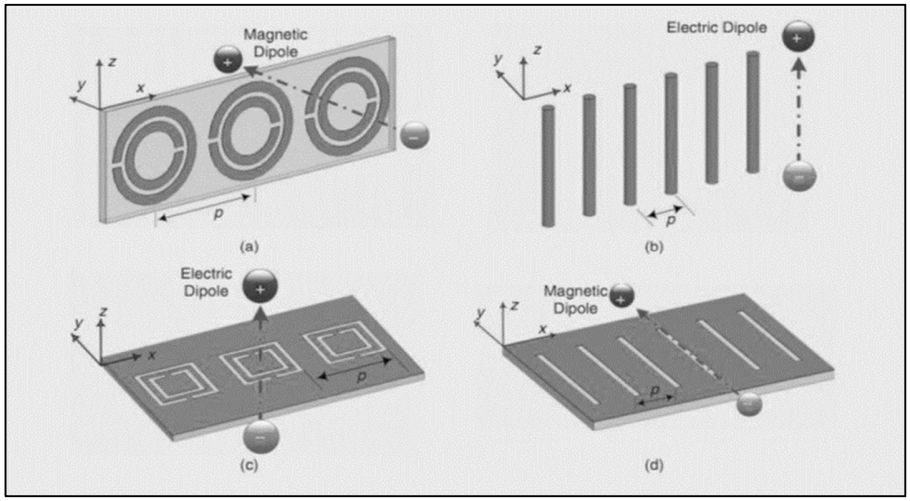

Figure 2.9 Split Ring Resonators (SRR) and Complementary Split Ring Resonators (CSRR).

2.4.3 Refractive index of metamaterials

Metamaterials have anti-parallel properties because its permittivity and permeability have negative values. Metamaterials, Left-handed materials (LHM), negative-refractive index materials (NIM), double negative materials (DNG), and backward-wave materials have been regarded as the same terms [46]. In this section, we will present a general analytical approach about the refractive index in Metamaterials. Ziolkowski and Heyman in [51]

thoroughly analyzed this concept mathematically and had shown that in DNG media the refractive index could be negative, the refractive index can be expressed as follows:

$$\epsilon = |\epsilon| e^{j\phi_\epsilon} \qquad \phi_\epsilon \in [\frac{\pi}{2}, \pi] \tag{2.37}$$

$$\mu = |\mu| e^{j\phi_\mu} \qquad \phi_\mu \in [\frac{\pi}{2}, \pi] \tag{2.38}$$

Where refractive index is given by

$$n = \sqrt{\epsilon\mu} = \sqrt{|\epsilon||\mu|} e^{\frac{j}{2}(\phi_\epsilon + \phi_\mu)} \tag{2.39}$$

For small losses case assumption, both permittivity and permeability can be written as

$$\epsilon = \epsilon' + j\epsilon'' \tag{2.40}$$

$$\mu = \mu' + j\mu'' \tag{2.41}$$

And

$$\sqrt{\epsilon} = \sqrt{\epsilon_r \epsilon_o - j\epsilon''} \approx -j\left(\sqrt{\epsilon_r \epsilon_o} + j\frac{\epsilon''}{2\sqrt{\epsilon_r \epsilon_o}}\right) \tag{2.42}$$

$$\sqrt{\mu} = \sqrt{\mu_r \mu_o - j\mu''} \approx -j\left(\sqrt{\mu_r \mu_o} + j\frac{\mu''}{2\sqrt{\mu_r \mu_o}}\right) \tag{2.43}$$

$$\begin{aligned} n = \sqrt{\epsilon\mu} = & -\left[\left((|\epsilon_r||\mu_r|) - \frac{\epsilon''}{\epsilon_o}\frac{\mu''}{\mu_o}\right) + j\left(\frac{|\epsilon_r|\epsilon''}{\epsilon_o} + \frac{|\mu_r|\mu''}{\mu_o}\right)\right] e^{\frac{j}{2}(\phi_\epsilon + \phi_\mu)}{}^{\frac{1}{2}} \\ & \approx -\sqrt{\epsilon_r \mu_r}\left[1 + \frac{j}{2}\left(\frac{\epsilon''}{|\epsilon_r|\epsilon_o} + \frac{\mu''}{|\mu_r|\mu_o}\right)\right] e^{\frac{j}{2}(\phi_\epsilon + \phi_\mu)} \end{aligned} \tag{2.44}$$

It can be seen from equation (2.44) that the real part of the refractive index is negative, and imaginary part as well because of nature of DNG materials [52]. If we neglect the losses, the negative refractive index can be easily shown to be negative. In lossless case $\phi_\epsilon + \phi_\mu$ are equal to 0, and substituting in equation (2.44), exponent $e^{\frac{j}{2}(\phi_\epsilon+\phi_\mu)}$ will be equal to -1 and refractive index will be expressed:

$$n = -\sqrt{\epsilon\mu} = -\sqrt{|\epsilon||\mu|} \tag{2.45}$$

Physically, as a consequence of negative refractive index, many interesting properties of a wave propagating in metamaterials medium can be concluded. When n is negative and by applying Snell's law, it can be shown that a reversed angle of transmission can be obtained, that is; applying Snell's law between two different mediums, one is DPS medium and the other is DNG medium as shown in Figure2.10. The angle of refraction in DNG medium is illustrated in equation (2.46).

$$\theta_t = n_2 \sin^{-1}\left(\frac{n_1}{|n_2|}\sin(\theta_i)\right) \tag{2.46}$$

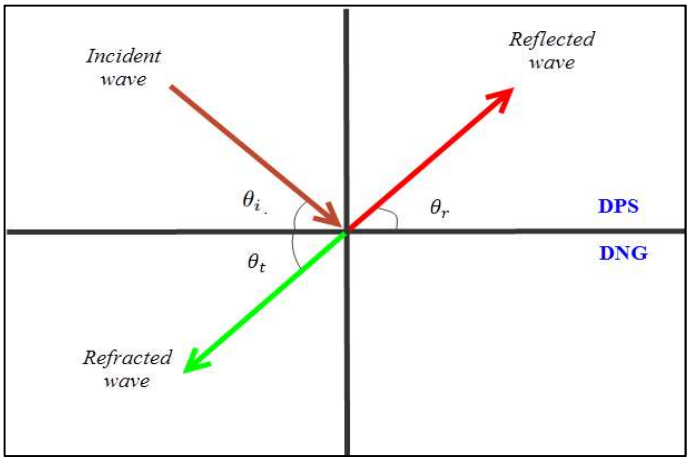

Figure 2.10: Wave reflection between DPS and DNG mediums.

CHAPTER 3

LITERATURE REVIEW

3.1 Ferrite based microstrip antennas

Ferrite materials have been widely used in designing microwave control devices, where DC magnetizing field is used to implement external control [12], [13], [16-18]. Their high dielectric constant, anisotropic and non-nonreciprocal properties made them very popular to control radiation pattern, resonance, polarization and gain characteristics of microstrip antennas. Figure 3.1 summarizes the existing research papers on different types of ferrite based antennas. The literature needs to be carefully reviewed to determine the best-suited approach in designing the proposed patch antenna.

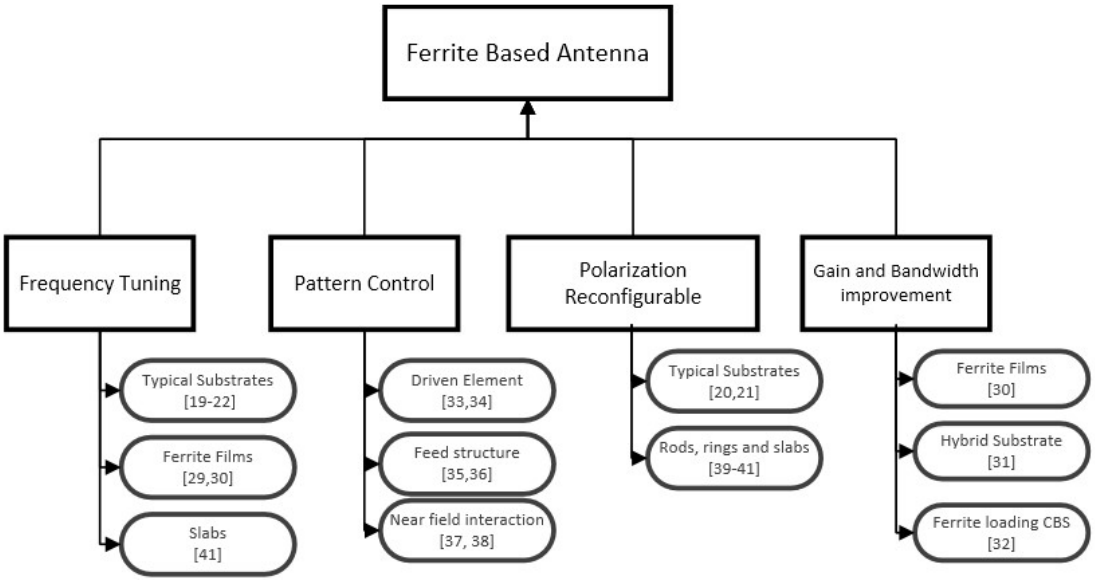

Figure 3.1: Summary of existing ferrite based reconfigurable microstrip antennas.

Tuning the resonant frequencies of a microstrip patch antennas using magnetic materials was demonstrated in 1992, where a simple patch with $1.8\ cm \times 1.4\ cm$ dimensions was designed on a magnetic substrate with $\epsilon_r = 14$ and saturation magnetization $4\pi M_s = 2500\ G$ [19]. It was shown that by changing the external magnetizing field (H_0), the permeability of the ferrite substrate can be changed, resulting in a change in the resonant frequency. Theoretical formulas of permeability for both transverse and axial directions of the applied magnetizing field were derived. In [20,21], Pozar has studied a patch antenna on magnetized ferrite substrate, where a probe fed square patch was designed on a ferrite substrate with $\epsilon_r = 15$ and $4\pi M_s = 1720\ G$. Using a permanent magnetic, a perpendicular magnetic biasing field was applied on the antenna. It was demonstrated that changing magnetic bias changed the antenna resonant frequency up to 16% for transverse biasing and up to 40% for axial biasing. In reference [22], a ferrite substrate with $\epsilon_r = 14.8$, $4\pi M_s = 3000\ G$ and $\Delta H = 450\ Oe$ was used to construct the patch antenna. It was demonstrated that by changing the magnetic biasing field of 60 kA/m, a tuning frequency range of 800 MHz was achieved. But this class of ferrite based tunable antennas often requires high magnetic biasing, generated through bulky electromagnets. This was one of the major drawbacks in integrating these antennas with indoor communication devices and sensors [18].

To overcome these problems, some researcher's integrated thin ferrite films on the dielectric substrates of the patch antenna [29, 30]. These configurations not only demonstrated required tuning and miniaturization, but it also improved the antenna gain. In [29], a simple rectangular patch antenna was designed on a normal dielectric substrate

to operate at 2.1 GHz, and NiCo-ferrite films were put above the patch, as shown in Figure 3.2.

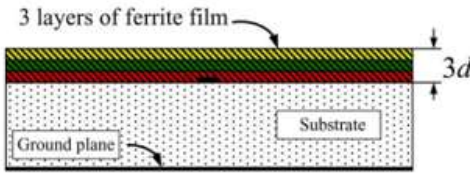

Figure 3.2 Self-Biased ferrite films over patch antenna [29].

This configuration introduced a tuning range of 14 to 40 MHz, with an enhancement in both efficiency and gain. Authors in [30] also showed that increasing the thickness of the ferrite film improves tuning range and miniaturization. An additional 40 MHz tuning range was demonstrated by increasing the thickness of the ferrite film by 10 mm. These antenna configurations also demonstrated low loss and improved size, gain and bandwidth.

Other researchers proposed a different type of solutions for enhancing the gain and miniaturization of the ferrite-based antennas. Ferrite-dielectric hybrid substrates were employed for this purpose. The hybrid substrate of reference [31] is shown in Figure 3.3, where a 5.8 GHz antenna is designed on a composite ferrite-dielectric substrate. The thickness of the substrate was h=3.2 mm and ϵ_r for ferrite and dielectric materials were ϵ_r =10 and 4.5, respectively. Note that the discontinuity has decreased the surface waves on the substrate and increased the gain of the antenna by about 4 dBi. Embedding ferrite material also enhanced the gain and the bandwidth of the cavity-backed antennas, as presented in reference [32].

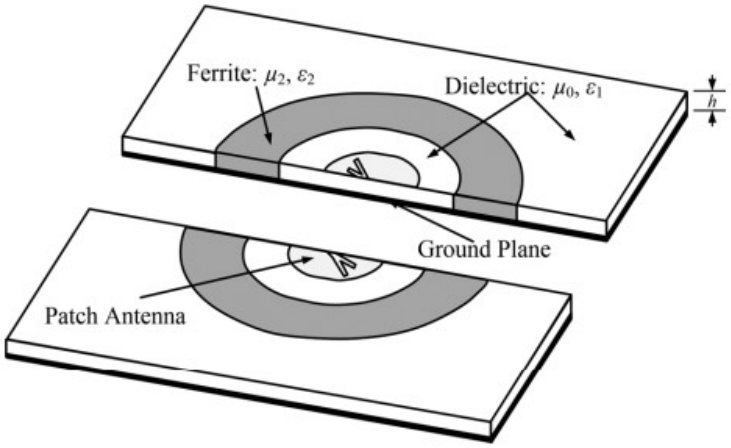

Figure 3.3 Antenna based on hybrid ferrite-dielectric hybrid substrates [31].

The design of ferrite based pattern reconfigurable patch antennas, available in the literature, are as follows: using driven antenna element [33, 34], using tunable factor from a feed structure [35, 36] and using magnetic-superstrate [37, 38]. In [33] and [34], the interaction between EM wave and the ferrimagnetic material were exploited for pattern reconfiguration. It was shown that by changing the external bias, a pattern control could be achieved.

In another approach, pattern reconfigurable microstrip antenna was proposed, where digital and analog phase shifts related to the ferrite substrate produced the required pattern control [35, 36]. Authors in [37] have introduced two YIG ferrite rods with $\epsilon_r = 15.4$ and $4\pi M_s = 1950G$ and $\Delta H = 10\ Oe$ in the near field region of a 10 GHz patch antenna. A beam scan of 30° was achieved by changing the external magnetizing field. The proposed design is shown in Figure 3.4. In reference [38], superstrate is used to realize pattern control of a patch antenna. Embedding ferrite rods, slabs or rings within the dielectric substrate of a patch antenna is a new trend to introduce tunable properties. In [39], frequency and polarization tunable patch antenna is presented.

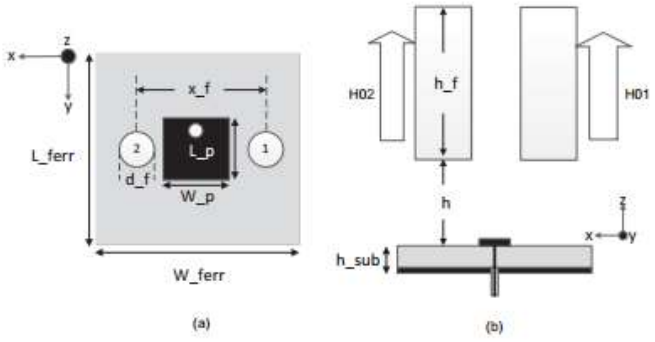

Figure 3.4: Ferrite superstrate based scan characteristics of a patch antenna [37].

In [39], polarization and frequency tunable patch antenna is presented. As shown in Figure 3.5, this design places a magnetized ferrite (YIG) cylinder underneath the 14 GHz patch to introduce tunable polarization properties (RHCP and LHCP). The microstrip patch antenna loaded with multiple magnetized ferrite disks were investigated in reference [40], where the axial ratio and return loss of the antenna depends on the position and the number of the ferrite disks.

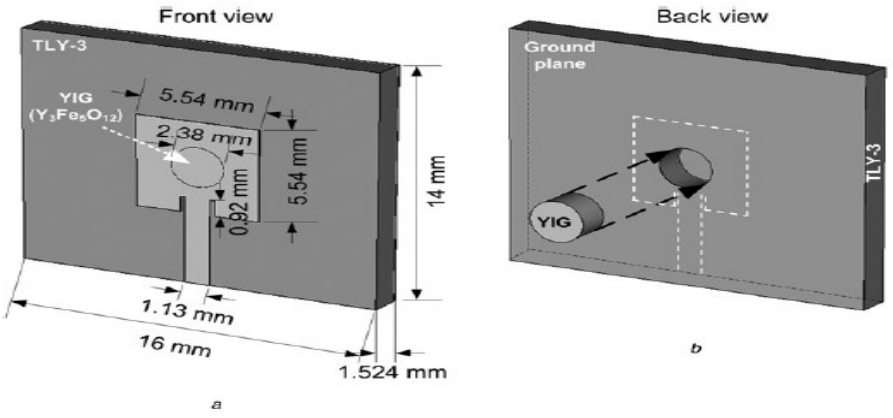

Figure 3.5: polarization and frequency tunable patch antenna with embedded ferrite slab [39].

As shown in Figure 3.6, this antenna was composed of a grounded coplanar waveguide (GCPW) with two YIG slabs positioned under the radiating patch. The antenna demonstrated multimode response with lower mode radiating a circularly polarized wave

and higher mode radiating a linearly polarized wave. A similar antenna is presented in reference [41], where changing the magnetization of ferrite slabs can achieve multiple resonant frequencies with different polarizations [41]. In this design, the frequency and polarization tuning was optimized by inserting the ferrimagnetic slabs within the non-radiating edges of the substrate. The antenna also demonstrated a frequency tuning range of 8.1% in the lower frequency band 5.5% in the higher frequency band.

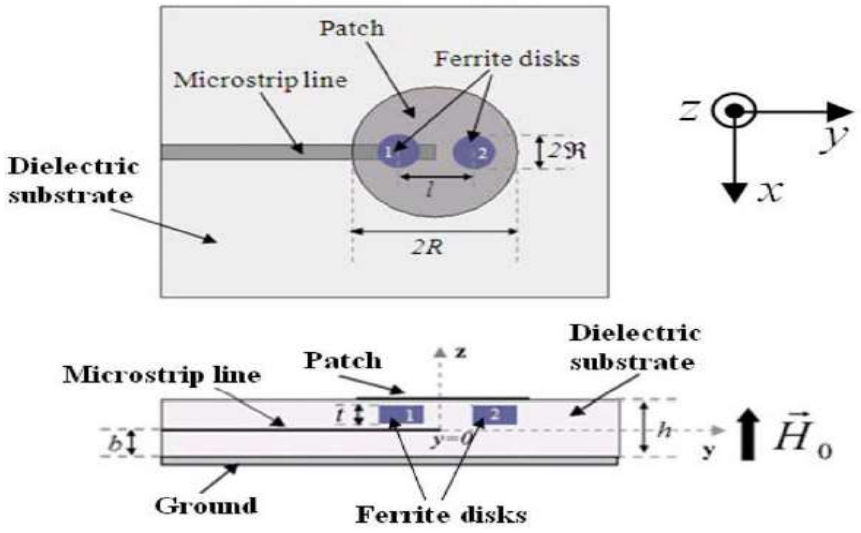

Figure 3.6: Ferrite based circular patch antenna with dual polarization [40].

As a summary, ferrite materials are widely used to design antennas with externally tunable operating frequency, polarization, and pattern configurations. They are also used to enhance the bandwidth and gain of microwave antennas. Although using typical ferrites substrates may introduce additional losses, small ferrites slabs integrated into hybrid substrates or ferrite films are promising techniques for designing reconfigurable antennas with simple configurations. Tables 3.1, 3.2 and 3.3 show comparative summary for all designs presented in this section.

Table 3.1 Summary of ferrite based frequency tuning designs.

Tunable Factor	Reference number	Type	Bias magnitude	Bias Direction	Tuning	Tuning BW
Frequency tuning	[19]	Typical Substrate	0.2 T	Transversal	750 MHz	-
			0.2 T	Axial	1 GHz	-
	[20], [21]		N/A	Transversal	1.1 GHz	16%
				Axial	2.2	40%
	[22]		0.75 T	-	800 MHz	400%
	[29]	Self-biased films			14-40 MHz	2%
	[30]				40 MHz	5%
	[41]	Slabs	0.15 T	Transversal	280 MHz, 260 MHz	8.1 % and 5.5%

Table 3.2 Summary of ferrite based pattern control designs.

Tunable Factor	Reference number	Type	Bias magnitude	Bias Direction	Tuning
Polarization	[20], [21]	Typical Substrate	N/A	Axial and transversal	Circular polarization, RHCP and LHCP
	[39]	Rod under patch	0.4 T	Transversal	Elliptical changing with bias direction
	[40]	Disks under patch	0.28 T	Transversal	Dual band circular polarization
	[41]	Slabs	0.06 T , 0.15 T	Transversal	Linear and Circular

Table 3.3 Summary of ferrite based Polarization tuning designs.

Tunable Factor	Reference number	Type	Bias magnitude	Bias Direction	Tuning
Pattern Control	[33]	Typical Substrate	0.03 T	Transversal	Reducing RCS
	[34]		0.13 T	Transversal	Change RCS
	[37]	Near field superstrates	0.188 T	Transversal	30 Degree
	[38]		-	-	37 Degree

3.2 Metamaterials in antenna applications

Metamaterials or engineered materials are widely used to improve antennas properties including impedance bandwidth, gain and directivity. Commonly used metamaterial consists of a periodic arrangement of Split Ring Resonators (SRRs), where SRR units are typically made of two conducting "C" shaped wire loops that have a gap in the opposite directions. SRR responds to an alternating magnetic field of EM wave, which introduces rotating currents in the conductor, similar to that of magnetic moments in magnetized ferrite material. In recent years, metamaterials are widely used in microwave devices, including absorbers [54, 55], power dividers [56, 57], antennas and many other applications [58-64]. In the field of antennas, integrating metamaterial can introduce tunable properties in addition to enhanced antenna response.

Split ring resonator (SRR) and complementary split ring resonator (CSRR) are the most commonly used components of the metamaterial. In reference [58], SRR is integrated within the feed line of a patch antenna to introduce band-stop properties to suppress spurious radiation. In [59], it is shown that SRR can enhance the gain of a conformal printed antenna. The design consisted of a simple rectangular patch operating at WiMAX band (2.50-2.69 GHz) and a thin layer of metamaterial superstrate, composed of S-shaped split ring resonators. The antenna configuration, shown in Figure 3.7, demonstrated an enhanced gain of 1.8 dB.

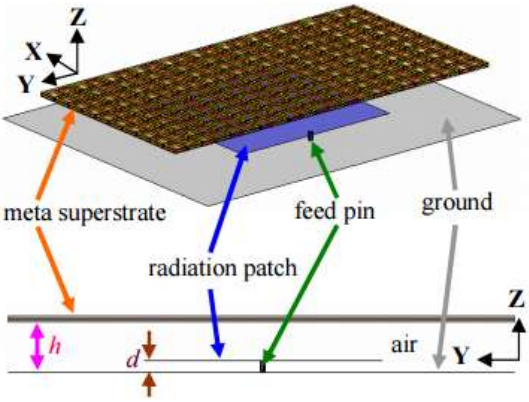

Figure 3.7: Gain enhancement of a patch antenna with metamaterial superstrate [59].

Another important application of metamaterial is to alter the physical dimension of a printed antenna. This requires optimal embedding SRR and CSRR structures within the substrate, which changes the effective permittivity or permeability of the structure to tune resonant frequency. In [68], a compact patch antenna using split-ring resonators (SRRs) embedded within the substrate has been designed. The resonance frequency of the antenna shifts from 6.6 to 4.67 GHz, which represents 29.3% reduction of the antenna size. In [50], metamaterials are also used to reduce the dimension of a circular patch antenna operating at 2 GHz. In reference [60], embedding a complementary split-ring resonator (CSRR) within a rectangular L-S band patch antenna tuned the operating frequency from 3 to 3.5 GHz. In [62], SRR's are used to introduce dual-band (1.5 GHz and 2.5 GHz) operation, which enables multiple simultaneous application of a single patch antenna. In [63], a dual-band antenna for GSM and WiMAX bands (1.8 and 3.5 GHz) is designed by integrating complementary split ring resonators (CSRR).

In the literature, metamaterial is also employed to steer the main beam of a printed antenna. Authors in [64] proposed loading CSRR units on the non-radiated edges of a 2 GHz patch antenna to steer the main beam towards $\theta=\mathbf{46^0}$. In reference [65], an SRR integrated

magnetized ferrite superstrate of a microstrip patch introduced beam scanning, which depended on the magnitude and direction of the external magnetizing field. A maximum scan of $\pm 30^{o}$ is demonstrated in this design. In reference [65], an SRR integrated ferrimagnetic superstrate is introduced on a Microstrip patch antenna to introduce beam scan, where the scan depended on external magnetic biasing of the ferrite material. A maximum scan of $\pm 30^{o}$ is demonstrated in this design. Table 3.4 below lists the reference material related to metamaterial based antennas based on their application.

Table 3.4 Summary of metamaterials based antenna references.

Tunable Factor	Reference number	Type	Configuration	Tuning
Gain improvement	**[58]**	S shape SRR	Rectangular patch	Gain = +1.8 dB
	[59]	stacked S-shaped split-ring	Rectangular patch	Gain = +2 dB
Antenna Miniaturization	**[68]**	SRR	Rectangular patch	1.93 GHz
	[60]	CSRR	Rectangular patch	0.5 GHz
	[61]	CSRR	Circular patch	4.5 GHz
Pattern Control	**[64]**	CSRR	Rectangular patch	46 degree
	[65]	SRR	Rectangular patch	30 degree
Dual band	**[62]**	SRR	Rectangular patch	1.5 GHz and 2.5 GHz
	[63]	CSRR	hexagonal patch	1.8 GHz and 3.5 GHz

In our design, metamaterials will be integrated within ferrite material to provide controllable enhancements to antenna performance.

3.3 Conclusions

In this chapter, a comprehensive literature review of previous works in both ferrite and metamaterial based antenna has been presented. It has been shown that ferrite was used in antenna applications as a driven element, self-biased films and integrated within the substrate. Even using ferrite substrate can provide large tuning in terms of frequency, pattern and polarization, but it requires high external biasing fields and it shows large losses. On the other hand, integrating ferrite films increasing the size of the antenna with small amount of tuning. Using of ferrite-dielectric composition was one of the best solutions in terms of efficiency and gain of designed antenna. Metamaterial has been also used in enhancing the performance of the antenna and adding reconfigurable characteristics.

This work will introduce microstrip antenna printed over ferrite-dielectric substrate. With low magnetization value and proper direction, tuning range with about 870 MHz will be achieved which provides wider tuning range compared with proposed designs in the literature. On the other hand, by integrating resonating structure within the slabs, the tuning range will be extended and controllable pattern can be achieved. This coupling will provide extended frequency tuning range up to 1.44 GHz in addition to 25^{o} of beam steering controlled by 0.062 Tesla magnetization field.

CHAPTER 4

DESIGN OF FREQUENCY RECONFIGURABLE ANTENNA

In this chapter the design and modeling of frequency tunable patch antenna, based on a dielectric-ferrite composite substrate will be proposed. In this design, two rectangular ferrite slabs are embedded within the dielectric substrate to introduce efficient frequency tuning mechanism. Using a finite element based full wave solver (HFSS®), the position of the externally magnetized ferrite slabs is optimized to maximize the gyrotropic interacts between the ferrite material and the magnetic field component of the EM wave. Parametric investigations are conducted to improve the antenna performance for different magnetization directions of the ferrite material. Although, electromagnetic can be used to externally magnetize the ferrite part of the substrate, permanent magnetic (NdFeB) are also suitable for this application. Magnetostatic simulation software Ansoft (Maxwell®) used to simulate the permanent magnets to study the magnetic field generated and used to magnetize ferrite slabs.

4.1 Design of patch antenna with ferrite slabs

Initially, probe-fed Microstrip patch antenna, operating in the C-band, was designed and optimized using professional software (HFSS). The patch was based on Roger RT\duriod 5880 substrate with dielectric constant of 2.2 and height of 3.2 mm. The optimized

dimensions of antenna are shown in Figure 4.1, where L_p =22.5 mm, W_p =26 mm, f_l= 5.5 mm

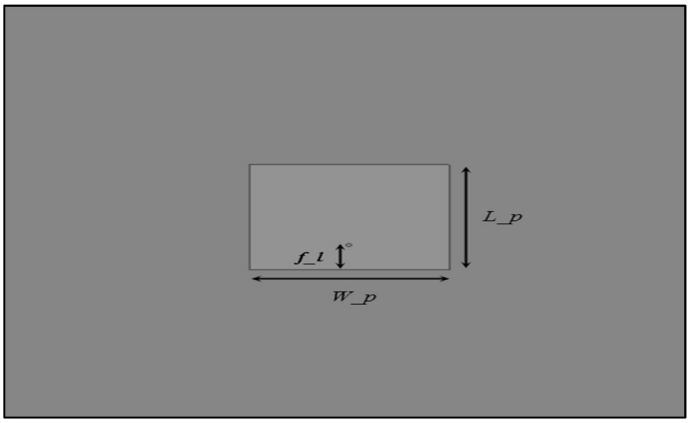

Figure 4.1: Optimized dimensions of Prob fed patch antenna.

The sumilated reflection coefficient of the antenna is shown in Figure 4.2. Note that the antenna resonates at 4.05 GHz and demonstrates an impedance bandwidth of 236 MHz with a maximum gain of 7.71 dB. To tune the resonance frequency of this antenna, ferrite slabs are optimally integrated with the substrate.

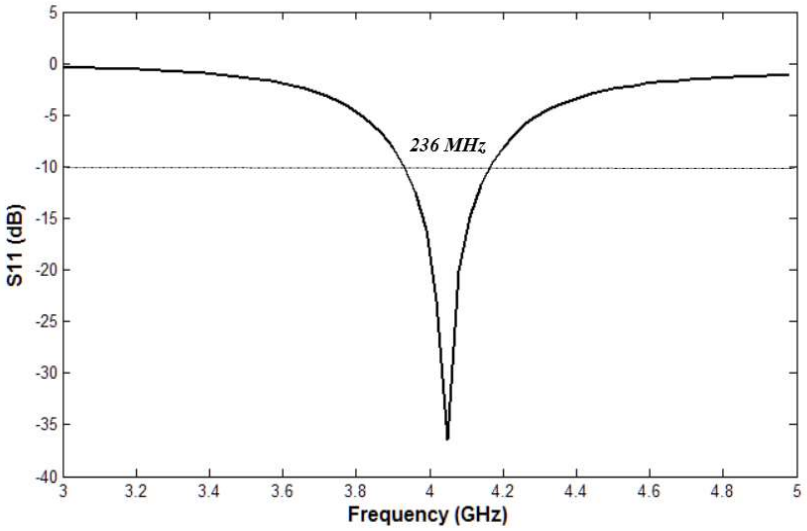

Figure 4.2: Reflection coefficient of the patch antenna.

4.1.1 Selection of ferrite material

The selection of the ferrite is determined by the material properties that best suits the design. As stated before, the absorption loss in ferrites is characterized by a parameter known as the resonance linewidth (ΔH). At microwave frequencies, garnets are found to be most suitable for our application due to low loss and suitable material properties. So Yttrium iron garnet (NG-1850), manufactured by TCI Ceramics, are integrated into the designed antenna. The specifications of the material according to their catalogue are shown in Table 4.1.

Table 4.1. Specifications of ferrite used in the design.

Parameter	Measured Value
Dielectric constant	15.0 +/-5%.
Magnetization Saturation (4πMs)	1850 +/-5% Gauss
Loss (I/Q)	0.00012
Line width	≤ 14.4 Oe

4.1.2 Position of ferrite slabs

Using the software, a through parametric analysis is performed to determine the best position to integrate the ferrite material it within the dielectric substrate. This analysis is based on known electric and magnetic field distribution on the patch antenna, obtained from its cavity model. It is observed that the maximum magnetic (H) field distribution occurs at the center of the non-radiating edge of the patch (H-Plane). The amplitude and

direction of the magnetic field distribution of a rectangular patch antenna are shown in Figures 4.3 and 4.4. Note that the maximum H-field distribution occurs at the center of non-radiating edges (along the y-axis) and it is perpendicular to the electric field distribution (along the x-axis) of the patch antenna.

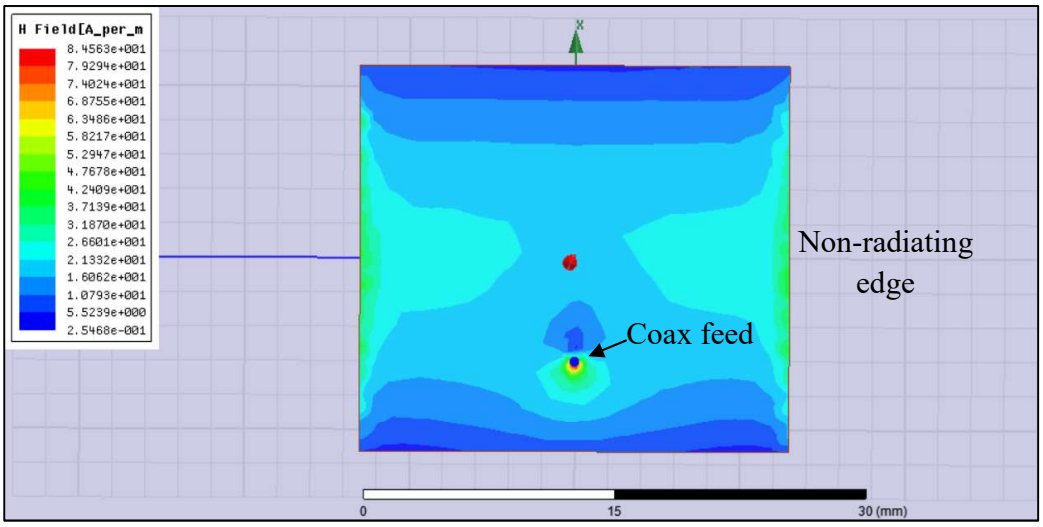

Figure 4.3: Amplitude of the Magnetic field distribution at 4 GHz (Magnitude).

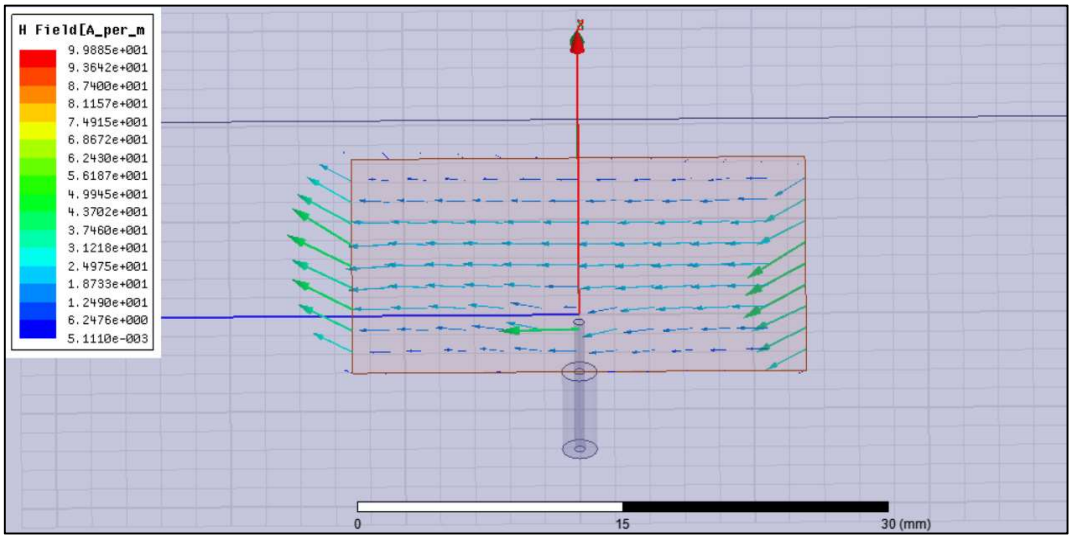

Figure 4.4: Magnetic field distribution at 4 GHz (Vector).

Thus, the center of the non-radiating edge of the patch is found to be the best suited position to place the rectangular ferrite slabs to maximize the gyro-magnetic interaction between the magnetized ferrite material and the magnetic field of the antenna. The simulated solutions demonstrated that two opposite biased ferrite slabs provided better frequency tuning compared to a biased single ferrite slab. It is also noted that the radiation efficiency of the antenna deteriorates, if the dielectric substrate under the center of the patch is replaced with a ferrite material. The two ferrite slabs embedded within the dielectric substrate of the patch antenna is shown in Figure 4.5.

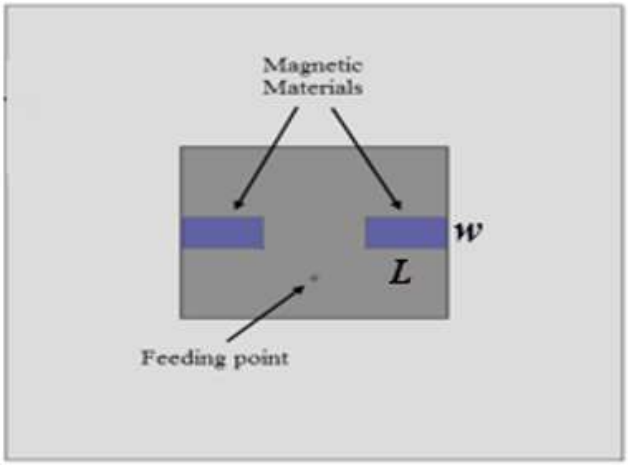

Figure 4.5: Schematic diagram of patch antenna with embedded ferrite slabs.

4.1.3 Dimensions of ferrite slabs

To study how the dimensions of the ferrite slabs are affecting the resonance behavior of the patch antenna, a comprehensive parametric analysis is conducted. From the theory, it is clear that changing the percentage of the embedded ferrite material under the patch will change the effective permeability of the substrate, which in return changes the resonance

frequency. The simulated return losses of the antenna with different length and width of the unmagnified ferrite slab are plotted in Figures 4.6 and 4.7.

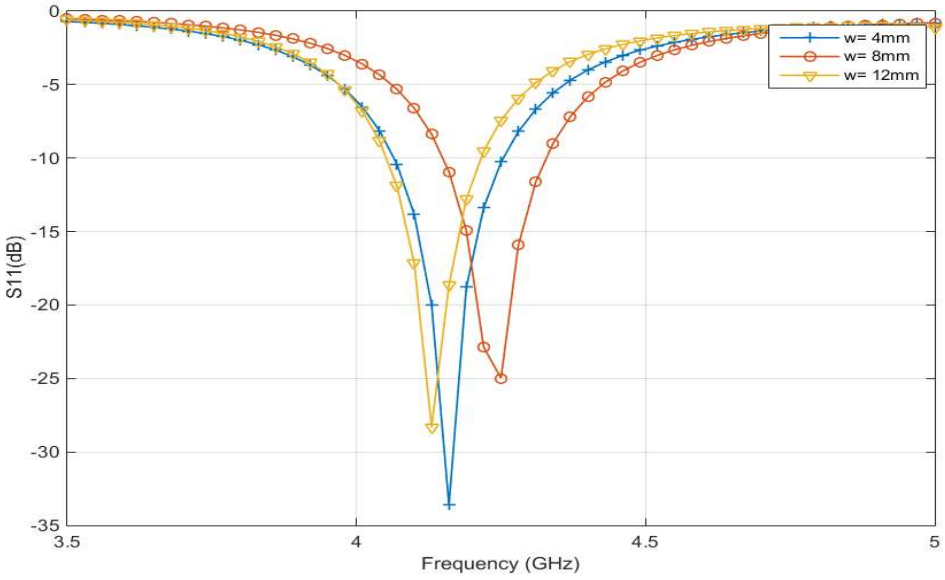

Figure 4.6: The effect of changing the length of ferrite slabs on the resonance.

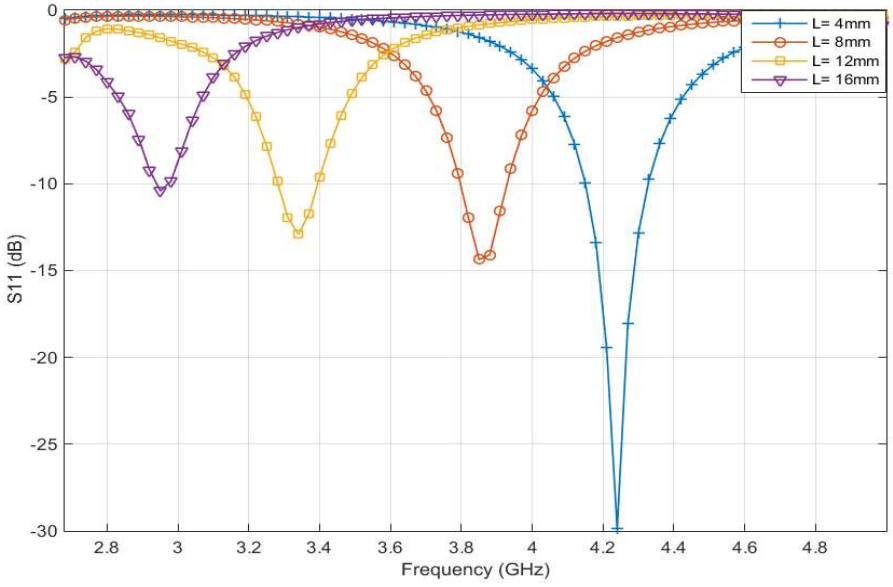

Figure 4.7: The effect of changing the width of ferrite slabs on the resonance.

Note that the change in width (W) of the ferrite slab causes more magnetic field to interact with the ferrite material and produces a larger change in resonant frequency (fr), compared to that of slab length (L). But this antenna size reduction through frequency tuning comes at cost of increased return loss, as demonstrated in Figure 4.7. Table4.2 summarizes the values of resonance frequencies and return loss of different length and width of ferrite slabs.

Table 4.2 Resonance frequency and S11 values for different dimensions of the slabs.

Parameter	Value	Related Resonance	|S11| value
Length (L)	4mm	4.16	-33.61
	8mm	4.25	-24.98
	12mm	4.13	-28.31
Width (W)	4mm	4.24	-29.87
	8mm	3.85	-14.35
	12mm	3.34	-12.9
	16mm	2.95	-10.40

Note that the change of width by $\Delta W=12$ mm leads to hard tuning of the resonant frequency by $\Delta f=1.3$ GHz or 30% of the resonant frequency (fr). Thus, for the required patch antenna with acceptable return loss and tunable range, the selected ferrite slab dimensions are W=4mm and L=8mm. Although these parameters resulted in an antenna with fr=4.2GHz, re-optimization of the antenna to get fr=4GHz can be performed in the later stage, once the effect of the external magnetizing field is studied.

4.2 Effect of external magnetization field

In the earlier chapter, the external magnetizing effects of microwave ferrite material were discussed. The source of tuning was mainly due to the tensor permeability of the material, which can be expressed by

$$\mu_{eff} = \frac{\mu - \kappa}{\mu}$$

Where, μ and κ are functions of both magnitude and direction of the external DC magnetic biasing field (H_{dc}). It was also clear from the earlier discussion that efficient pressing of the ferrimagnetic dipoles require H_0 to be applied in the perpendicular plane to that of the magnetic field component of EM wave (H_{EM}). In Figure 4.4, it is clear the h_{EM} fields for the patch antenna remains in y-direction. So, H_{dc} can be applied in either x-axis or z-axis direction. But from an experimental point of view, applying magnetic biasing field (H_{dc}) in z-direction is more practical and adopted in the simulated model. In order to provide the external magnetic field to ferrite material, neodymium permanent magnets (NdFeB) will be practically used. The simulation of the magnets has been studied in the next subsection.

4.2.1 Permeant magnet design

NdFeB magnets are the strongest commercially magnets that can provide large magnetic fields with small sizes compared with standard coils There are many categories of these magnets that differ in their size and physical properties. The most important factor in choosing the magnet that fits our design is its size, since it affects how many fields it can provide, and the degree of uniformity of magnetic field that passes to the slabs. Uniform magnetic field is important to care about in ferrite design, so we have chosen a magnet that has larger dimensions than the slabs are.

To study the direction and magnitude of the magnetic field provided by the magnet, Ansoft Maxwell® magnetostatic software was used to simulate NdFeB magnets with (10× 10 × 5) mm dimensions (known as N-42 type magnet) above copper sheet in vacuum medium. The magnet has the properties shown in Table 4.3 .

Table 4.3: Properties of N-42 permanent magnet.

B_r		H_{cB}		H_{cJ}		BHmax	
mT	gauss	kA/m	Oersteds	kA/m	Oersteds	kJ/m3	MGOe
1,280	12,800	915	11,500	955	12,000	318	40

Where B_r is the Residual Induction, H_{cB} is the coercivity, H_{cJ} is the Intrinsic coercivity, and BHmax is the maximum product energy. The generated magnetic field values generated by the magnet at different axial distances were simulated and extracted from software. Table 4.4.

Table 4.4: Magnetic field values with different distances from the magnet.

Distance [mm]	Mag_B [Tesla]
0.0	0.379
0.5	0.346
1.0	0.312
1.5	0.278
2.0	0.247
2.5	0.216
3.0	0.187
3.5	0.161
4.0	0.140
4.5	0.119
5.0	0.101

Figure 4.8 also shows the simulated of magnetic field values generated with respect to all distances from the magnet.

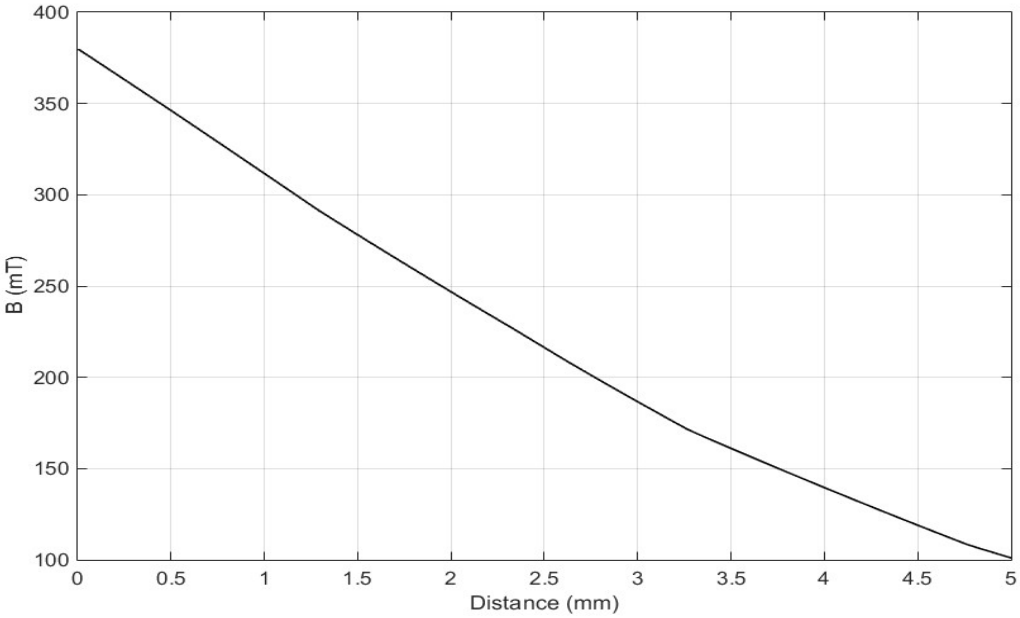

Figure 4.8: Simulated magnetic field (B) with distance from the magnet.

Figure 4.9 shows the model of the magnet over a copper sheet with 5mm distance below the magnet and the magnetic field produced around the magnet. It can be shown that the magnetic field that going through the sheet is approximately uniform at the distance of 5 mm and the maximum value of the field needed for our design (0.1 T).

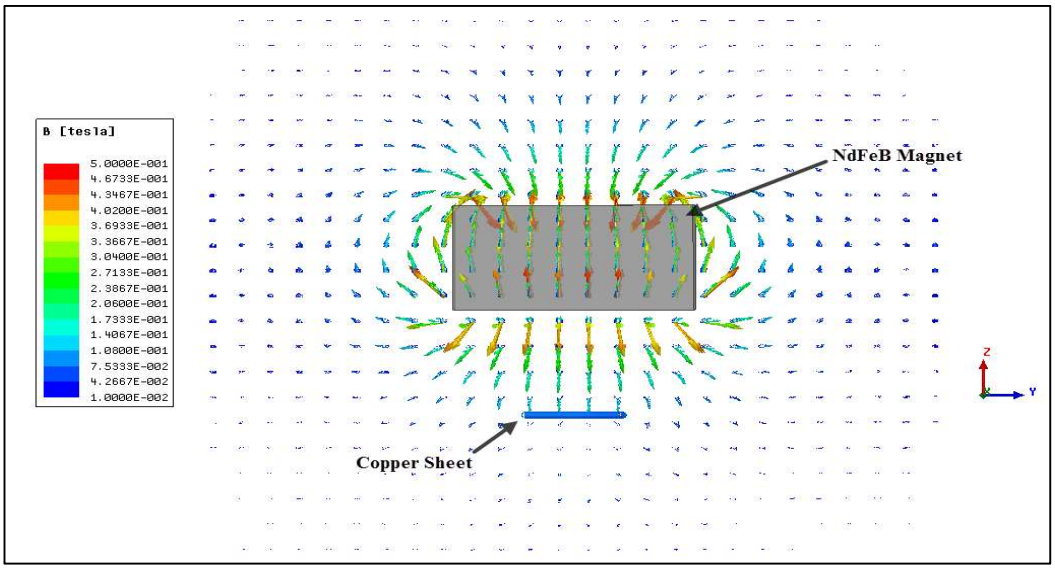

Figure 4.9: Magnetic field from NdFeB magnet over copper sheet.

4.2.2 Frequency tuning

To study the effect of both direction and magnitude of biasing field an applied field (Hdc) starting from 10 kA/m and up to 80 kA/m (0 to 0.1 Tesla) was applied on the slabs in two different directions:

1. When both the ferrite slabs are magnetized in the same direction, either in +z or – z axis.
2. When the ferrite slabs are magnetized in reverse direction the other.

In case-1, externally magnetizing the ferrite slabs in the same direction demonstrates lower frequency tuning range with higher return loss. This is shown in Figure 4.10. Note that a resonant frequency tuning of Δf=0.15GHz (considering three left most curves) is achieved for ΔH_{dc}=25.8mT. It is also clear from this figure that this configuration of the antenna also generates a higher order mode at 5.3 GHz.

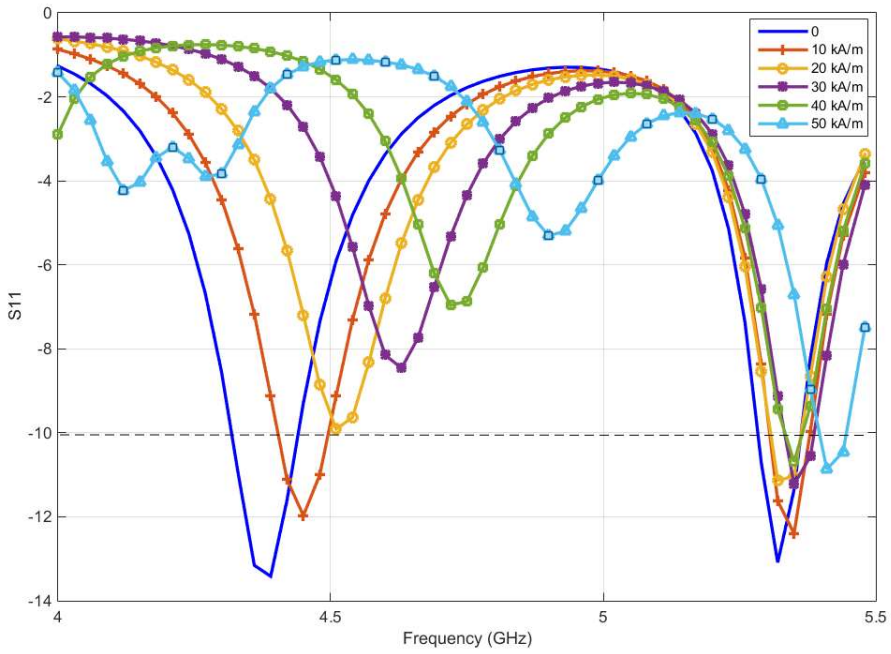

Figure 4.10: The effect of applying external magnetic field in the same direction.

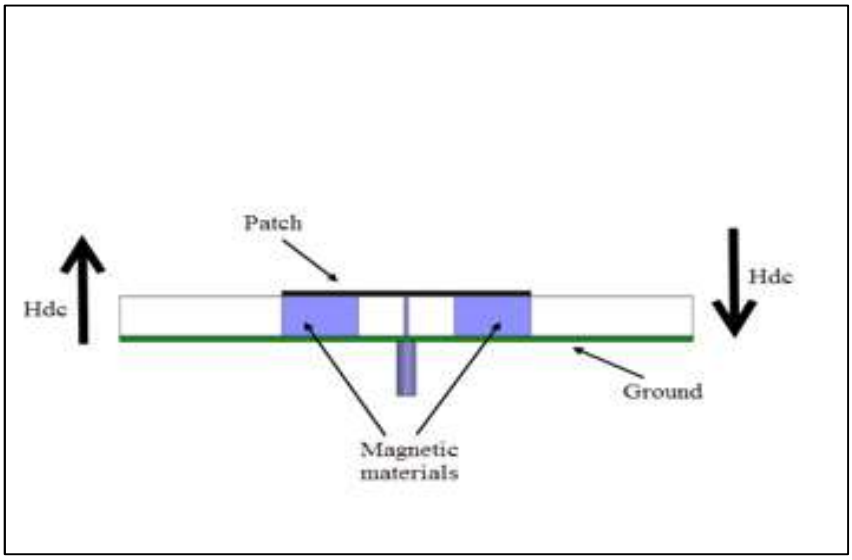

Figure 4.11: The effect of applying external magnetic field in the same direction.

In case-2, the ferrite slabs are externally magnetizing in the opposite direction, as shown in Figure 4.9. The simulated return loss, gain and radiation patterns resulted from this antenna configuration are discussed below:

Return Loss: Figure 4.11 shows the effect on the return loss (S11) of the antenna for changing the magnetic bias up to 80 kA/m (0.1T), in opposite directions. Note that by increasing the magnetic bias ΔH_{DC}=0.1T, the resonance frequency of the patch antenna increased from 4.2 GHz to 5.12 GHz, with a tuning range of Δf_r=870MHz. The broad tuning range is the result of cumulative gyrotropic interaction between the oppositely magnetized ferrite slabs to alternating magnetic field component of the EM wave (H_{EM}). Note that the return loss of the antenna ranges from -25 dB to -11 dB for no-magnetization to maximum available magnetization state. The resonance frequency versus applied magnetic field plot is also shown in Figure 4.12.

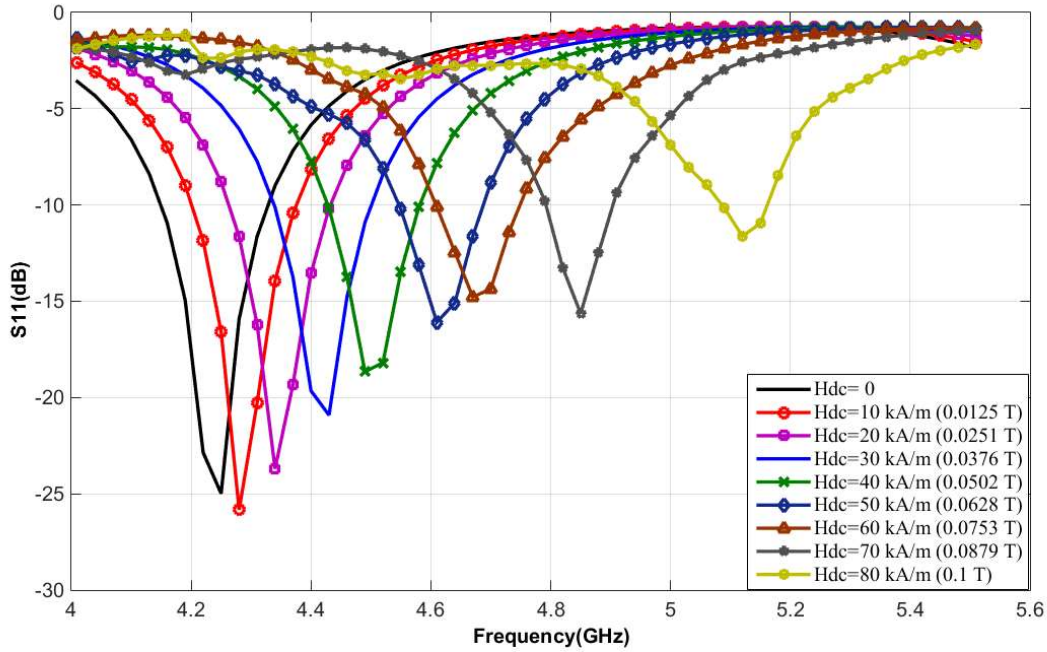

Figure 4.12: The effect of applying external magnetic field in opposite direction.

Gain and Radiation Patterns: Using the professional software, the gain and efficiency of the designed patch antenna are studied to determine the cost involved due to introducing the frequency tuning properties. As expected, the antenna gain reduces from 7.7 dB for no bias to 2.1 dB for the maximum bias of 80kA/m. This is because increasing the magnetic biasing led to increased interaction and absorption within the ferrite material. Table 4.3 summarizes the gain and efficiency of the antenna related to the different magnetic biasing state of the antenna.

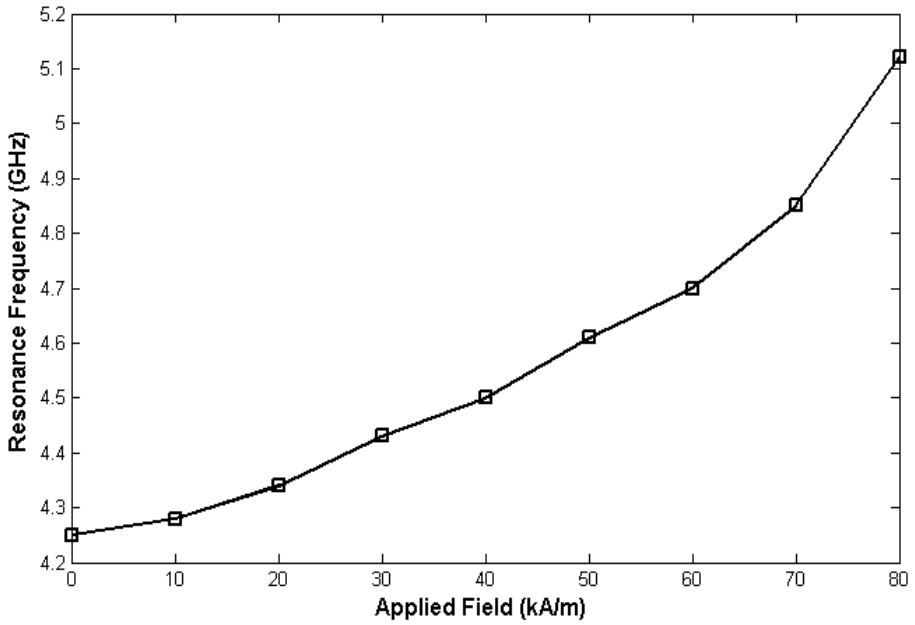

Figure 4.13: Resonance frequency of the patch with respect to external bias.

The E and H-plane (ϕ= 0° and 90°) radiation pattern of the designed antenna is plotted in Figure 4.12.

Table 4.5: Resonance frequency, maximum gain and efficiency of the antenna for different bias fields.

Magnetic Bias (kA/m)	Magnetic Bias (Tesla)	Antenna parameters		
		Resonance frequency (GHz)	Maximum Gain (dB)	Efficiency
0	0.0000	4.25	7.7	92%
10	0.0125	4.28	7.6	89%
20	0.0251	4.34	7.7	89%
30	0.0376	4.43	7.4	82%
40	0.0502	4.49	7.1	77%
50	0.0628	4.61	6.5	67%
60	0.0753	4.7	4.8	46%
70	0.0879	4.85	4.1	42%
80	0.1000	5.12	2.1	26%

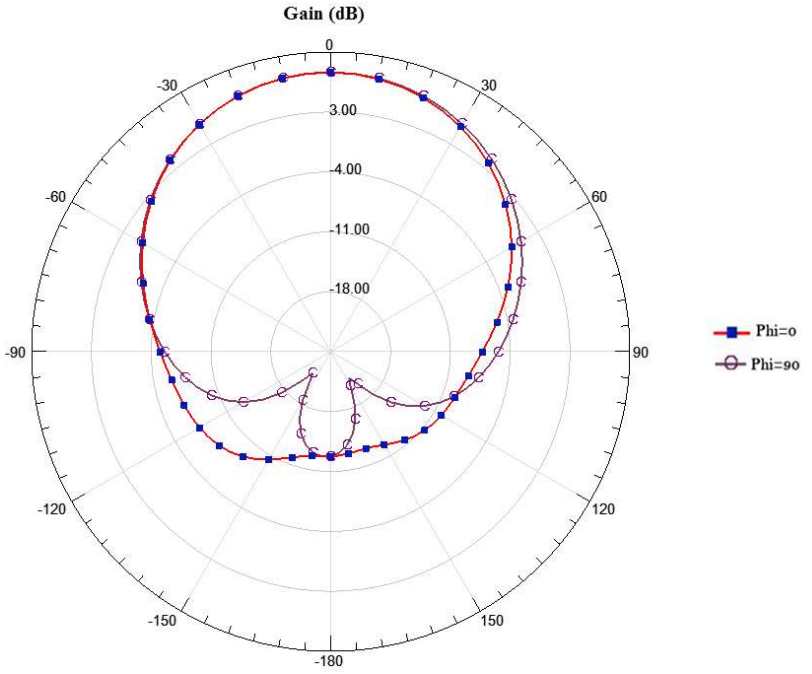

Figure 4.14: Radiation pattern for the antenna at 4.28 GHz with Hdc= 0.0125T.

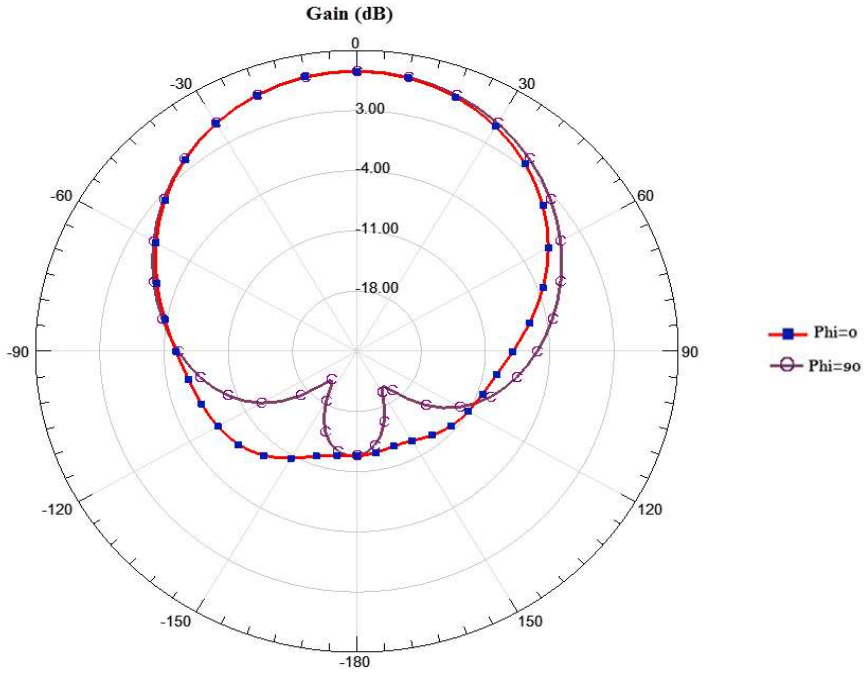

Figure 4.15: Radiation pattern for the antenna at 4.34 GHz with Hdc= 0.0251T.

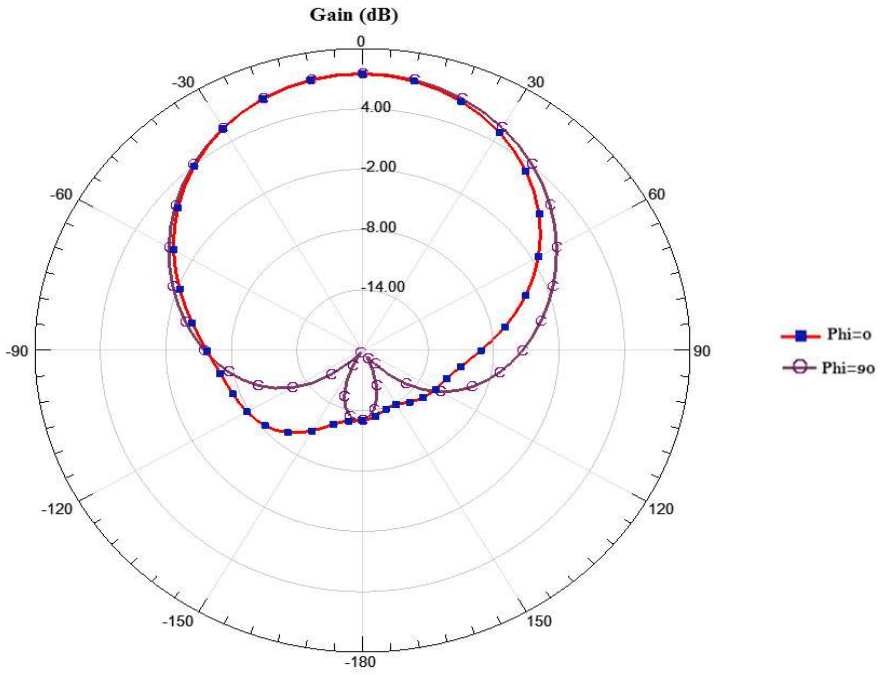

Figure 4.16: Radiation pattern for the antenna at 4.43 GHz with Hdc= 0.0376T.

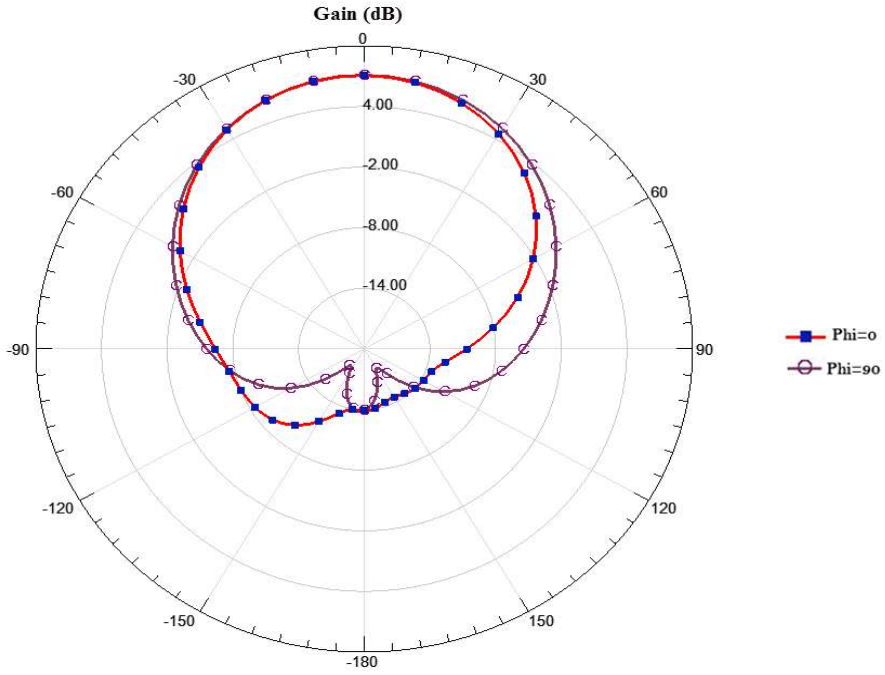

Figure 4.17: Radiation pattern for the antenna at 4.49 GHz with Hdc= 0.0502T.

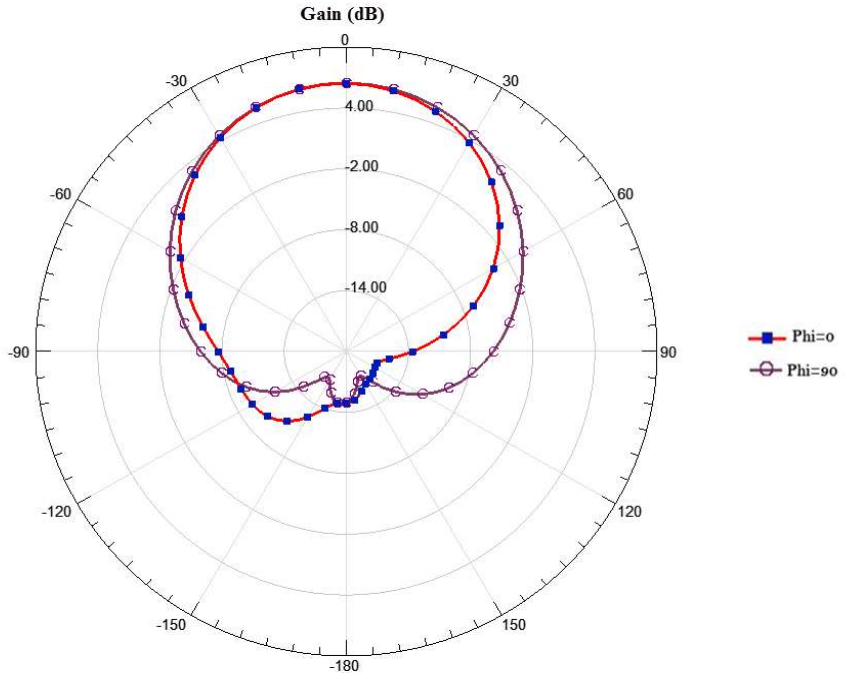

Figure 4.18: Radiation pattern for the antenna at 4.61 GHz with Hdc= 0.0628T.

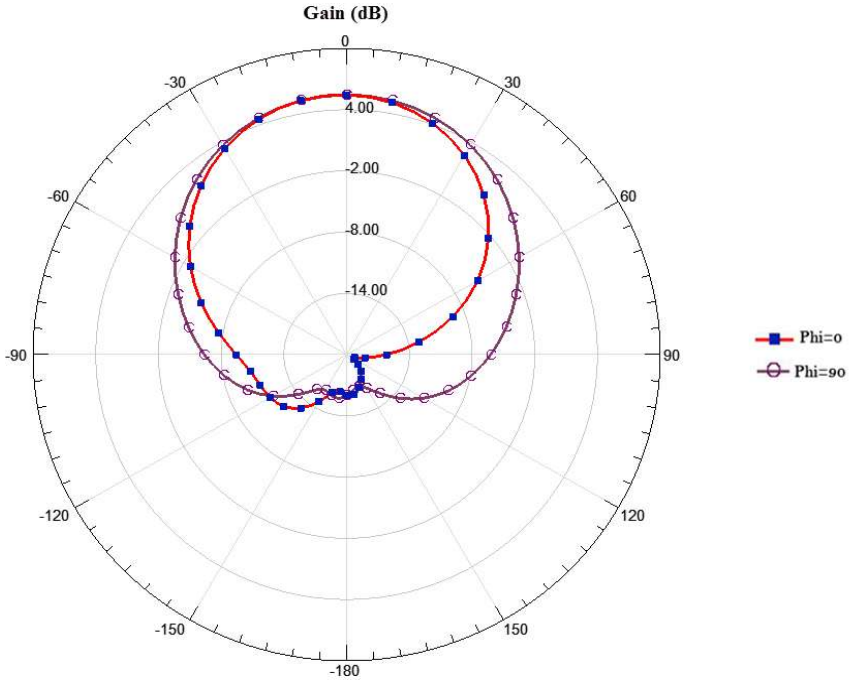

Figure 4.19: Radiation pattern for the antenna at 4.7 GHz with Hdc= 0.0753T.

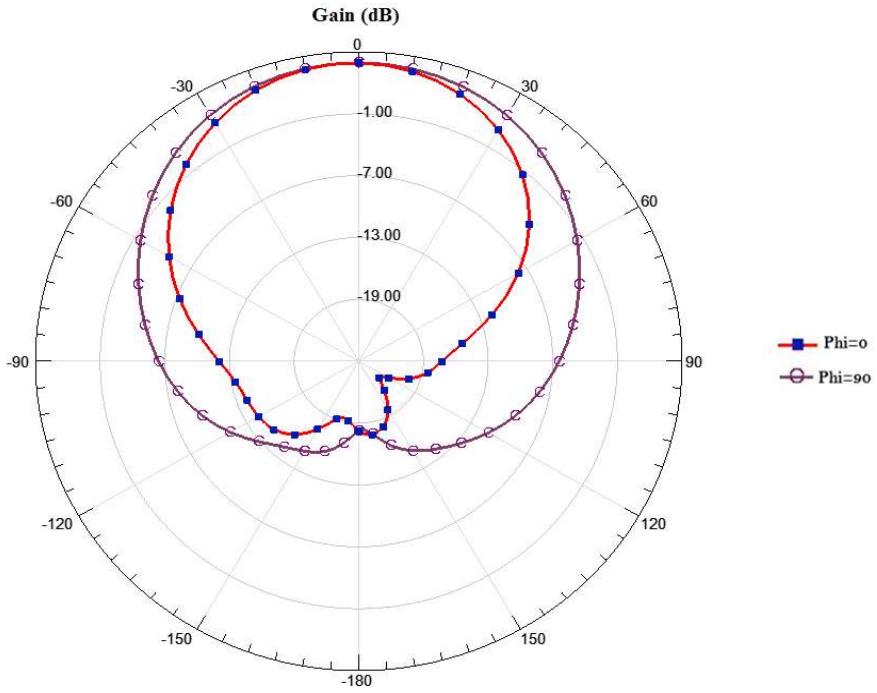

Figure 4.20: Radiation pattern for the antenna at 4.85 GHz with Hdc= 0.0879T.

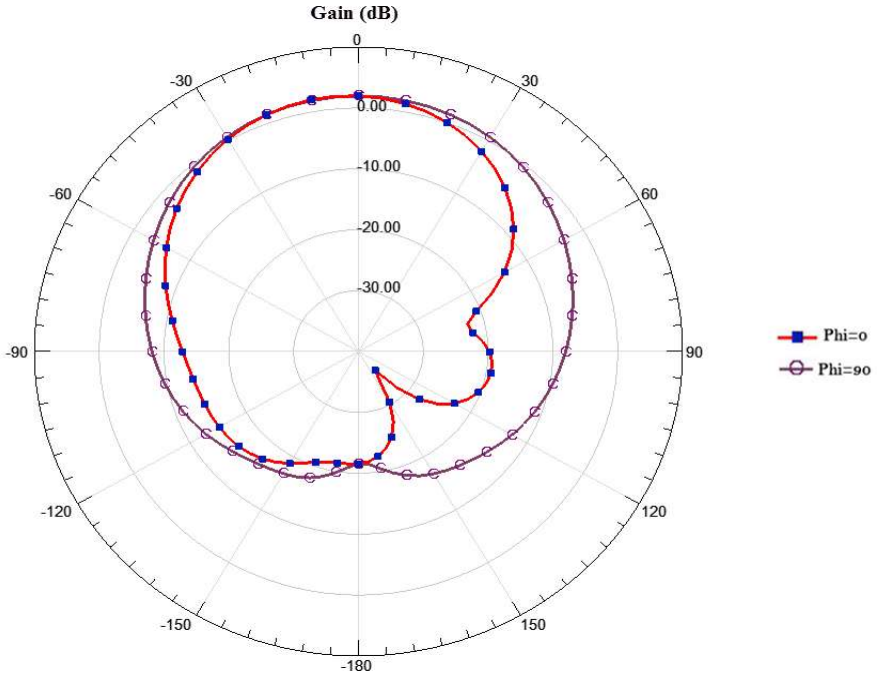

Figure 4.21: Radiation pattern for the antenna at 5.12 GHz with Hdc= 0.1T.

4.3 Conclusions

In this chapter, ferrite-dielectric based patch antenna was designed, by optimizing the position of ferrite slabs and with proper magnetization direction, frequency tuning of 870 MHz was achieved by applying up to 0.1 T. Which forms 20% of tuning from the center frequency and has larger tuning range rather than presented in the literature.

The average gain of the antenna in the tuning range is 5 dB, and good radiation patterns have been achieved. Permanent NdFeB magnets have been simulated in the magnetostatic simulator to provide the required magnitude and direction of the external magnetic field.

CHAPTER 5

DESIGN OF PATTERN AND POLARIZATION RECONFIGURABLE ANTENNA

In the previous chapter, the analysis of magnetically tunable patch antenna was studied. It was shown that by using a ferrite-dielectric substrate with proper magnetization, frequency tuning could be achieved with good gain. In this chapter, split ring resonators (SRR) will be integrated within the ferrite slabs to provide another source of internal magnetization within ferrite material. The aim is to constructively couple the ferrimagnetic resonance with the resonance behavior of the SRR to result in a larger net magnetic field. These magnetic couplings of the fields are realized here by optimally embedding SRR's within the ferrite part of the dielectric-ferrite substrate. This should introduce beam steering properties of the designed patch antenna in addition to improving the frequency tuning characteristics. On the other hand, it will be shown that using ferrite slabs and rods will provide a tunable polarization antenna. The Ansys High-Frequency Structure Simulator (HFSS®) is used to design SRR structures and finally optimally integrate them within the ferrite-dielectric substrate of the patch antenna.

5.1 Design of planar square split ring resonator (SRR)

SRRs in its simplest form are conductive metallic rings with a split inner circle embedded within an outer circle having oppositely positioned split. These structures are used to

construct meta-material with enhancing magnetic coupling properties. Thus, an electromagnetic (EM) wave with magnetic field components perpendicular to the plane of the SRR induces alternating currents on the rings [69], which in turn generates a magnetic moment normal to the SRR plane. The gaps are used to generate large capacitance to reduce the resonance frequency of the SRR. In this research work, metallic SRR's are designed and optimally positioned on NG-1850 ferrite substrate to resonate around 4-GHz. The optimized dimensions (L_1 = 3.2mm, L_2=2.7mm, g=0.3mm, h=3.2mm, t=0.0017mm) of the ferrite-based SRR are shown in Figure 5.1. The simulated reflection and transmission coefficients of the SRR structures are plotted in Figure 5.2.

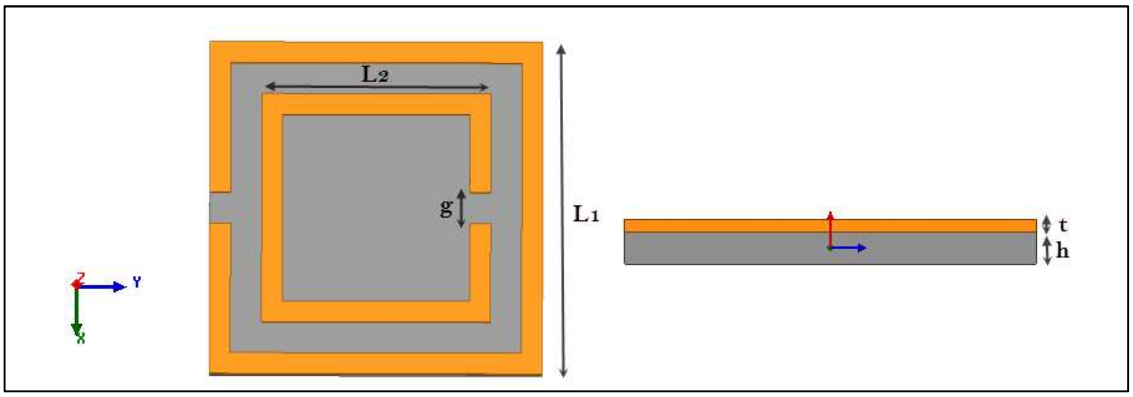

Figure 5.1: The designed SRR structure on NG-1850 ferrite material.

The frequency of 4-GHz is selected to magnetically couple the SRR resonance with that of the patch antenna, designed in chapter 4. The mathematical equations are used to extract the permittivity (ϵ_r) and the permeability (μ_r) values from the S-parameters [70]. These equations were implemented in MATLAB code which was used in the to extract both permittivity and permeability. The real and imaginary part of both effective permittivity and permeability of the designed SRR structure are shown in Figure 5.3 and Figure 5.4.

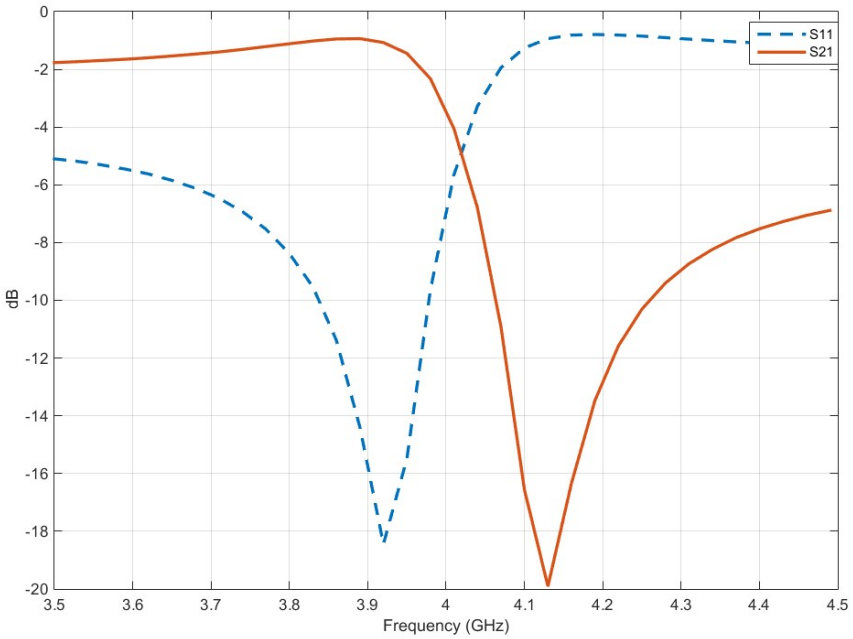

Figure 5.2: Transmission and reflection coefficients of the designed SRR structure.

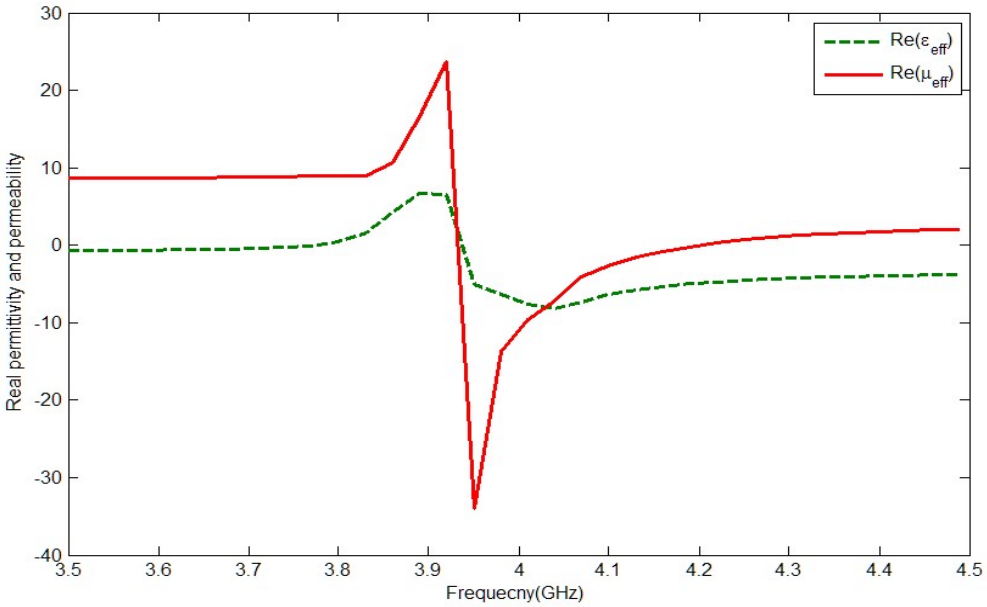

Figure 5.3 Real part of the effective permittivity and permeability of the designed SRR.

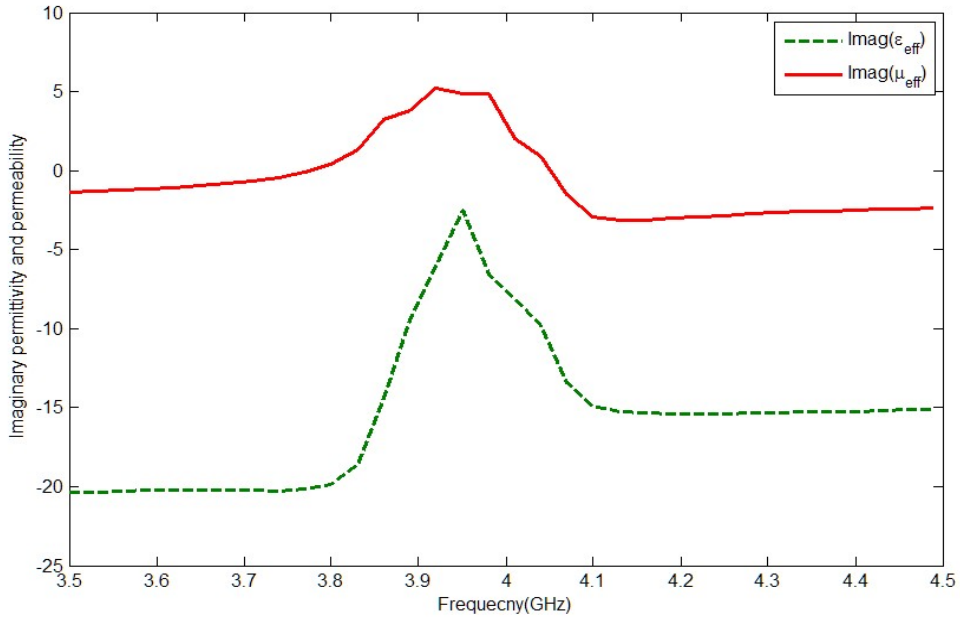

Figure 5.4: Imaginary part of effective permittivity and permeability of the designed SRR.

5.2 Magnetizing properties of embedded SRR's in a ferrite slab

This section studies the effect of the external magnetizing field on the interaction between the magnetized ferrite and the embedded SRR structures. The simulation model is created by embedding multiple SRR resonators within the ferrite material and placing them inside a rectangular WR187 waveguide. The dimensions of the waveguide (WG) and the position of the engineered ferrite material are selected to optimally excite the embedded SRR's using the magnetic field components of propagating EM wave. Figure 5.5 shows the simulated model with selected dimensions of the WG and the ferrite (NG-1850) material. Note that the cut-off frequency of the waveguide is 3.153 GHz. The simulated transmission (S21) and reflection (S11) for an un-magnetized (H_{dc}=0) ferrite material with embedded SRR are shown in Figure 5.6.

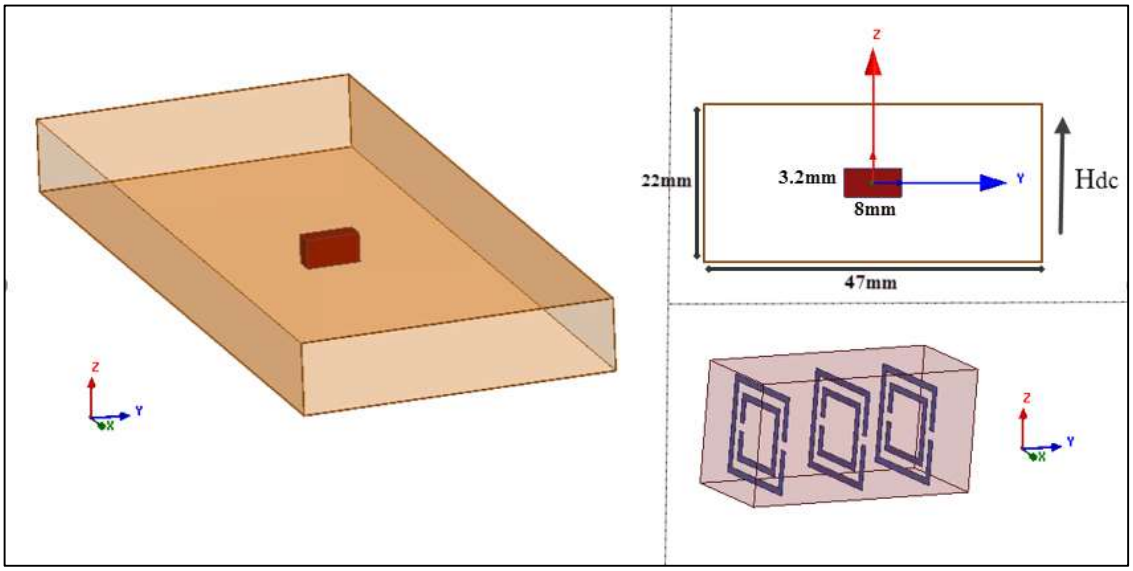

Figure 5.5: Ferrite slab with embedded SRRs inside WR187 waveguide.

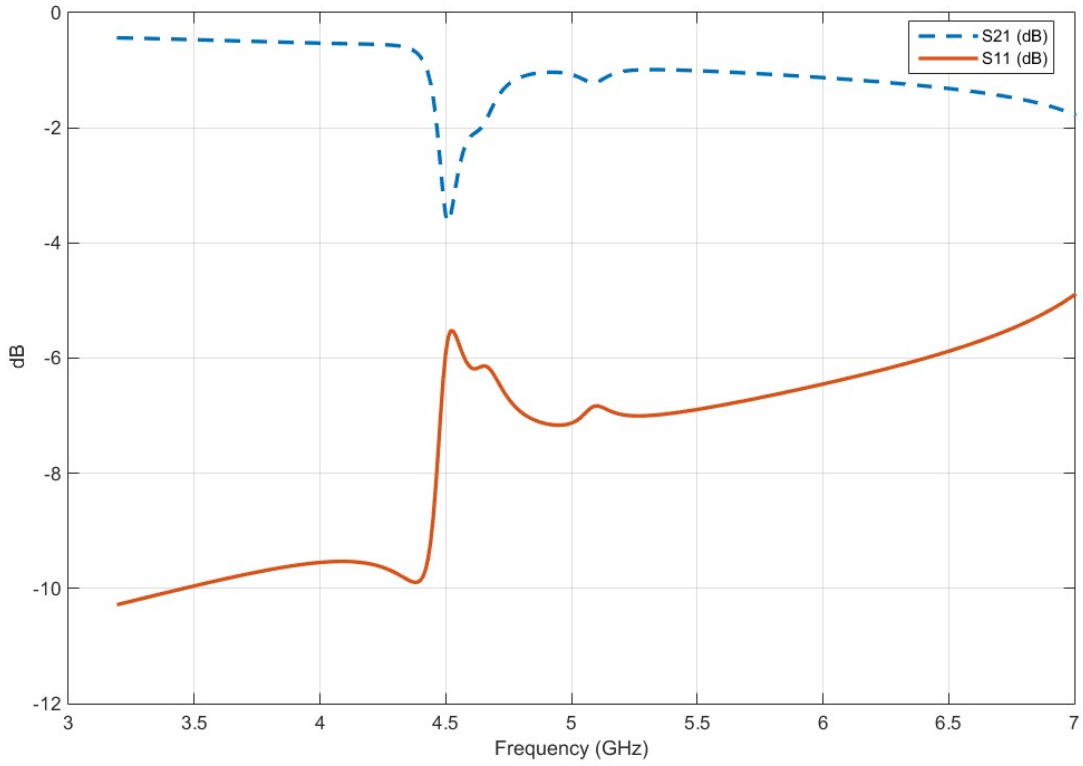

Figure 5.6: Transmission and reflection coefficients of the slab with no bias (Hex=0).

It was noted from the figure that when RF signal penetrates in the unmagnetized (H_{dc}=0) slab, the SRR embedded in the ferrite resonates at 4.5 GHz and demonstrates the highest insertion loss at the resonance frequency. Figure 5.7 shows both magnitude and vector of the magnetic field pattern of the excited SRR structures inside the ferrite with no bias. It can be noted that the magnetic field produced by the SRRs is almost perpendicular to the SRRs pattern plane and can introduce an extra magnetization field for the ferrite.

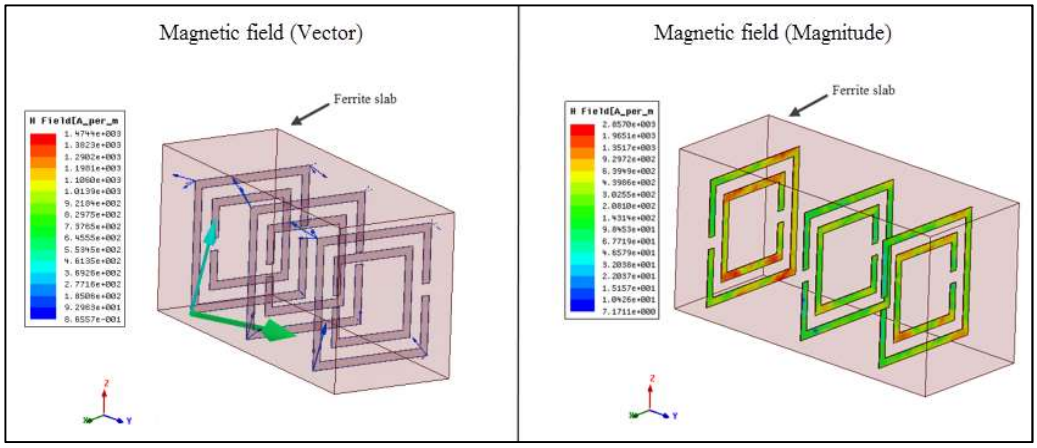

Figure 5.7 The electromagnetic excitation of embedded SRR structures with no bias.

Figure 5.8 shows the change in transmission responses of the SRR embedded ferrite material with changing values of the external magnetizing field (H_{dc}). Note that the increase in the transmission losses demonstrates an increased interaction of the SRR and propagating EM wave. This interaction depends on magnitude and direction of H_{dc}, as explained in earlier.

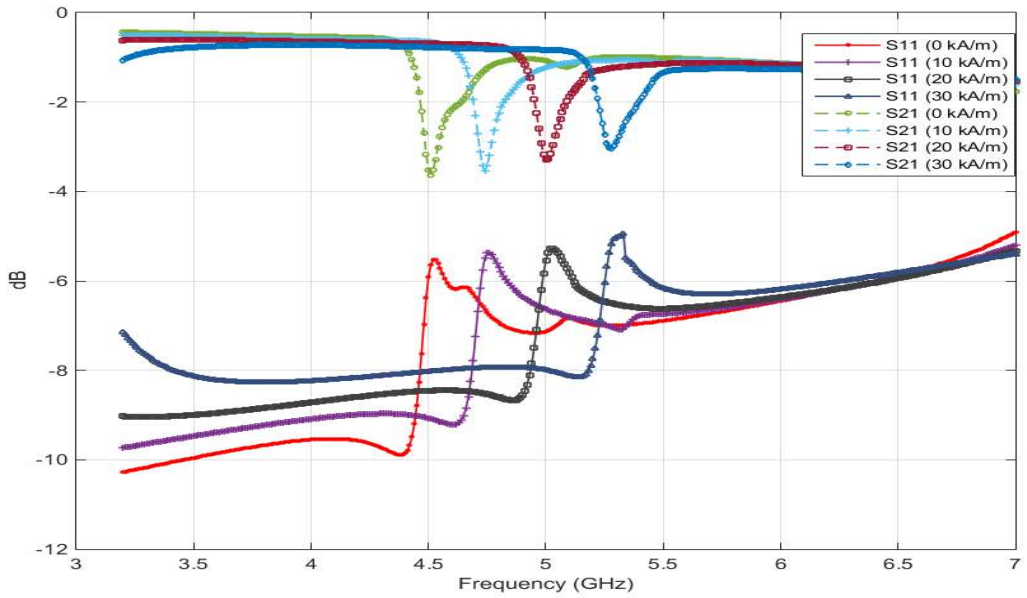

Figure 5.8 The transmission responses of SRR for changing external Magnetization (Hdc).

Thus, understanding the interaction between the magnetic field component and the magnetized SRR embedded ferrite slab is essential to optimally integrate them within the antenna substrate. The design needs to utilize the waves within the substrate to excite the SRR and reduce the external biasing requirement of the ferrite slab to achieve certain frequency tuning. In addition, SRR embedded ferrite slabs can also introduce beam steering of the patch antenna by altering the electric field and current distribution of the patch, as discussed in section 5.4.

5.3 Designing SRR composite substrate

The process of optimally integrating the SRR's within the ferrite part of the composite substrate is discussed here. Simulating software HFSS is used to optimize the location, number, orientation and dimensions of the SRR's to achieve required magnetic interaction

between the SRR embedded ferrite slabs and the magnetic field component of the wave excited underneath the patch antenna. The schematic diagram of the patch antenna, based on a SRR integrated ferrite-dielectric substrate is shown in figure 5.9. Note that only one SRR is embedded in the ferrite slabs and the orientation of the SRR structures in each slab are opposite to each other. Based on the theoretical predictions and simulated parametric study, the effect of SRR position is explained in the following section.

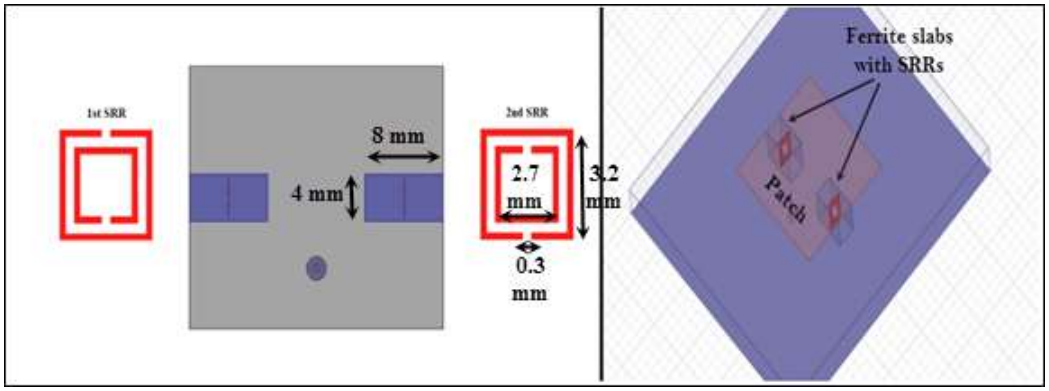

Figure 5.9 Two oppositely SRRs embedded below the patch in the ferrite slabs.

5.4 Optimizing the Position of SRR

Figure 5.10 shows the probe-fed patch antenna with SRR integrated ferrite slabs, centrally located at the non-radiating edge. The position of the SRR is varied a long distance 'd', starting from the central region of the patch towards the non-radiating edge. The simulated reflection coefficients of the antenna for different SRR positions without biasing the slabs are shown in Figure 5.11 and Figure 5.12. In both figures, the lower resonance is produced by the patch antenna (see chapter 4) and the SRR structure produces the upper resonance (see section 5.2). Note that changing 'd' mainly affects the patch resonance due to a change

of magnetic properties of the composite substrate. Embedding the SRR closer to the center of the patch produces larger reflections resulting in lower radiation efficiency.

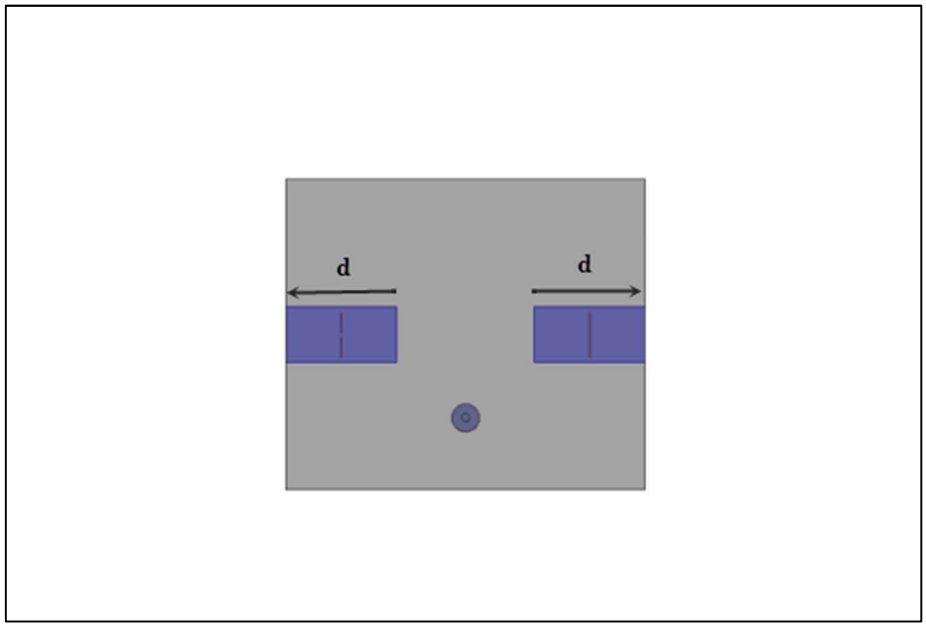

Figure 5.10: Two oppositely SRRs are embedded below the patch in the ferrite slabs.

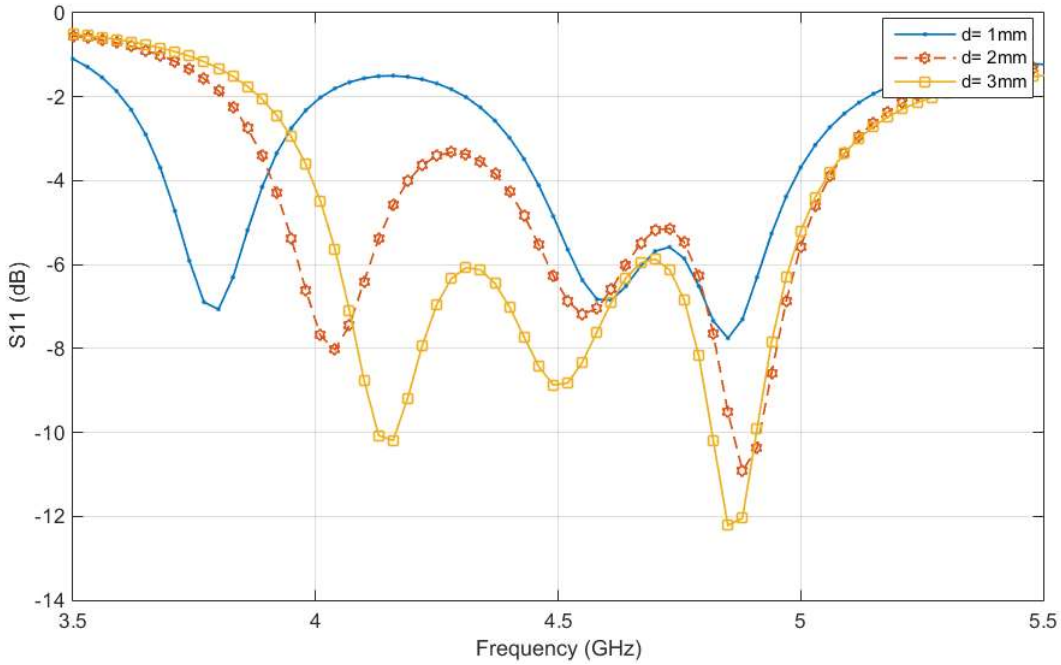

Figure 5.11 Reflection coefficient of the patch for d=1,2,3 mm (d=1mm is closest to patch center).

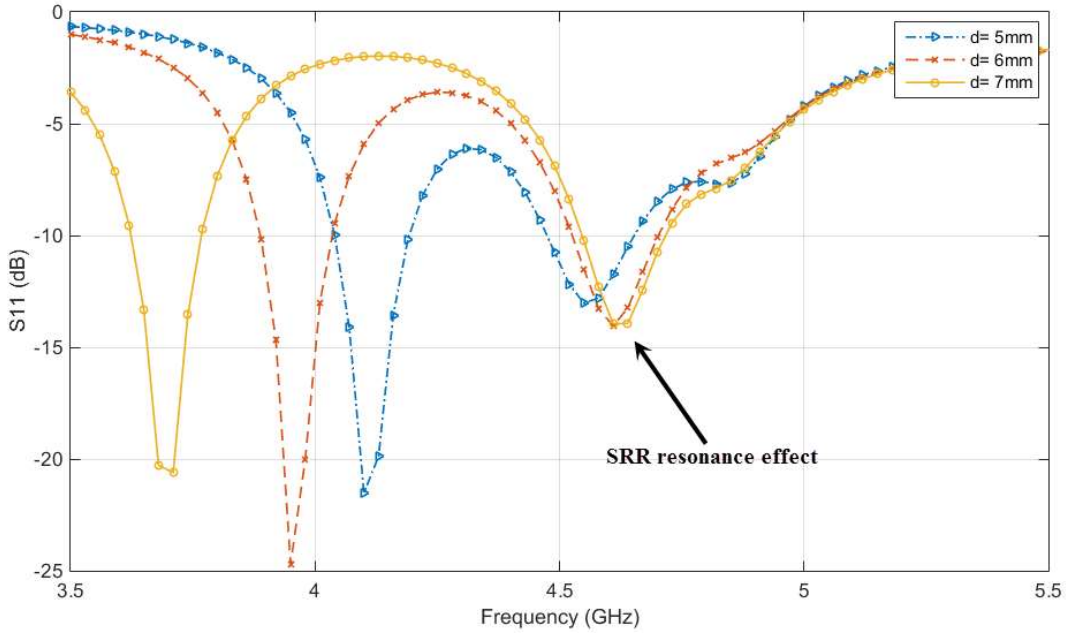

Figure 5.12 Reflection coefficient of the patch for d=5, 6 and 7 mm.

The summary of the antenna S11 responses of different SRR positions form unmagnetized ferrite (Hdc=0) is shown in Table 5.1. Note that the first resonance of the antenna when SRRs are closer to the edge of the patch (d=5mm), occurs at 4.12 GHz. By altering the position of the SRR by Δd=2mm, the 1st resonance can be tuned by Δf_{r1}=0.44 GHz, whereas the 2nd resonance remains un-tunable.

Table 5.1 Summary of antenna response for different SRR positions.

Position (d)	First Resonance	Second Resonance	Tilting - second resonance
	Frequency	Frequency	
5 mm	4.12 GHz	4.57 GHz	+15º
6mm	3.95 GHz	4.61 GHz	+15º
7mm	3.68 GHz	4.61 GHz	+20º

The radiation patterns related to the tabulated 1st and 2nd resonance frequencies of the antennas for d= 5mm are plotted in Figure 5.13. It is clear that the radiation patterns shift towards the +θ-angles for the 2nd resonance. The antenna gain related to other 'd' values are listed in Table 1.

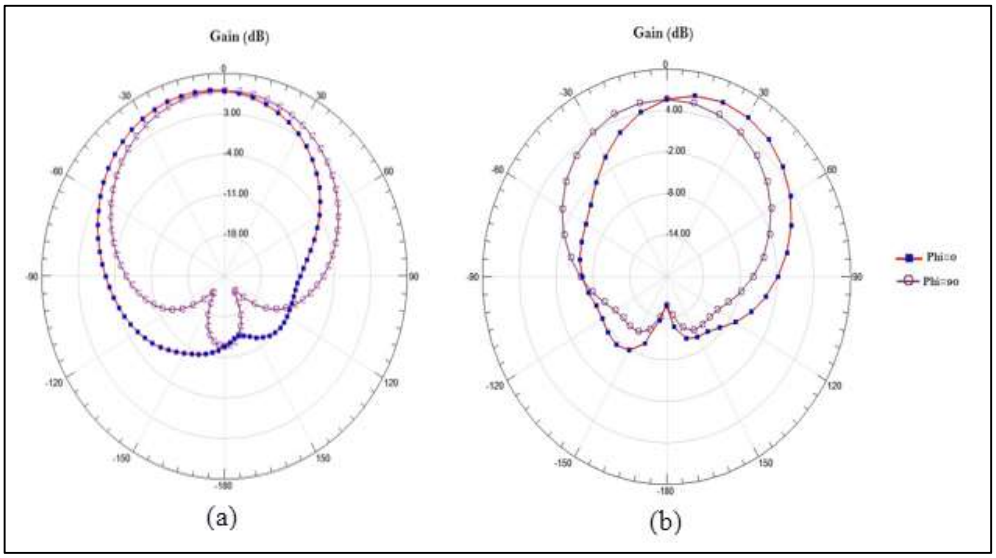

Figure 5.13 Radiation patterns of the antenna with d=5mm at (a) 4.12 GHz and (b) 4.57 GHz.

5.5 Frequency tuning properties of the antenna

To investigate how these resonance behaviors are affected by external magnetizing field, the patch antenna with SRR-integrated ferrite-dielectric substrate is magnetized. Figure 5.14 plots the tunable range of the 1st resonance of d=7mm case for changing external magnetizing field (Hdc) of the antenna. It is clear from the schematic diagram, plotted in the offset of the figure, that the SRR integrated ferrite slabs are magnetized with oppositely directed Hdc's. Note that by increasing the magnetic bias ΔHdc=0.1T (80 KA/m), the resonance frequency of the patch antenna increased from 3.68 GHz to 5.12 GHz, with a

tuning range of Δfr=1.44 GHz. Comparing this figure with Figure 4.12 of the earlier chapter, it can be concluded that integrating SRR increased the frequency tuning range by around 40%.

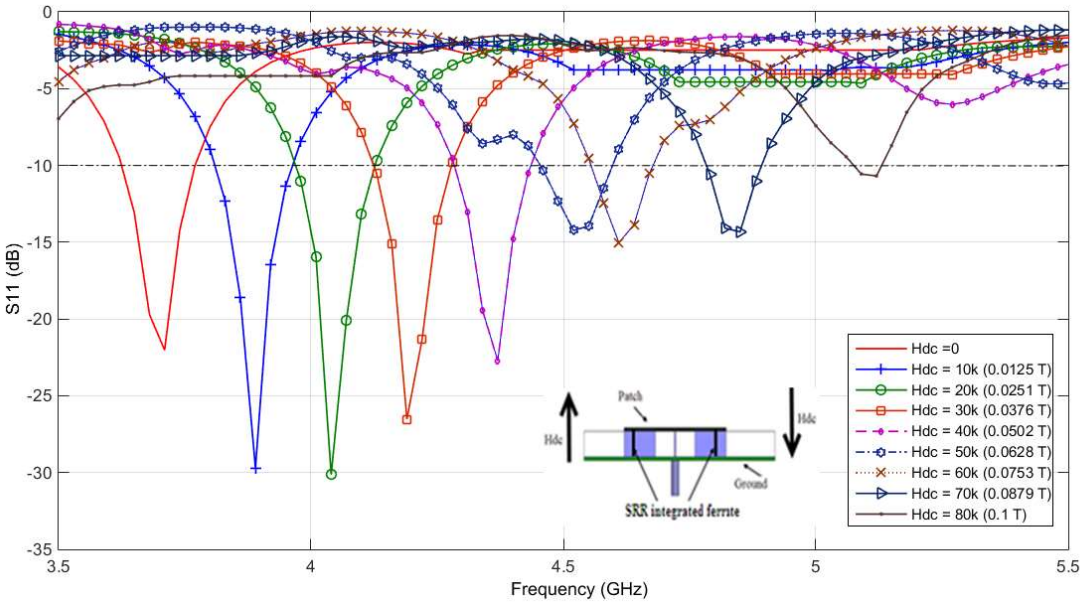

Figure 5.14 Frequency Tuning of the antenna for changing magnetizing field with d=7mm.

5.6 Beam steering properties of the antenna

To understand the beam scanning properties, Figure 5.15 plots the electric field distribution of the patch antenna with d=7mm for Hdc=0 and 0.06T (50KA/m), respectively. Note that at H_{dc}=0.06T, the direction of the main beam changes, as the excited SRR's alters the electric field distribution of the antenna. Figure 5.16 plots the simulated reflection response of the designed SRR integrated ferrite-dielectric substrate based patch antenna for two different magnetic biasing. Note that the impedance bandwidth of the antenna slightly reduces with increasing H_{dc}.

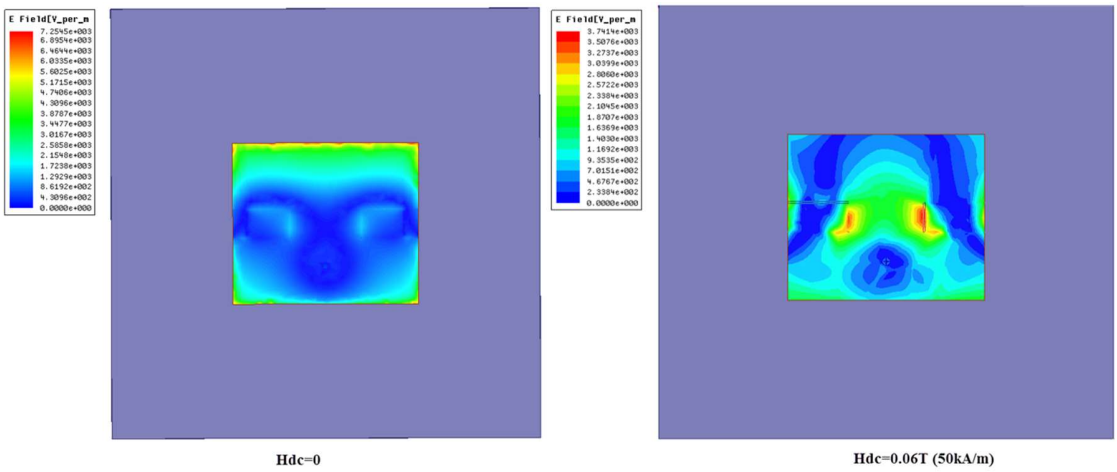

Figure 5.15 Electric field distribution of the patch for two different magnetic biasing.

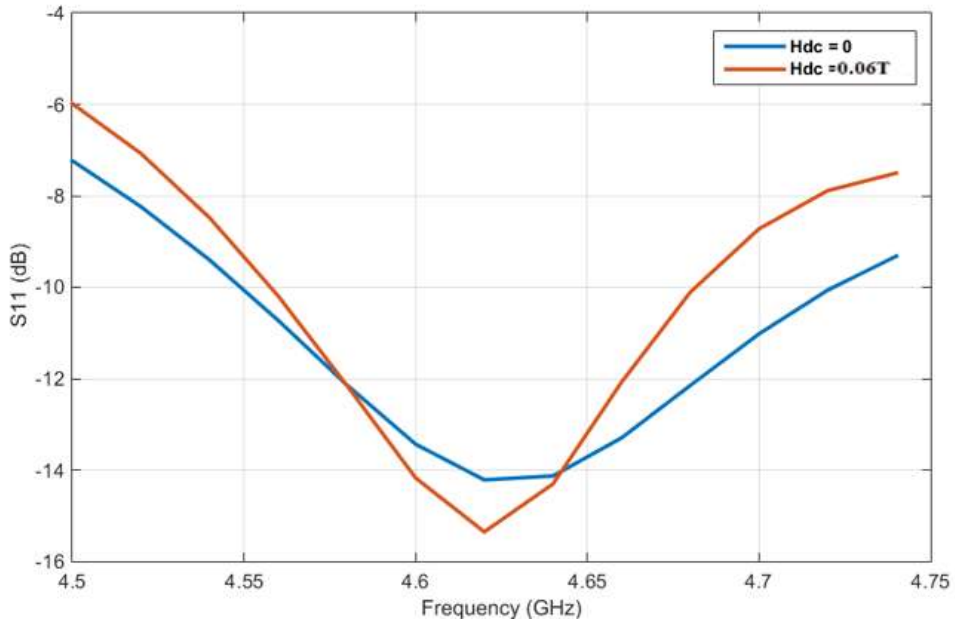

Figure 5.16 Reflection responses (S11) of the antenna (with One integrated SRR) for two values of Hdc.

The radiation pattern of the 4.61GHz antenna is plotted in figure 5.17, for two different values of H_{dc}. Note that the main beam of the antenna for no-bias (H_{DC}=0) case is steered and the maximum gain goes towards θ=+20° in the E-plane. But when HDC=0.06T are oppositely applied in both the ferrite slabs, the main beam is steered towards the broad-

side direction (θ=-5°). As expected, the gain of the antenna is compromised to facilitate the beam scanning behavior. Figure 5.18 shows the absolute radiation pattern for the two values.

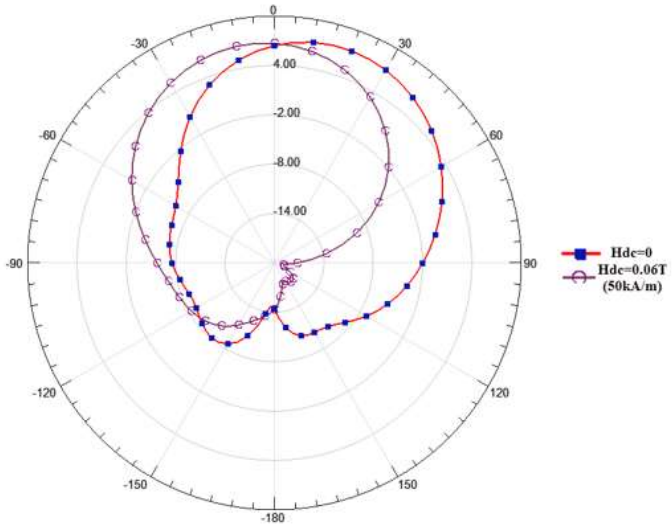

Figure 5.17 Radiation pattern of the antenna (with One integrated SRR) for two values of Hdc.

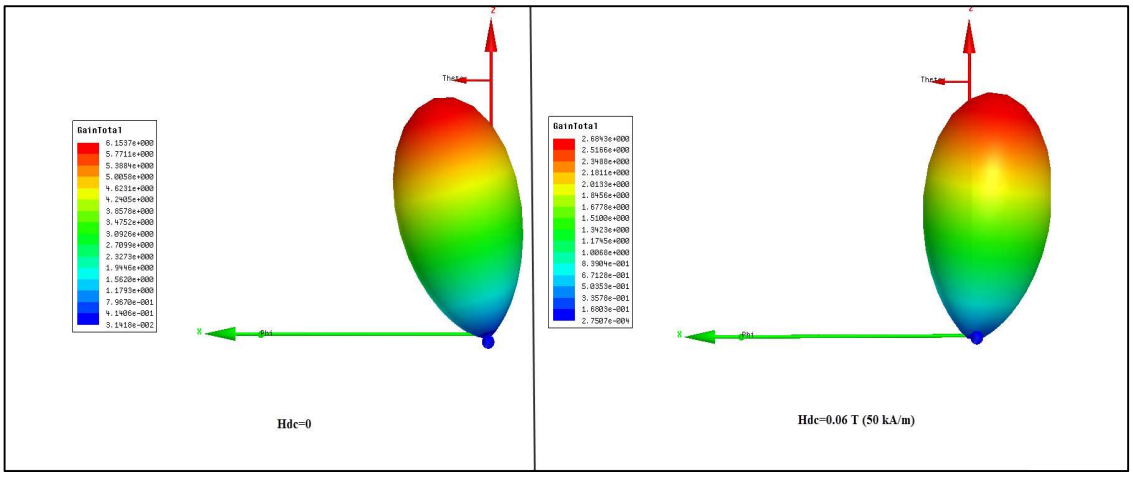

Figure 5.18 3D Radiation pattern of the antenna (with One integrated SRR) for two values of Hdc.

5.7 Antenna Resonance with Multiple SRRs

Since metamaterials are arranged in pattern configurations and usually constructed as arrays of electrically conductive elements, multiple SRRs were integrated and optimally embedded within the ferrite slab underneath the patch. The schematic diagram of the patch antenna with two embedded SRR's within the ferrite slabs are shown in Figure 5.19 The change in the reflection responses of the antenna with changing 'd' are plotted in Figure 5.20.

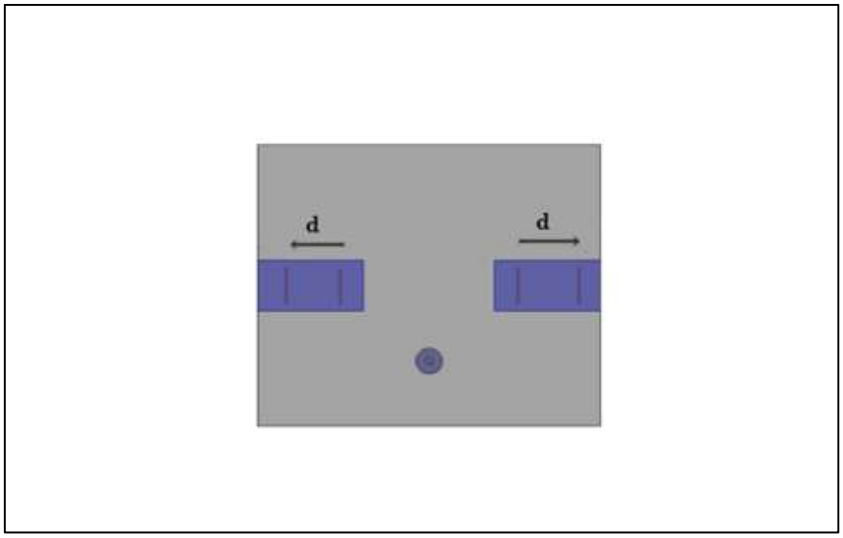

Figure 5.19 Patch antenna with two embedded SRR's within the ferrite slabs.

Note that by increasing distance ('d') between the SRR's, the frequencies of upper and lower resonance move away from each other and demonstrate larger S_{11} values indicating increased impedance mismatch.

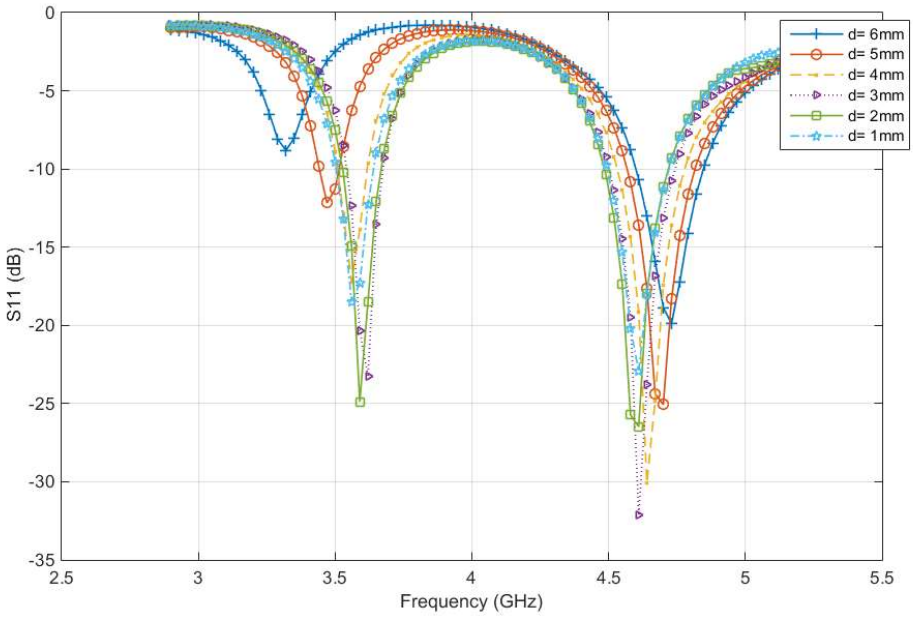

Figure 5.20 S11 for different distances between the two SRRs.

Figure 5.21 shows the radiation patterns for the maximum distance (6mm) and the minimum distance (1mm) between the two SRRs, respectively. It is clear that positioning SRR's towards the center reduces the beam scanning behavior of the antenna.

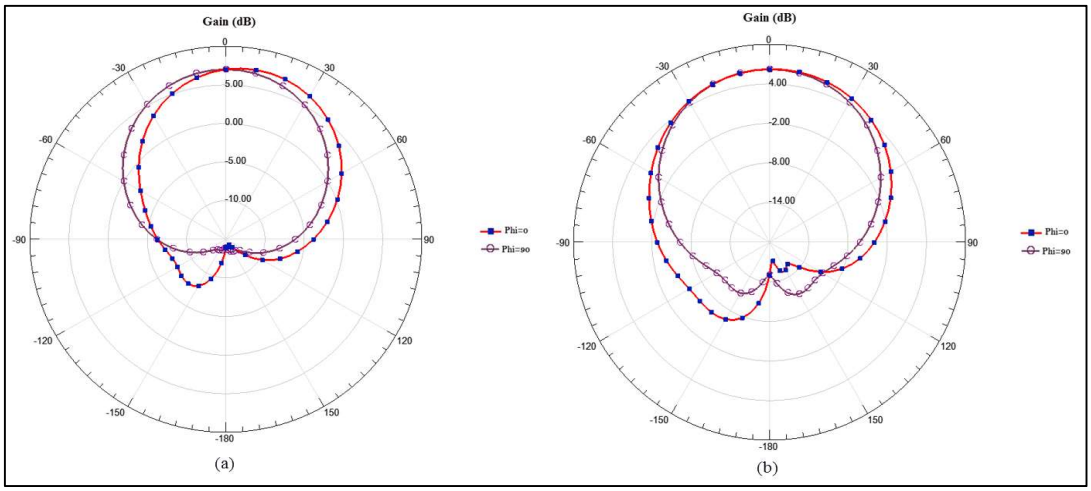

Figure 5.21 Radiation pattern of two SRR integrated antenna with (a) d= 1mm, (b) d=6mm.

The design of the patch antenna with three integrated SRR's within the ferrite slabs of the substrate is shown in Fig 5.22. The distance between the SRR structures is optimized to be 1 mm. Both reflection coefficient and radiation pattern of the un-biased (H_{dc}=0) antenna with three embedded SRRs are shown in Figures 5.23, 5.24 and 5.25, respectively. Note that compared with one SRR case, the 1st resonance of this antenna demonstrates increased beam steering for the un-bias case, whereas the 2nd resonance is associated with a broadside radiation pattern.

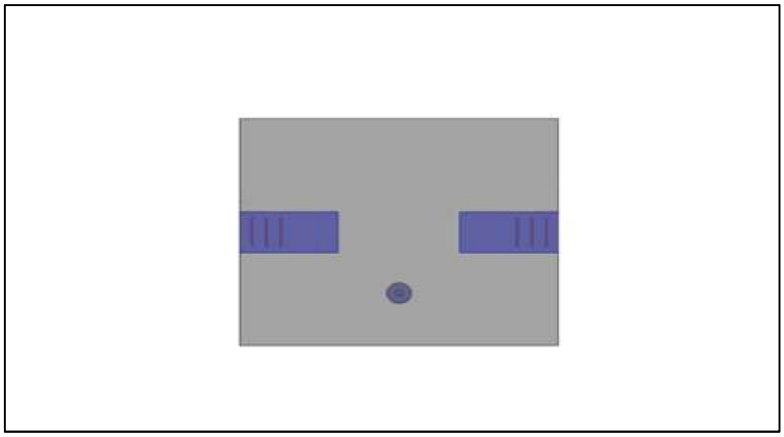

Figure 5.22 Patch antenna with three embedded SRR's within the ferrite slabs.

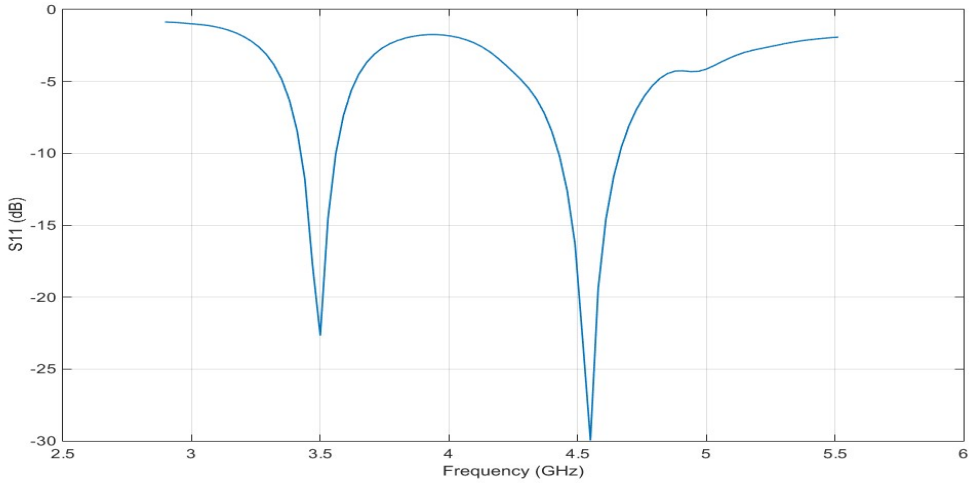

Figure 5.23 Reflection response of the antenna with three embedded SRR in the ferrite slabs.

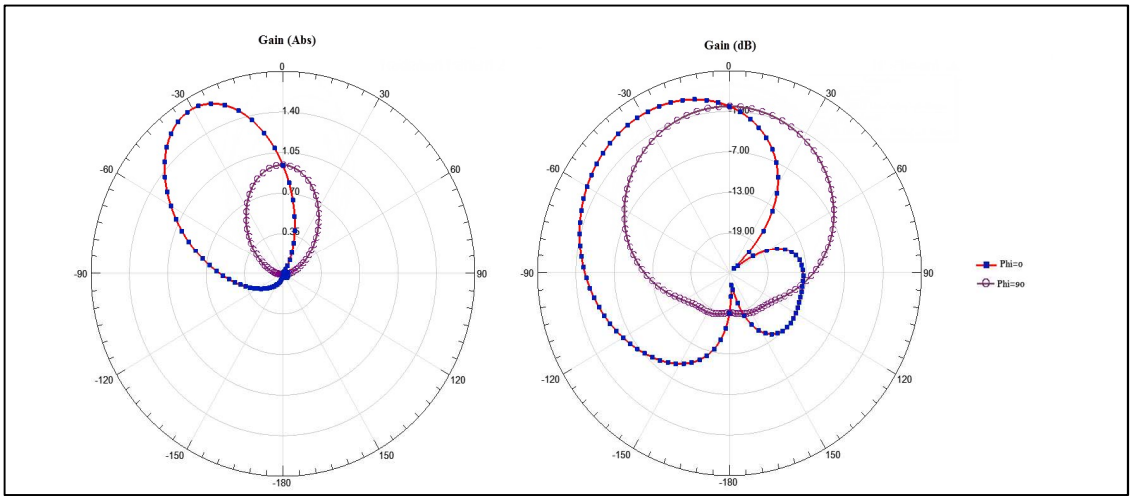

Figure 5.24 Radiation pattern at the first resonance of patch with 3 SRRs.

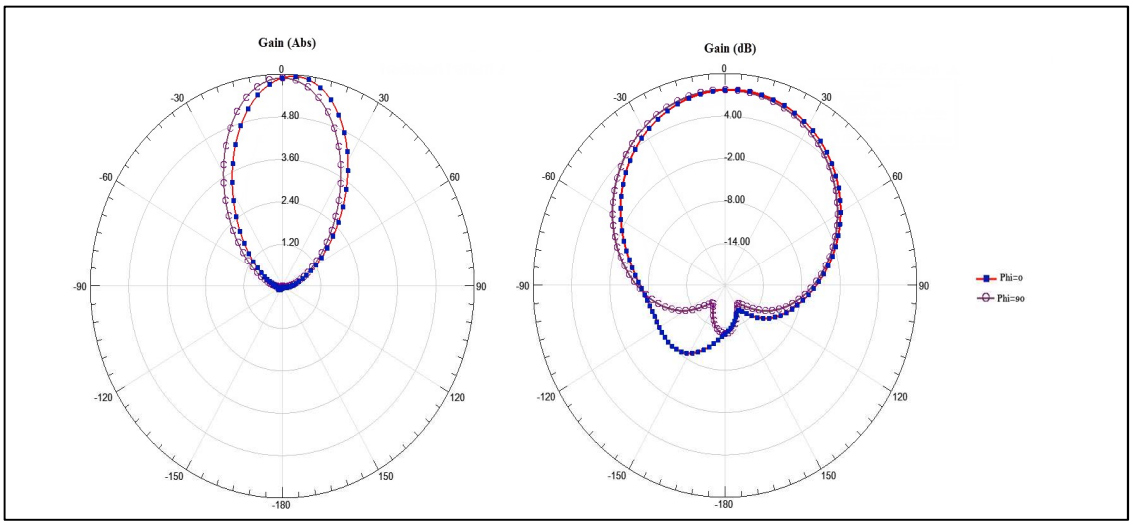

Figure 5.25 Radiation pattern at the second resonance of patch with 3 SRRs.

5.8 Design of polarization reconfigurable antenna

In this section, ferrite based microstrip patch antenna is designed with controllable polarization capability. It will be shown that by using the rod in the center of the patch, about circular polarization will be achieved and by applying different magnetic bias direction, the polarization changes between right-handed circular polarization (RHCP) and

left-handed circular polarization. On the other hand by inserting ferrite slabs, the axial ratio getting larger and the patch act as about elliptical polarized that also can be controlled by changing the magnetic bias direction.

It is known in the literature that simple patch antenna with one feed has a linear polarization. Figure 5.25 shows the axial ratio of the patch presented in chapter 3 in dB. It can be shown that at 4 GHz the axial ratio is about 57 dB which indicates that the simple patch has a linear polarization.

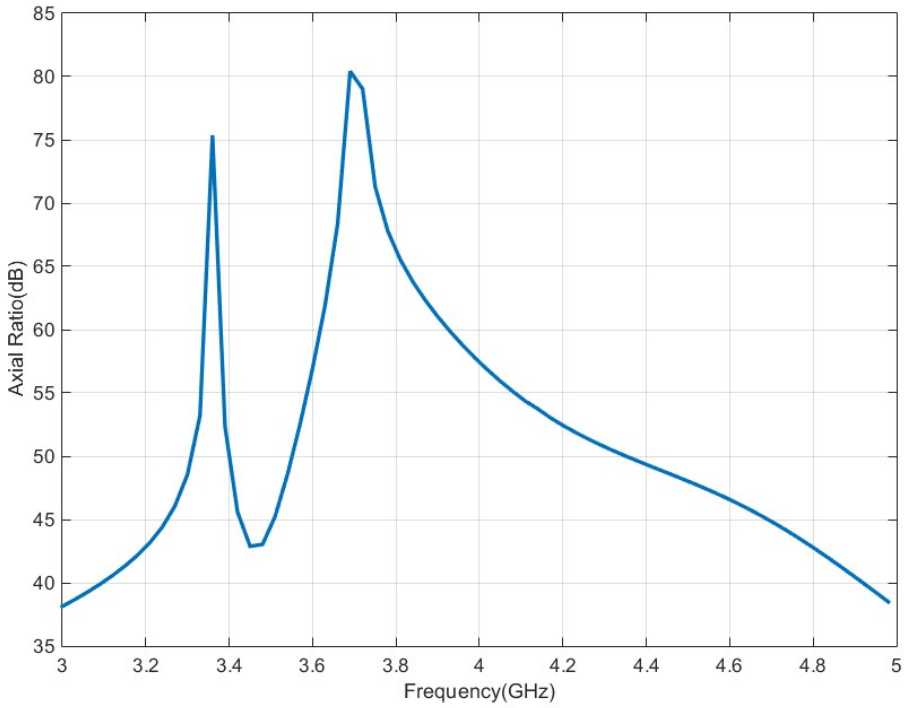

Figure 5.26 Axial ratio of simple patch antenna operating at 4 GHz.

After embedding 3mm radius YIG NG-1850 ferrite rod at the center of the patch designed previously to operate at 4 GHz as shown in Figure 5.26, and by applying a magnetic bias

in the +z direction the resonance frequency of the antenna shifted to 3.48 GHz as shown in Figure 5.27.

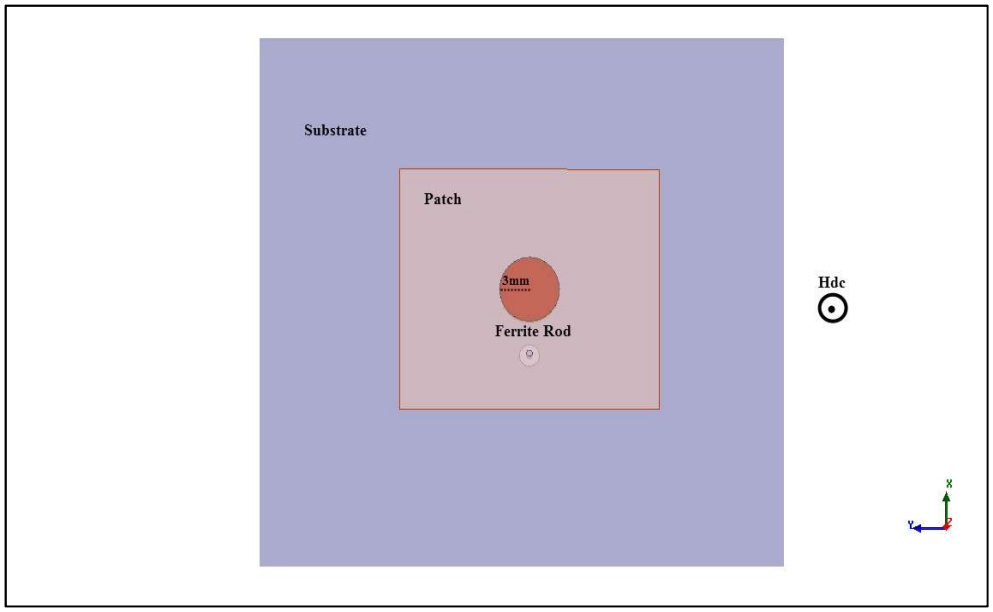

Figure 5.27 Designed Patch with embedded rod.

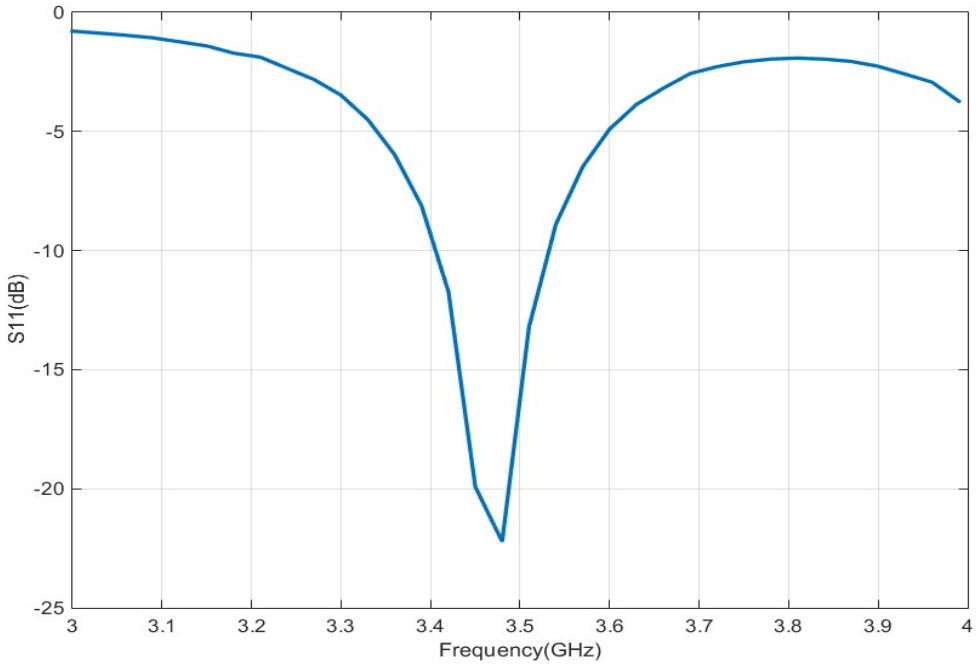

Figure 5.28 Return loss of the ferrite rod embedded antenna.

Figure 5.28 shows the axial ratio of the antenna with embedded ferrite rod; it can be shown that at 3.48 GHz, the axial ratio is 3.16 dB which indicates that the radiation of the patch is circularly polarized. Figure 5.29 shows the electric field distribution on the patch which shows that the right-handed circular polarization of the patch, by changing the direction of the magnetic bias, the patch starts to radiate LHCP as illustrated in figure 5.30.

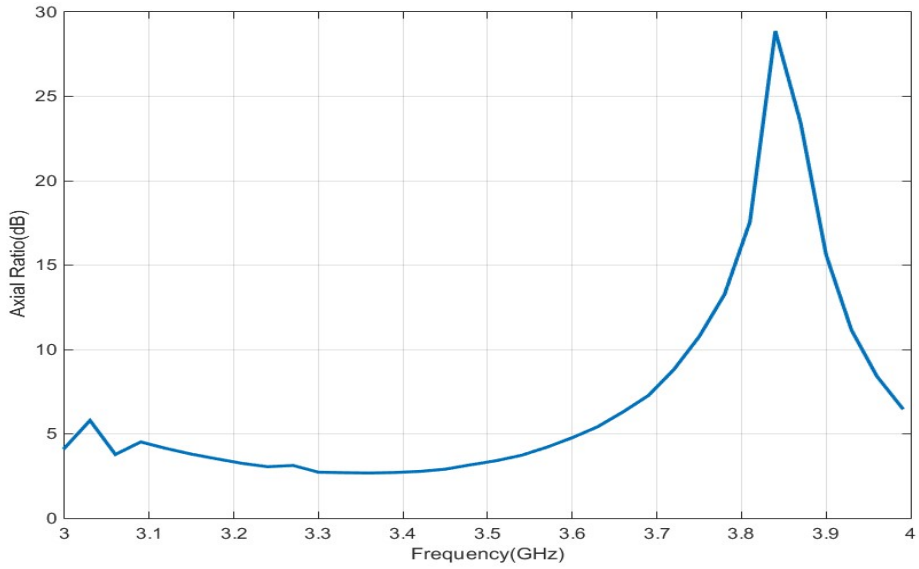

Figure 5.29 Axial Ratio of the patch with embedded ferrite rod.

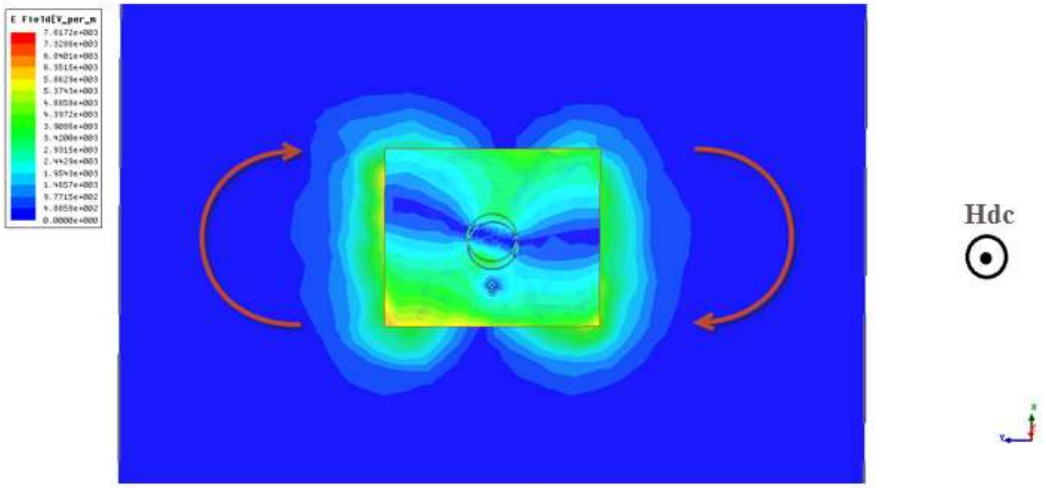

Figure 5.30 Electric field changes when Hdc in +z (RHCP).

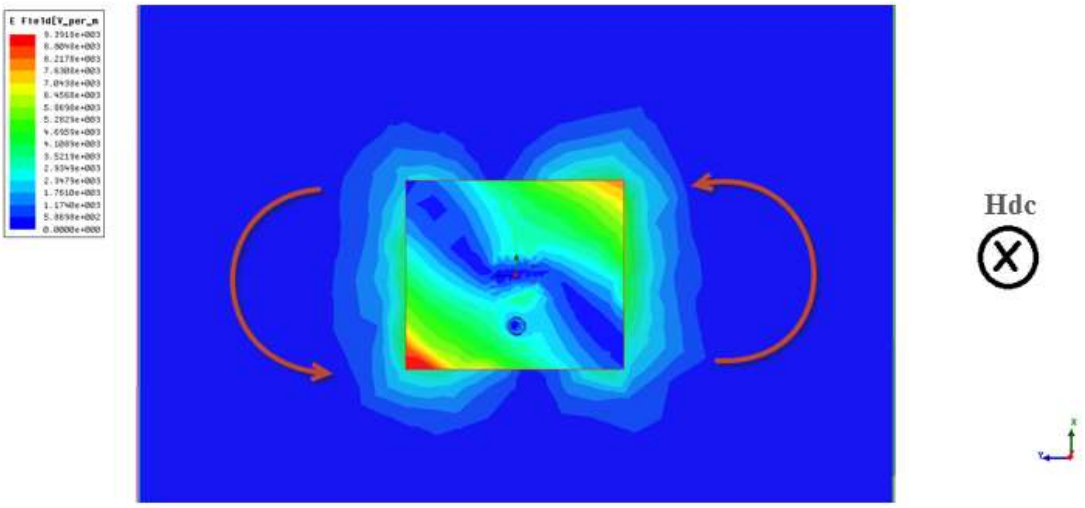

Figure 5.31 Electric field changes when Hdc in -z (LHCP).

By embedding slabs under the patch, it was noted that the axial ratio of the patch has been changed, and around elliptical polarization is achieved. Figure 5.31 shows the patch after embedding two slabs in addition to the rod; the antenna resonates at 4.48 GHz as shown in Figure 5.32.

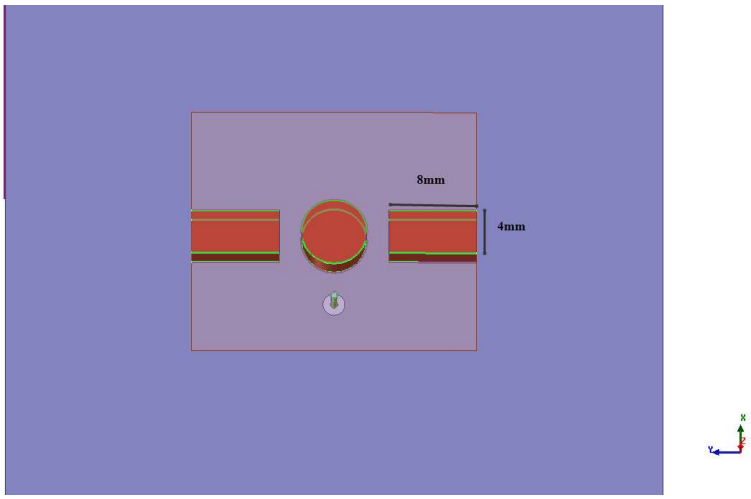

Figure 5.32 Designed patch with ferrite rod and slab embedded.

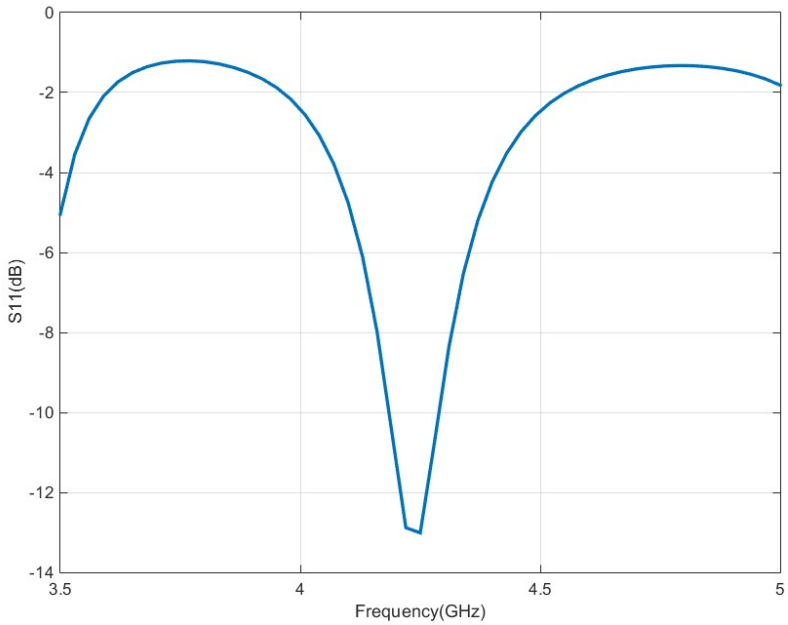

Figure 5.33 Return loss of the patch with rod and slabs embedded.

Figure 5.33 shows the axial ratio with respect to the frequency to the patch with embedded rod and slabs. It can be shown that the axial ratio at the resonance frequency has been increased and reached to 15 dB, which indicates that the antenna has elliptical polarization.

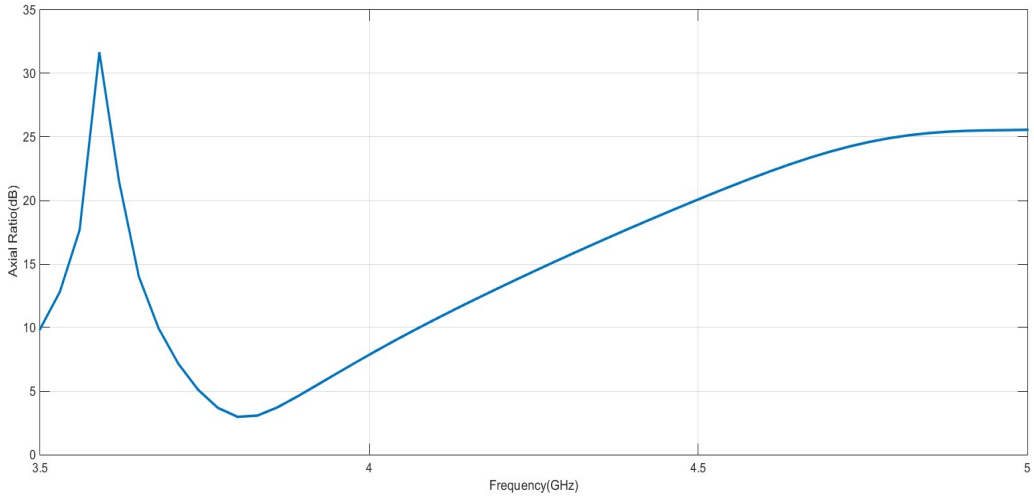

Figure 5.34 Axial Ratio of the patch with embedded ferrite rod.

By applying the external magnetization field on +z direction, it was noted that the polarization is right-handed elliptical polarization. Figure 5.34 shows the flow direction of the electric field distribution upon the patch when the applied field in +z direction. Figure 5.35 indicates that by reversing the direction of the external field, the polarization became to be left handed.

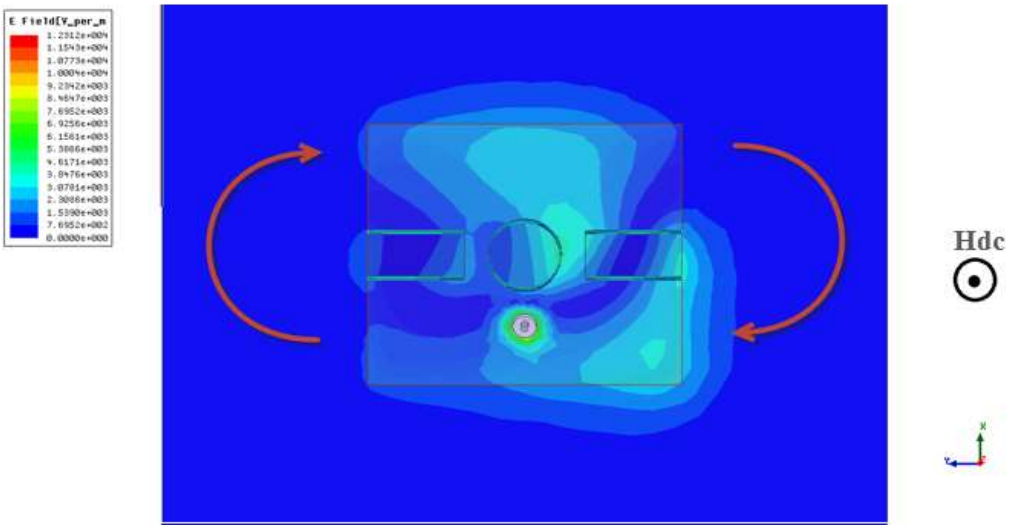

Figure 5.35 Electric field changes when Hdc in +z (Right handed elliptical).

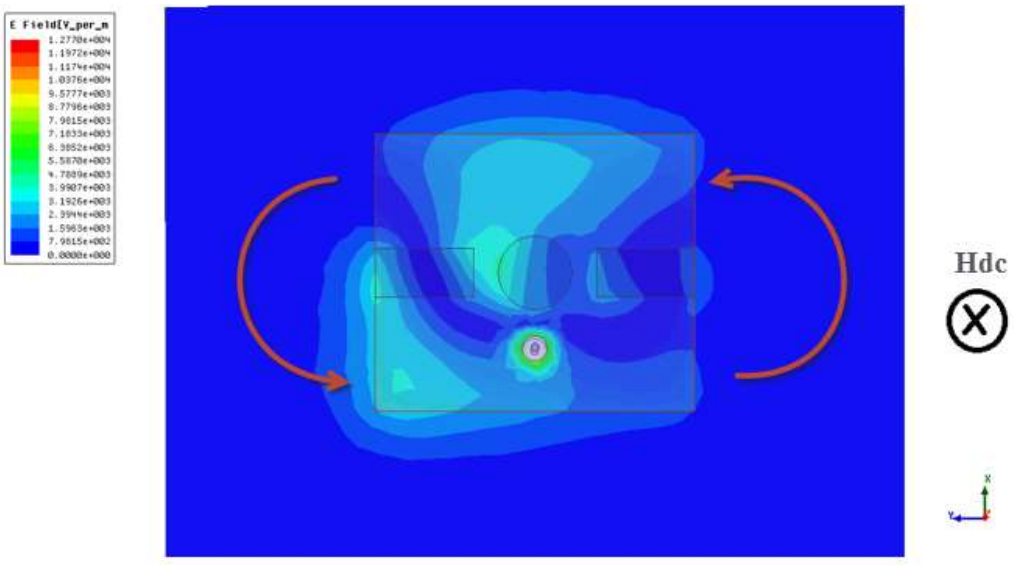

Figure 5.36 Electric field changes when Hdc in -z (Left handed elliptical).

5.9 Conclusions

Novel ferrite-metamaterial based microstrip antenna has been proposed. Split ring resonators (SRRs) have been designed with ferrite and embedded within the slabs. The transmission characteristics were studied. MATLAB was used to extract the permittivity and permeability of the SRR using theoretical approach presented in the literature.

The slabs were integrated within the dielectric substrate of the patch antenna, which increased the tuning range of the patch to reach 1.44 GHz that is forming 40% of the center frequency. This integration has also introduced beam steering of the patch, where the radiation pattern of the antenna showed 25^{o} of beam scanning of the maximum gain by applying a field of 0.062T.

Moreover, it has been shown that by integrating the ferrite within the dielectric substrate, the polarization of the antenna has been changed to elliptical, this polarization has been controlled between left-handed and right-handed by changing the direction of applied magnetic field.

CHAPTER 6

DESIGN OF 2×1 ARRAY WITH 3D SCAN CAPABILITY

A 2x1 linear array of microstrip antennas on with SRR integrated ferrite-dielectric substrate is designed to introduce three-dimensional (3D) beam scanning. Typical phased array technique is used to steer the main beam in the H-plane (y-axis), whereas external magnetic biasing field is used to steer the main beam in E-plane (x-axis). The simulated radiation patterns are presented to demonstrated 3D scan capability.

6.1 Design of 2×1 array on ferrite-dielectric substrate

Initially, a 2x1 array is designed using the coaxial fed patch on a ferrite-dielectric substrate with no integrated SRR. Figure 6.1 shows the linear phased array antenna with center to center separation distance of λ/2. The position and dimensions are optimized to achieved a required resonance frequency and radiation properties.

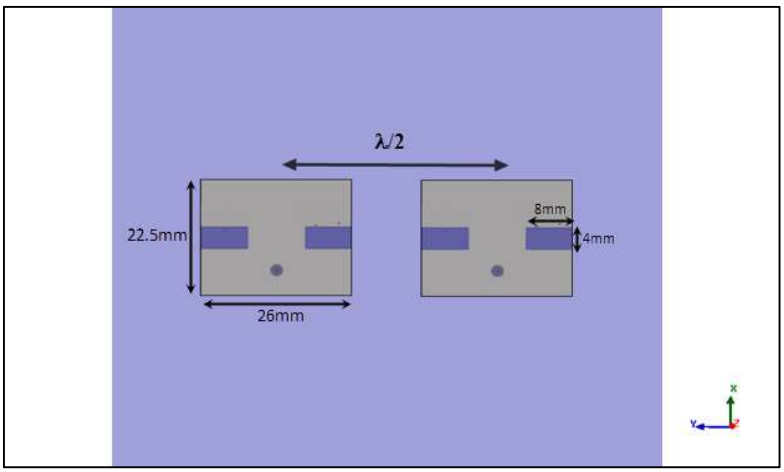

Figure 6.1 Schematic diagram of the 2x1 microstrip array with SRR embedded ferrite slabs.

The simulated reflection coefficient of the array antenna is shown in Figure 6.2. Note that the array antenna resonates at 4.1 GHz with -10 dB impedance bandwidth of 175 MHz. Figure 6.3 shows the E and H-plane radiation patterns of the 4.1 GHz array for the un-biased (H_{dc}) case and having equivalent patch excitation signals.

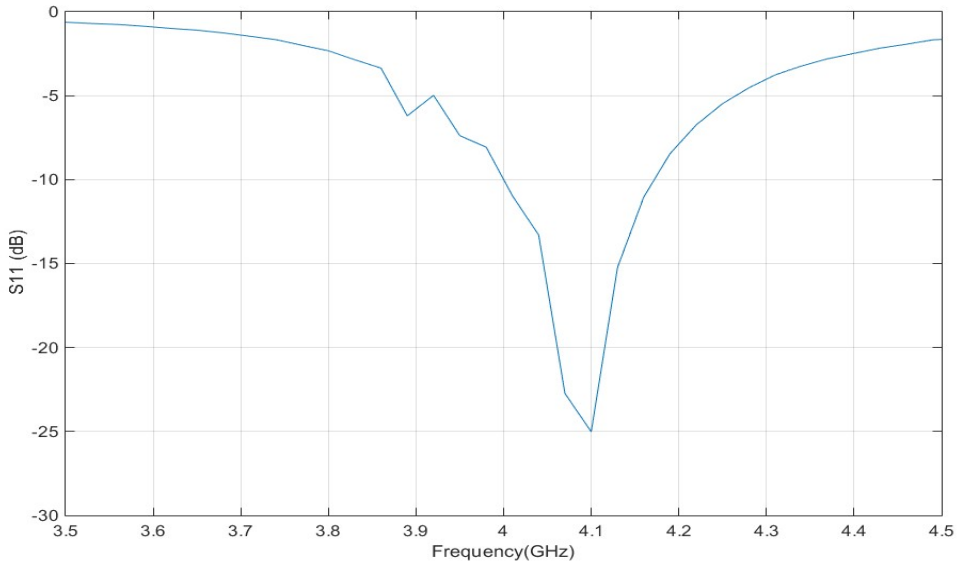

Figure 6.2 The Simulated reflection response of the 2x1 line phased array.

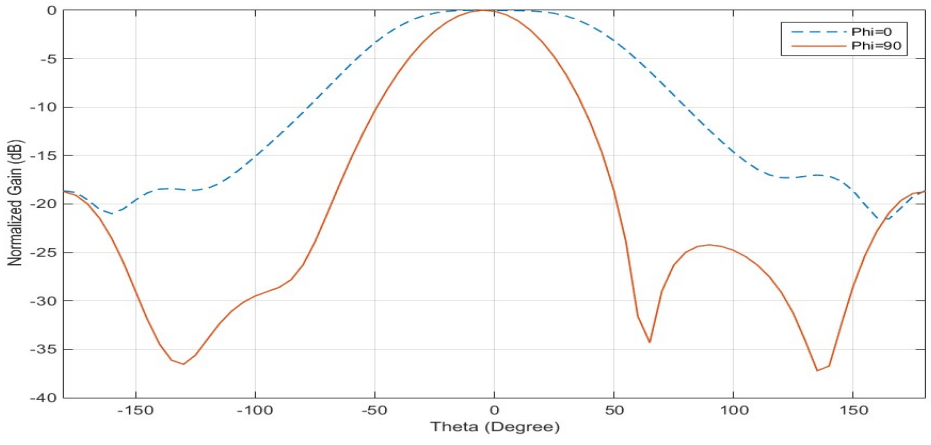

Figure 6.3 E and H-plane radiation patterns of the array when Hdc=0.

6.2 Design of SRR integrated array antenna

SRR elements were embedded within each ferrite slab at distance of 2 mm from the edge of the patch antenna. The 2x1 array antenna with integrated SRR's is shown in Figure 6.4. The dimensions and integration process of SRR elements remained similar to that explained in chapter 5.

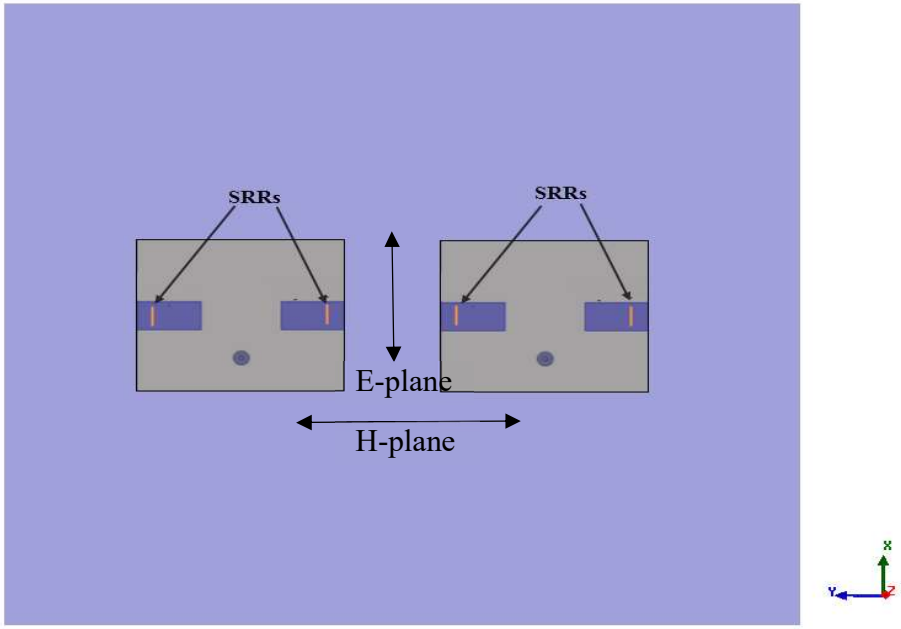

Figure 6.4 The designed 2x1 microstrip array with SRR's embedded in the ferrite slabs.

For uniform excitation signals of the patch elements (β=0), the reflection response of the array is shown in Figure 6.5 for un-biased (H_{dc}=0) ferrite material. The impedance bandwidth of the two resonance frequencies at 3.89 GHz and 4.46 GHz is 120 MHz. The normalized radiation patterns relate to the 1st and 2nd resonance is plotted in Figures 6.6 and 6.7. Note that at 3.89 GHz, the array beam demonstrated no tilting in H-plane (at

phi=90), but 30° tilting in the E-plane (phi=0). Similarly, at 4.46 GHz, the array beam demonstrated no tilting in H-plane (at phi=90), but -40° tilting in the E-plane (phi=0). As demonstrated in chapter 5, applying appropriate Hdc can steer the tilted main beam in H-plane.

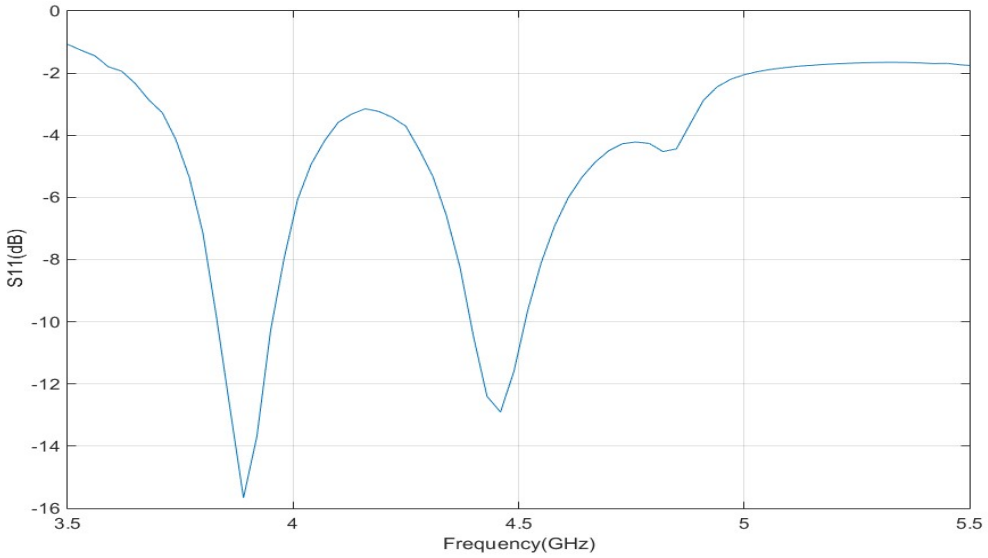

Figure 6.5 Reflection response of the 2x1 array with embedded SRR's with ferrite slabs.

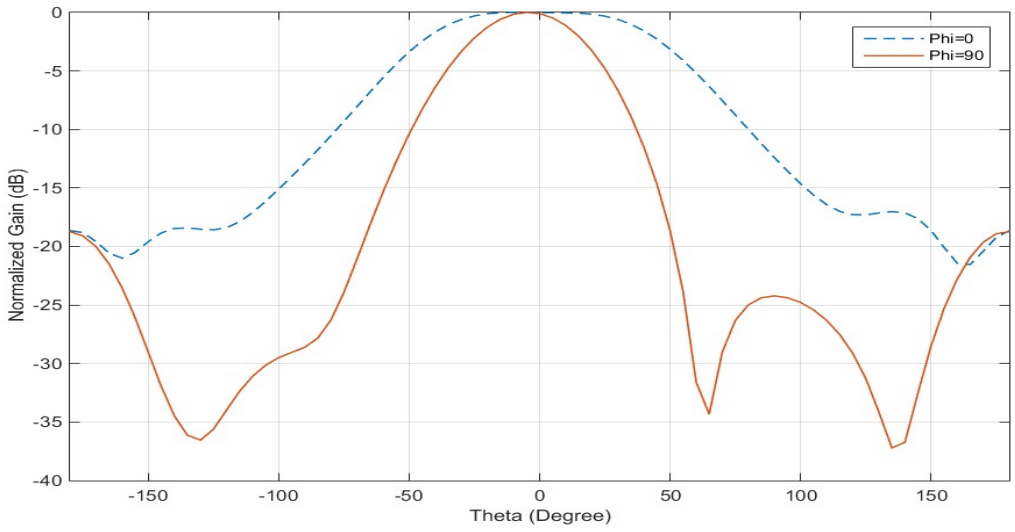

Figure 6.6 Radiation pattern of the SRR integrated array at 3.89 GHz (1st resonance).

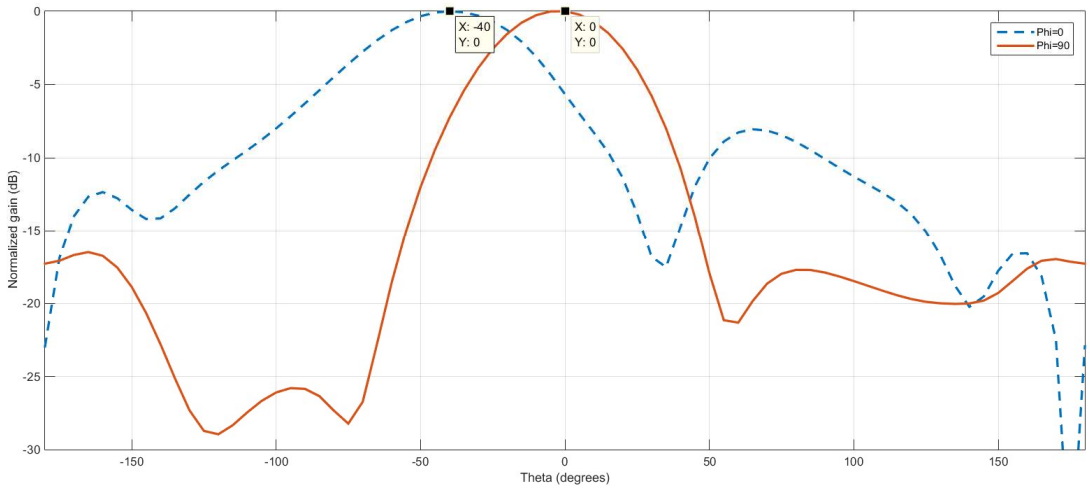

Figure 6.7 Radiation pattern of the SRR integrated array at 4.46 GHz (2nd resonance).

6.3 3D beam scan of SRR integrated 2×1 microstrip array

In order to achieve three-dimensional (3D) beam scan, the radiation pattern needs to demonstrate beam steering in both the H-plane (at phi=90) and the E-plane (phi=0) of the array antenna. It is already shown that optimally applied external magnetizing field allows beam steering in the E-plane (phi=0), whereas traditional phase array technique can be used to steer the main beam in the H-plane (at phi=90). In Figure 6.7, it was shown that embedding the SRR's within the non-magnetized (Hdc=0) ferrite slabs and uniformly (β=0) exciting the patch elements tilts the E-plane (phi=0) pattern by θ=-40 degrees. Figure 6.8 demonstrates that by magnetizing the ferrite slabs with the oppositely directed external magnetic field of HDC=0.065T, the main beam of the antenna is steered in the E-plane towards θ =-25 degrees. Note that this process has a minor effect on the H-plane direction of the main beam, which can be neglected or later corrected by exciting the patch elements with progressively phased (β) signals. To demonstrate beam steering in H-plane, the patch

elements of the array is excited by signals with a progressive phase shift of β=0º, 30º and 60º. Figure 6.9 shows the beam steering in H-plane due to different values of the β.

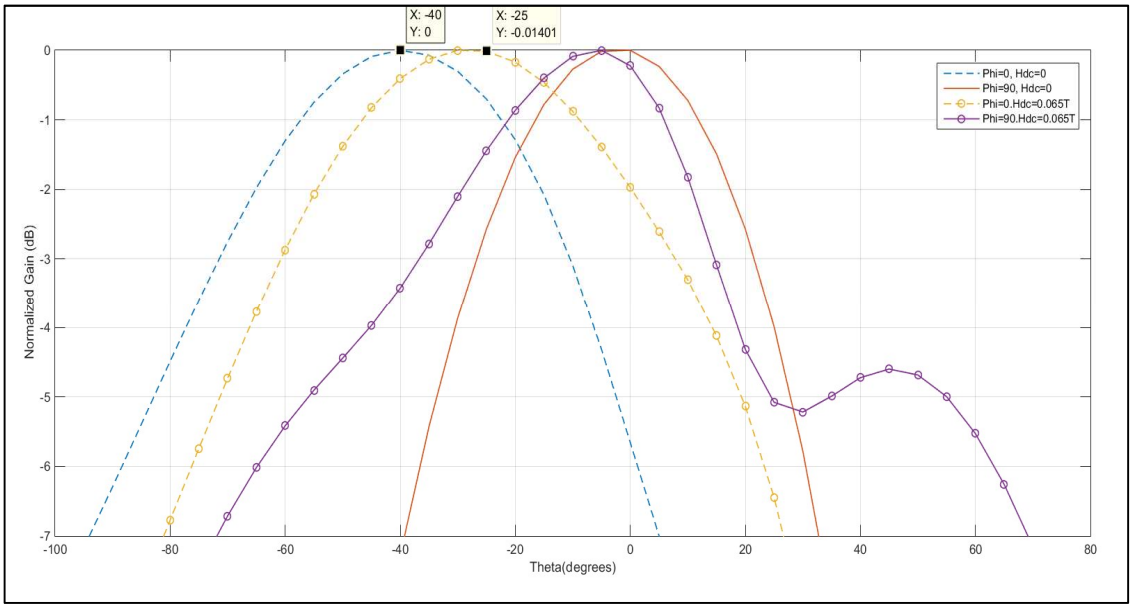

Figure 6.8 Radiation pattern of the uniformly excited array with changing the magnetic bias (Hdc).

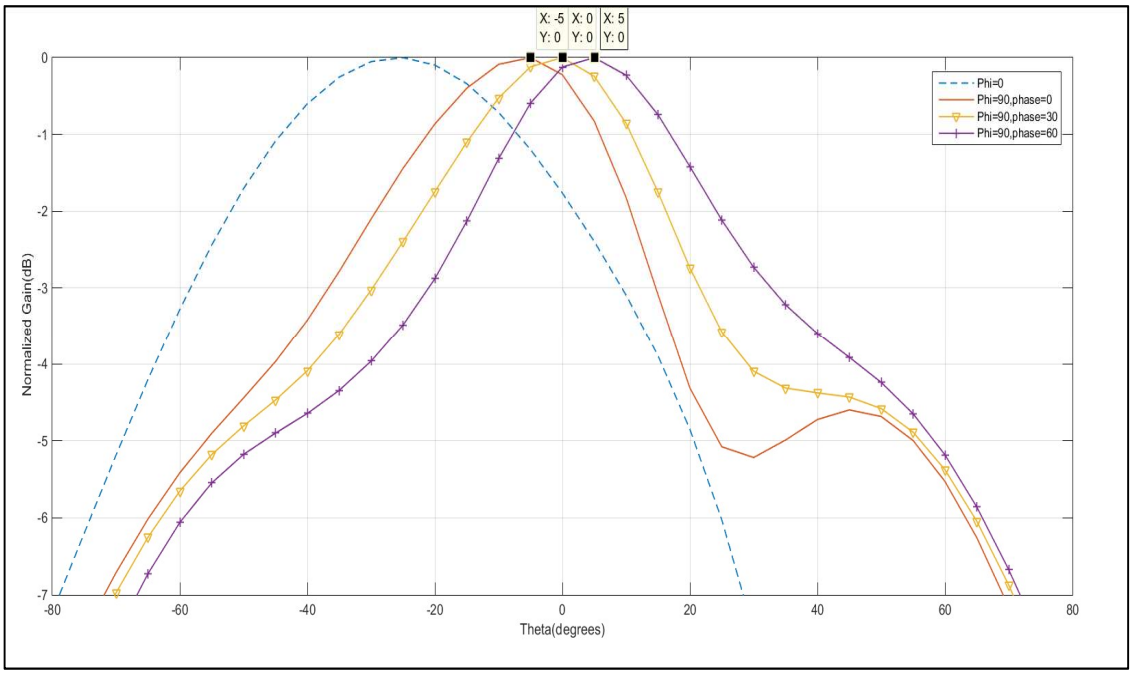

Figure 6.9 Radiation pattern of non-magnetized and non-uniformly excited array with β= 0º, 30º and 60º.

It clear from above section that 3D beam scan requires beam steering in both E and H-planes. Thus to achieve 3D beam steering, the SRR integrated ferrite slabs needed to be magnetized in addition to exciting the patch elements with progressively phased signals. Figure 6.10 shows a schematic figure where the main beam of the antenna is directed towards (ϕ,θ)=5°, -25°. Note that the main beam of the uniformly excited array antenna with θ=-25° in E-plane is achieved by properly applying an HDC=0.062T. Now, introducing progressive phase shift (β) in the excitation signal of the array elements, this beam is steered towards ϕ=5°.

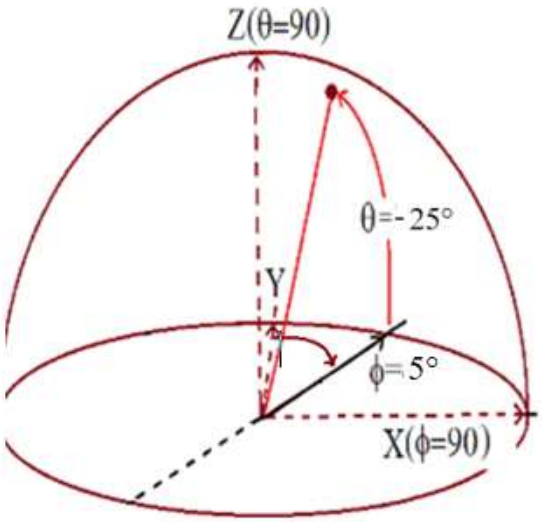

Figure 6.10 Schematic diagram of 3D steering towards ϕ=5° and θ=-25° for HDC=0.062 T and β=60°.

6.4 Conclusions

This chapter has introduced a design of ferrite-SRR based microstrip antenna array with 3D scan capability. The design consists of 2×1 microstrip patch elements that have the ability to scan in both E and H planes. It was shown that by integrating the SRR within the slabs the radiation pattern of the array showed tilting in the E-plane. By applying 0.062T of external magnetic field, the beam was steered by 15^{o}. Additionally, by changing the progressive phase shift of radiating patches by 90^{o} the array showed a tilting to 10^{o} in the H-plane. So by controlling both external magnetic bias and progressive phase shift, 3D scan can be achieved.

CHAPTER 7

EXPIREMENTAL RESULTS

This chapter presents the process involved in fabricating the prototype and experimentally validating the simulated results. The facilities available in the electrical engineering department in KFUPM are used to fabricate the SRR embedded ferrite slabs and integrate them within the antenna substrate. Vector network analyzer is used to experimentally observe the scattering parameters, and flatbed antenna radiation pattern measurement device is used to observe the radiation patterns of the antenna prototype.

7.1 Fabrication process

The optimized patch antenna is initially fabricated using LPKF ProtoMat E33 circuit board plotter. This machine is capable of fabricating single and double sided printed circuit boards with a minimum 2mm clearance between the tracks. Figure 7.1(a) shows one of the LPKF machine located in the PCB lab. The plotter can be controlled using a software called "Circuit-Pro". This software is a powerful tool that allows creating and editing the PCB layout, in addition to controlling the machine operation. The fabrication process starts by exporting the CAD HFSS and converting it into compatible CirciuitPro file as shown in Fig.7.1(b).

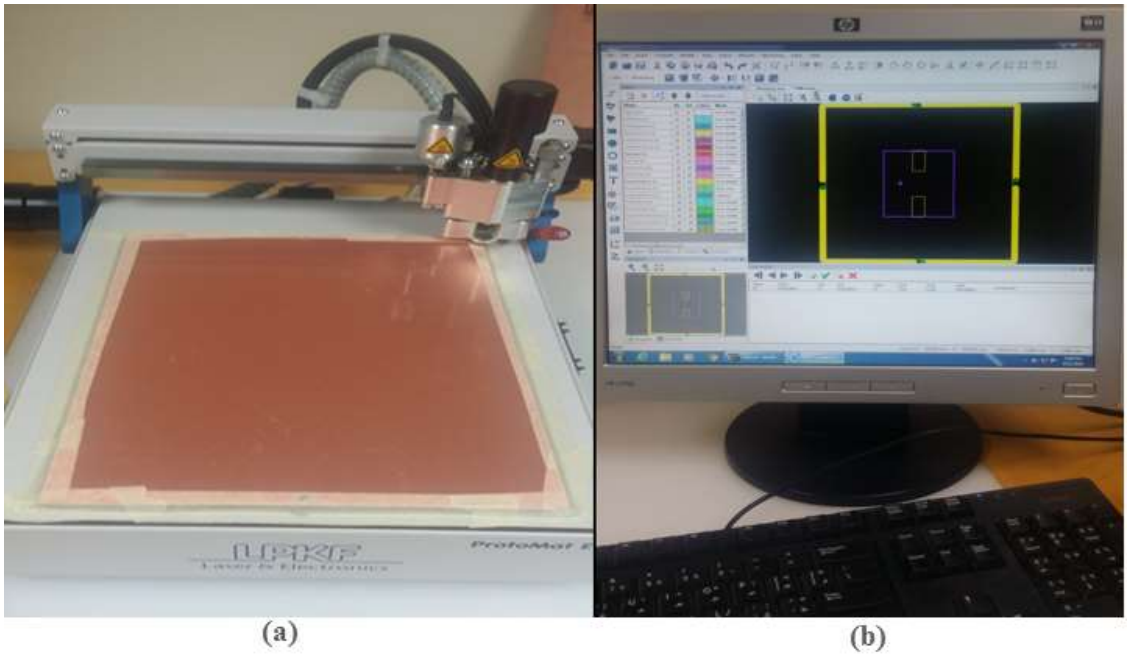

Figure 7.1 PCB plotter (a) LPKF Protomat E33, (b) CircuitPro software.

In the software, different layers are assigned to the patch and the ground plane. Milling and drilling dimensions and locations are imported from the CAD (HFSS). This allowes an accurate fabrication of the patch antenna excited with a coaxial feed. The slots required to integrated the SRR embedded ferrite slabs are also drilled underneath the patch antenna. Figure 7.2 shows the patch antenna on a Roger 5880 substrate with dielectric constant of 2.2 and height of 3.18mm. Note that Figure 7.2(a) shows the rectangular holes drilled to insert the SRR embedded ferrite slabs, which are shown separately. Figure 7.2(b) shows the antenna with integrated ferrite slabs. Copper tapes are used to cover the ferrite portion of the radiating patch and ground plane, as shown in Figure 7.3. A metal press available in the fabrication lab is used to correct the misalignment between the ferrite slabs and substrate heights.

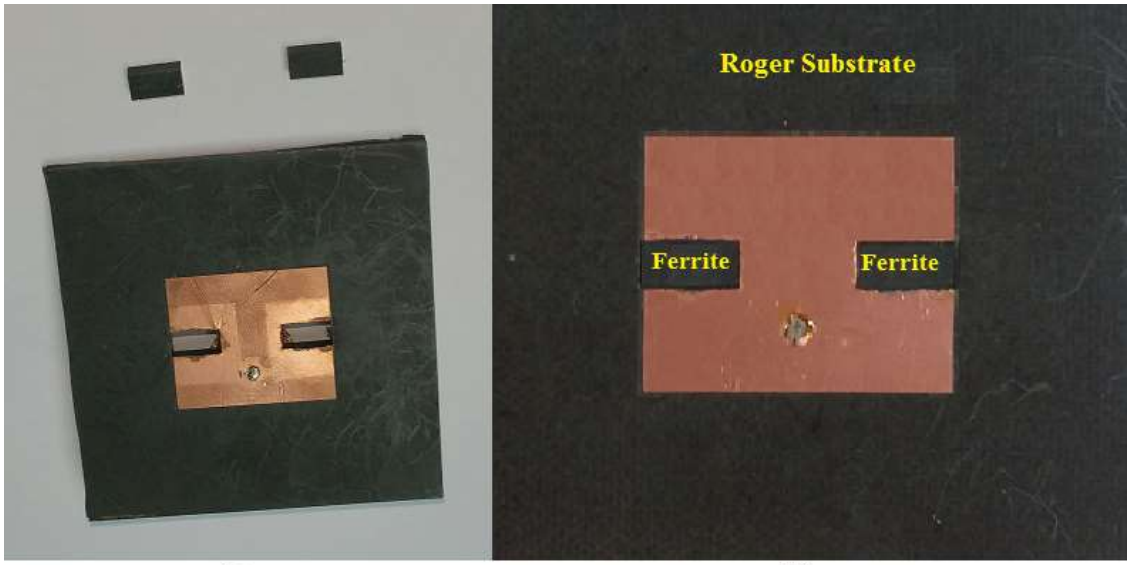

Figure 7.2 The fabricated antenna.

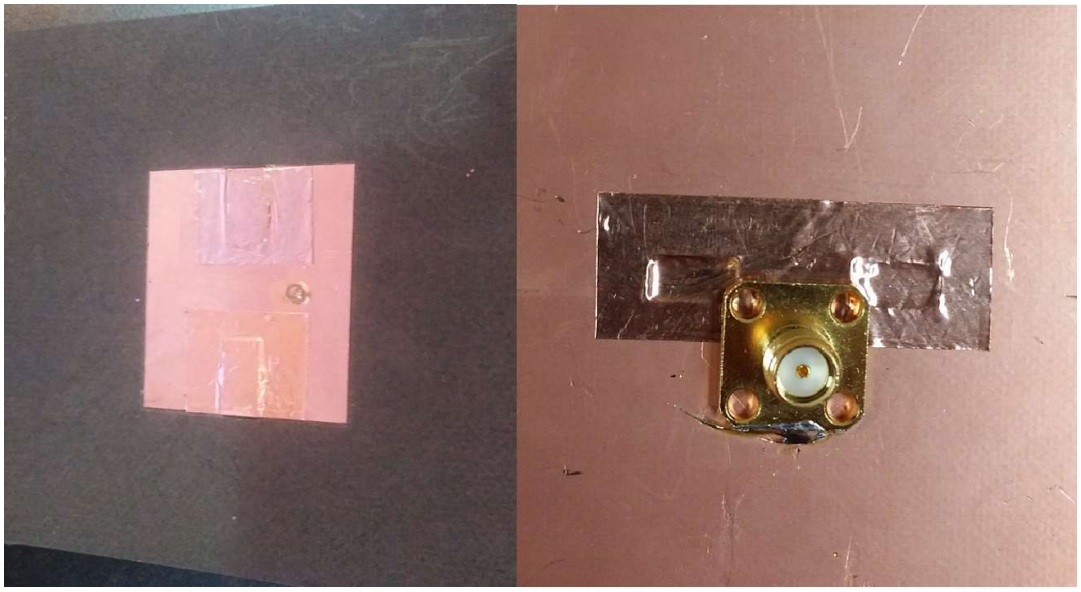

Figure 7.3 Front and back picture of the fabricated antenna.

7.2 Measurement setup

7.2.1 S-parameters measurements

Keysight Agilent E5071C network analyzer, available in Microwave Lab of KFUPM, is used to measure the reflection coefficient of the antenna. This two-port vector network analyzer, shown in Figure 7.4, has a frequency range of 20 GHz and measurement speed of 9 msec [71]. It is extensively used to measure the reflection and transmission characteristics of both active and passive circuits. MATLAB is used to arrange the measured data and superimpose them with simulated curves.

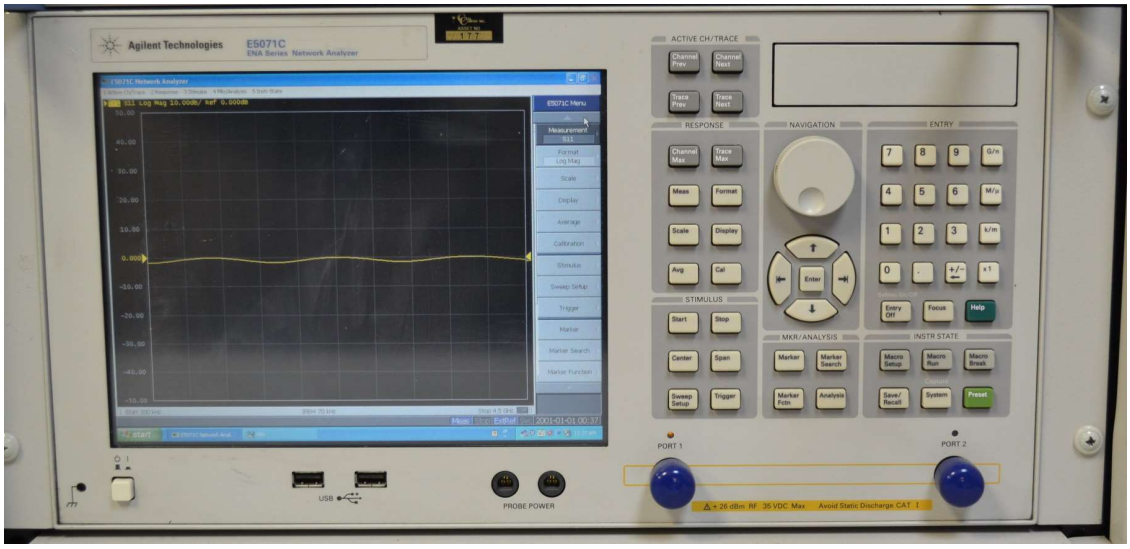

Figure 7.4 S-parameter measurements of the antenna using 20 GHz Vector analyzer.

7.2.2 Radiation pattern measurements

RFxpert flatbed antenna radiation patterns measurement device, available in the microwave lab on KFUPM, is used to monitor the beam steering properties of the antenna. This device

measures near field radiation properties to predict the far-field patterns of the antenna [72]. The tool is connected to a PC with special software to visualize both far-field and near-field real-time measurements. Figure 7.5 shows the typical RFxpert measurement setup which consists of an RF source, RFxpert scanner and PC software. Note that this device can also be interfaced with a vector network analyzer.

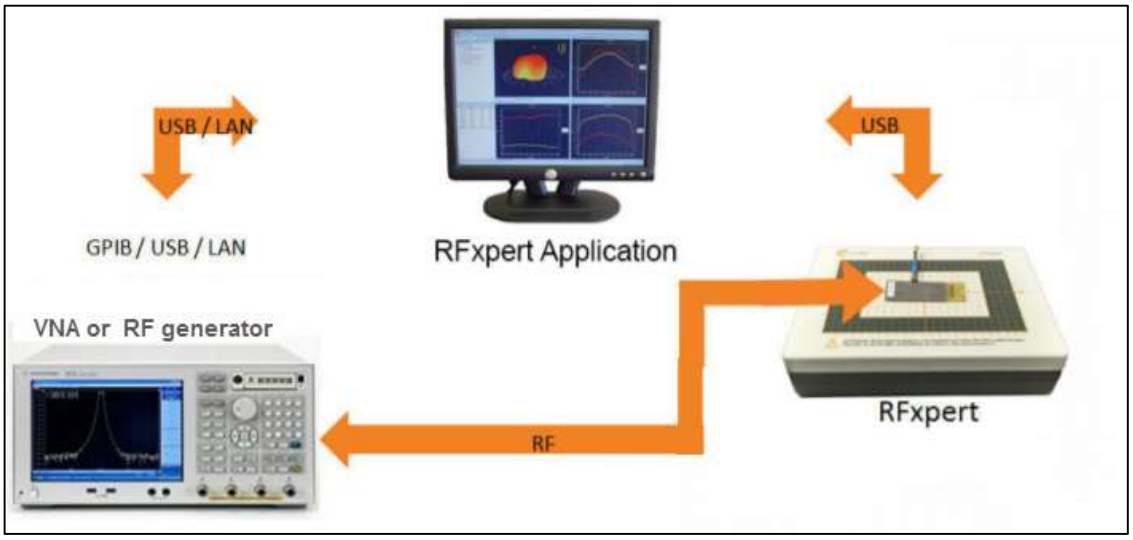

Figure 7.5 Radiation pattern measurement setup using RFxpert.

7.2.3 Calibrating external magnetic biasing fields

To provide external magnetic oppositely to the ferrite slabs, permanent N-42 type NdFeB magnets are used. The magnets were fabricated by a company, called e-magnets-UK. The dimensions of the magnets are 10 ×10 × 5 mm and it can provide up to about 0.45 T biasing field. Note that magnetic field of similar strength is used in earlier to generate simulated results of the designed SRR embedded ferrite integrated patch antenna.

Using a Tesla-meter and a flat probe, the magnetic field produced by the permanent magnet is measured. Figure 7.6 shows the measurement setup related to calibrating the magnet biasing of the SRR integrated ferrite slabs. Table 7.2 list the magnetic fields produced by N-42 magnetic at a different distance away from the magnetic. This table can be used to generate required magnetic biasing of the ferrite slabs depending on the distance between the ferrite slabs and the N-42 magnets.

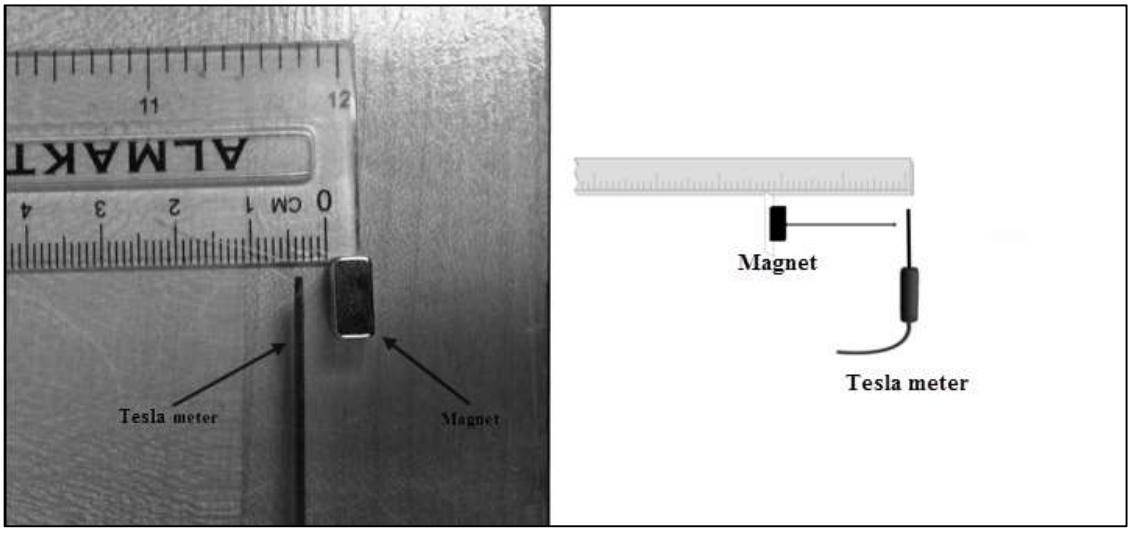

Figure 7.6 Measurement setup to calibrate magnetic biasing fields from N-42 magnet.

Table 7.1 Simulated and measured magnetizing fields of N-42 versus distance.

Distance [mm]	Mag_B Simulated [Tesla]	Mag_B Measured [Tesla]
0.0	0.379	0.360
2.0	0.247	0.230
5.0	0.101	0.105
6.0	0.086	0.093
7.0	0.079	0.085

Note that at a distance of 5 mm, there is a match between the simulated and measured results. With increasing distance, the mismatch between the simulated and measured values increases due to human errors of centering the gaussmeter probe in front of the magnet.

7.3 Antenna with embedded ferrite slabs

The vector network analyzer, shown in Figure 7.4, is used to measure the S-parameter responses of the ferrite integrated (without SRR) antenna, shown in Figure 7.3. The measurements started with placing the antenna within the measurement setup displayed in Figure 7.7. The measurement setup consisted of the RF generator, the antenna prototype placed above the RFxpert scanner and a PC with interface software.

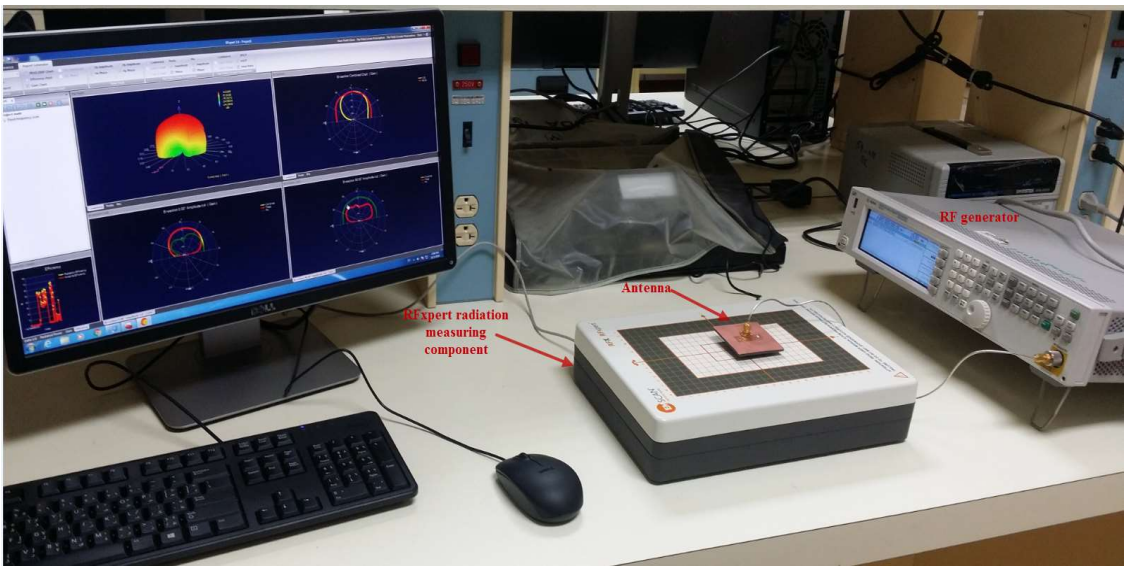

Figure 7.7 The Radiation pattern measurement setup in KFUPM lab.

Initially, the reflection and radiation measurements are made without the presence of any external magnetic bias. Figure 7.8 shows the reflection coefficient of both simulated and fabricated antenna with embedded ferrite slabs. The result shows a good match between the simulation and the measured resonance response at 4.3 GHz. Then a magnet is placed

at different distances from the antenna to generating changing external biasing (H_{DC}) values. Figure 7.9 and Figure 7.10 show the simulated and measured E-plane and H-plane radiation patterns of the antenna, respectively.

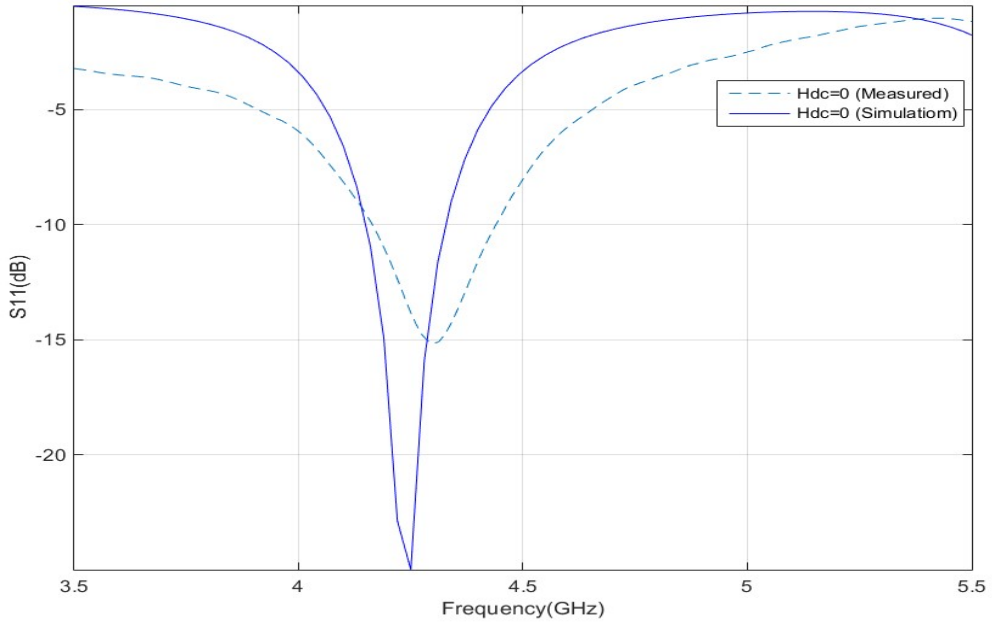

Figure 7.8 Reflection response of fabricated antenna with simulation (Hdc=0).

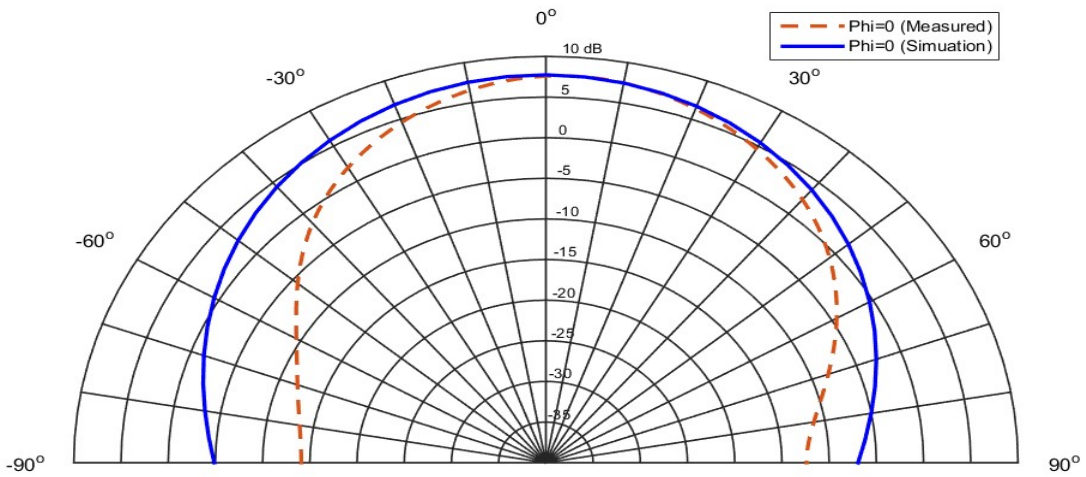

Figure 7.9 Radiation pattern of fabricated antenna at Phi=0 plane with Hdc=0

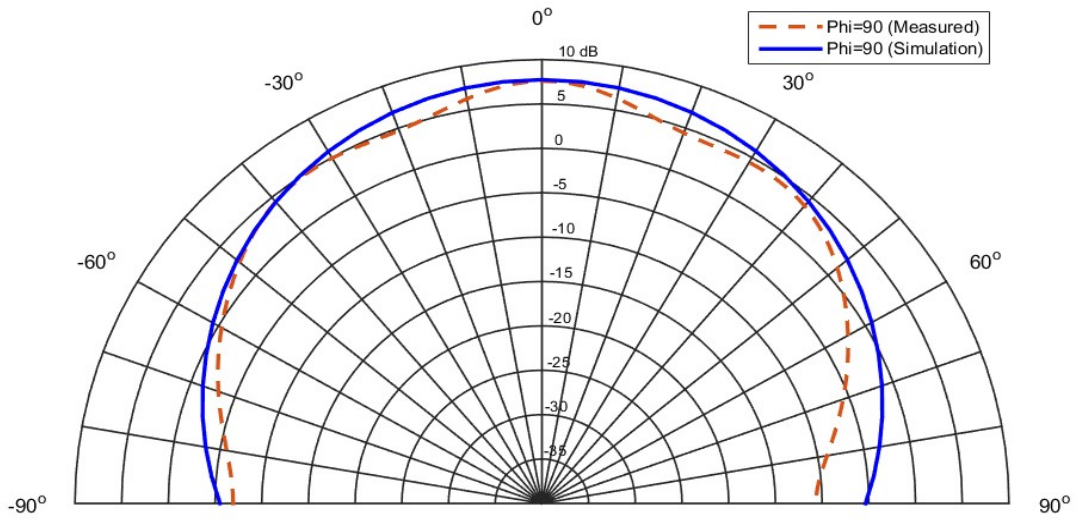

Figure 7.10 Radiation pattern of fabricated antenna at Phi=90 plane with Hdc=0.

To observe the effect of external magnetizing, permanent magnets is placed over the ferrite slab, and the change in resonant frequency and the radiation pattern is observed. When the magnetic is placed 7-mm above the antenna, it magnetized the ferrite slabs with an H_{DC}=0.09T. Consequently, the resonant frequency of the antenna is observed to move upwards in frequency scale, as shown in Figure 7.11. Although the simulated result displayed at 0.09T is 4.85GHz, the experimental results are 4.65GHz. Figures 7.12 and 7.13 superimpose the measured and simulated E-plane and H-plane radiation patterns of the antenna for Hdc=0.09T, respectively. Note that the measured patterns agreed well with the simulated results. Figure 7.14 shows a similar superimposed response of simulated and measured reflection responses for magnetic biasing of 0.1T. This magnetic bias is achieved by placing the magnetic 5 mm away from the patch. Note that the tuned frequency is experimentally observed at 5.05 GHz compared to the simulated 5.12 GHz. Which shows that the experimental tuning range is 750 MHz compared with 870 MHz of simulated one.

The main reason of this error is human inaccuracy during fabrication and the magnetizing process of the experiment.

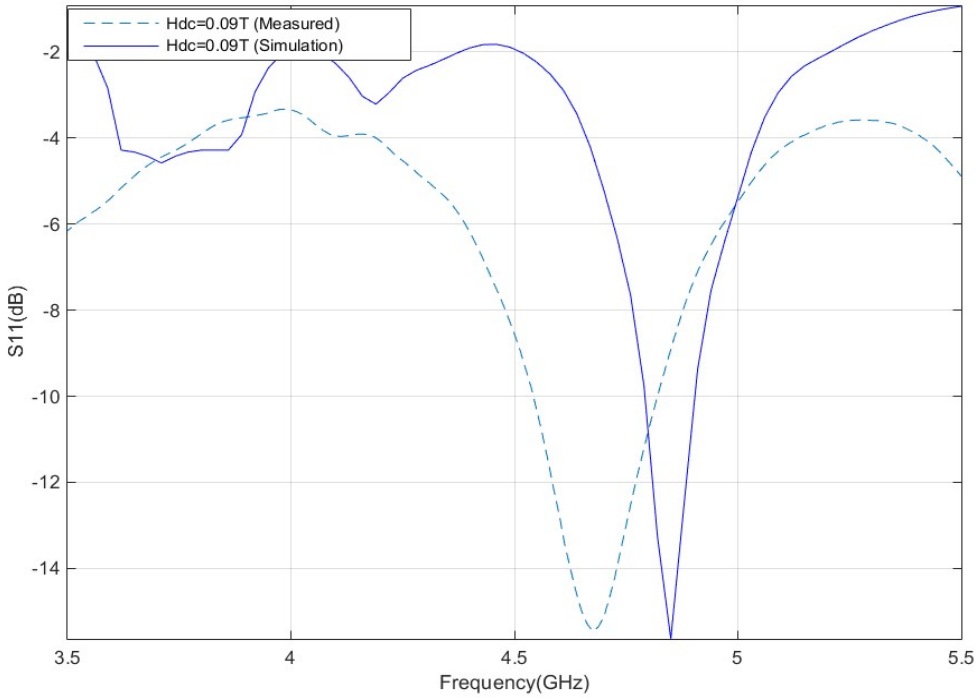

Figure 7.11 Reflection response of fabricated antenna with Hdc=0.09T.

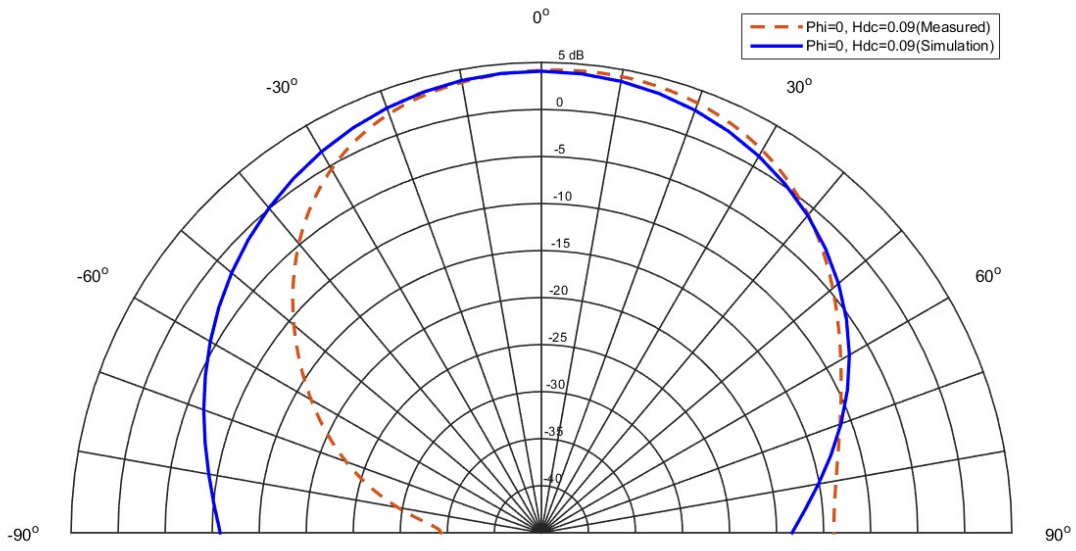

Figure 7.12 Radiation pattern of fabricated antenna for Phi=0 plane with Hdc=0.09T.

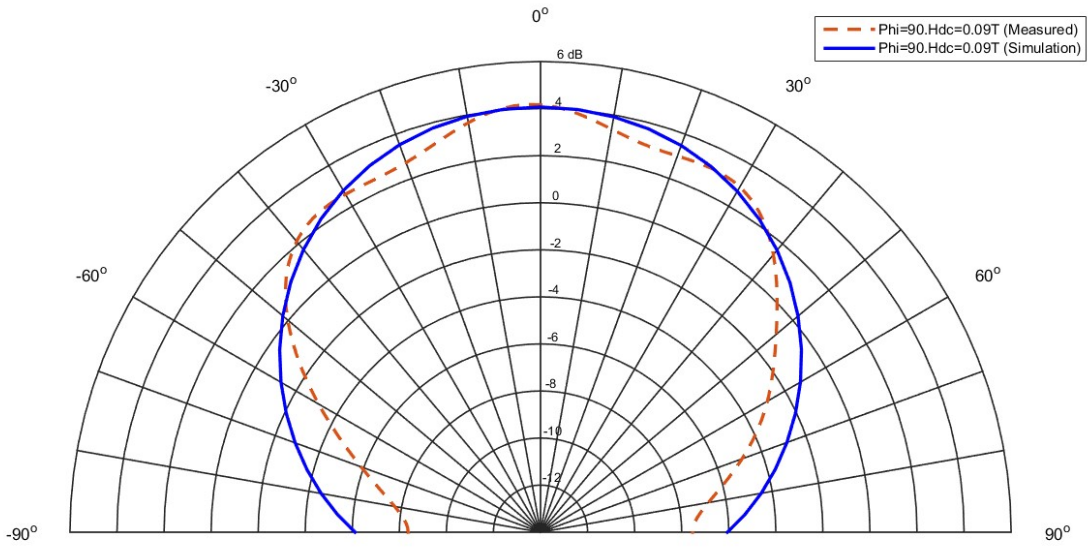

Figure 7.13 Radiation pattern of fabricated antenna at Phi=90 plane for Hdc=0.09T.

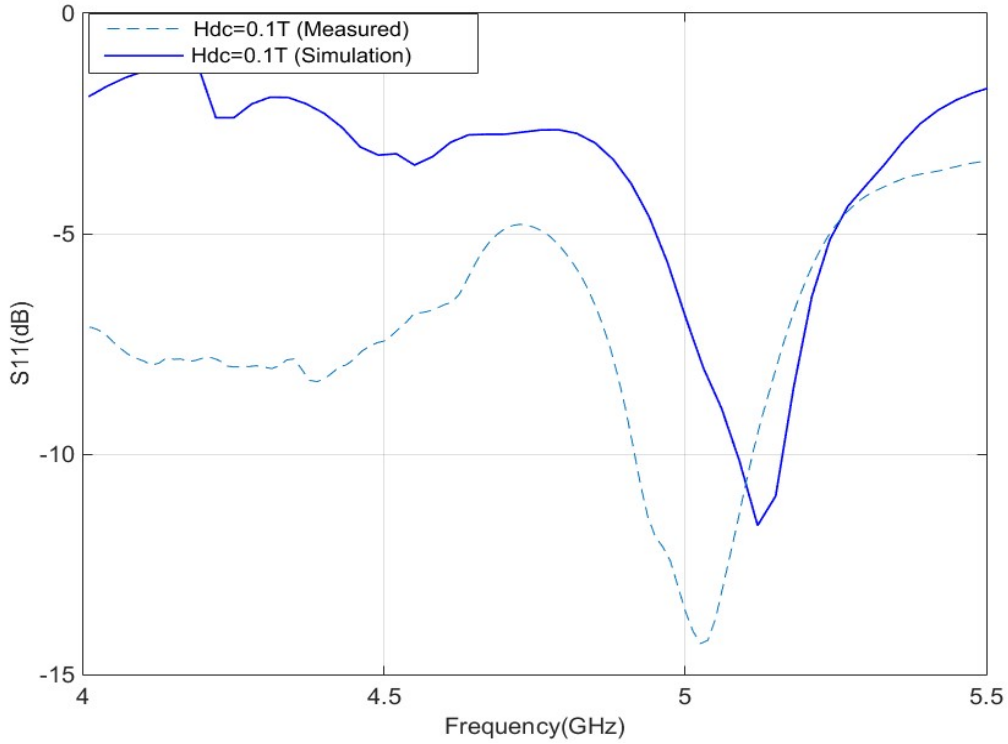

Figure 7.14 Reflection response of fabricated antenna with Hdc=0.1T.

7.4 Antenna with SRR integrated ferrite slabs

To investigate the effects of SRR shapes, they are optimally embedded within the ferrite slab as accurately as possible. This is realized by dividing the ferrite into two rectangular slabs of 6 mm and 2mm in lengths. The SRR structures, made of silver foil, are carefully integrated within the ferrite slabs. Since the in-house manual process in used for this fabrication process, human error is expected to degrade the measured results. Figure 7.15 shows the pictures of the fabricated antenna prototype with SRR integrated ferrite slabs, embedded within the dielectric substrate. The reflection response (S11) of fabricated antenna is measured without magnetic bias and plotted in Figure 7.16. The main difference between the simulated and experimental responses are due to human error and possible air gap, introduced by SRR shapes, in-between the two components of the ferrite slab.

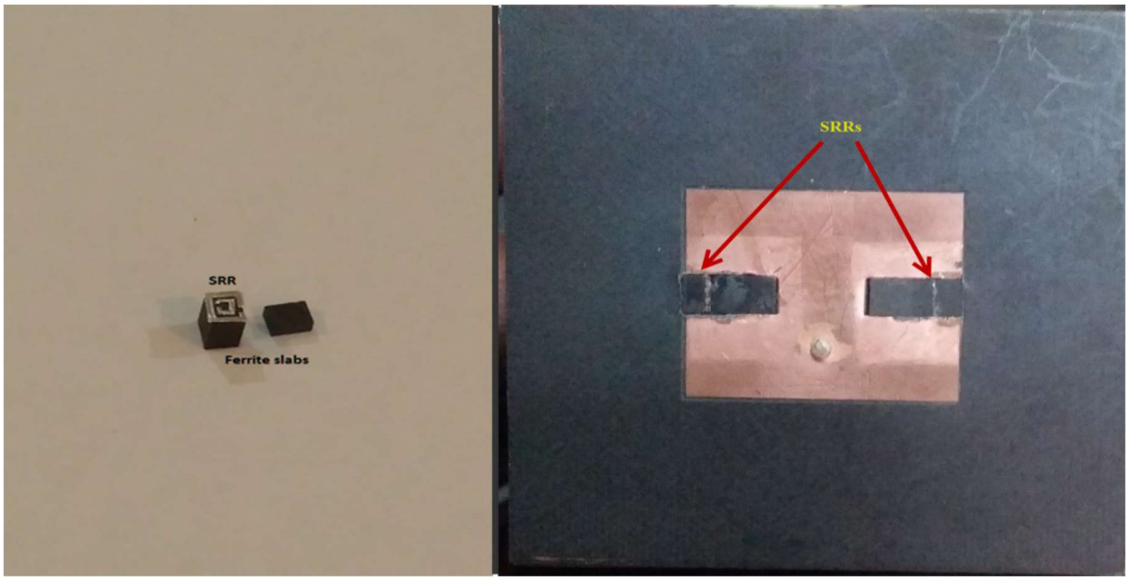

Figure 7.15 The fabricated antenna with SRR integrated ferrite slabs embedded within the substrate.

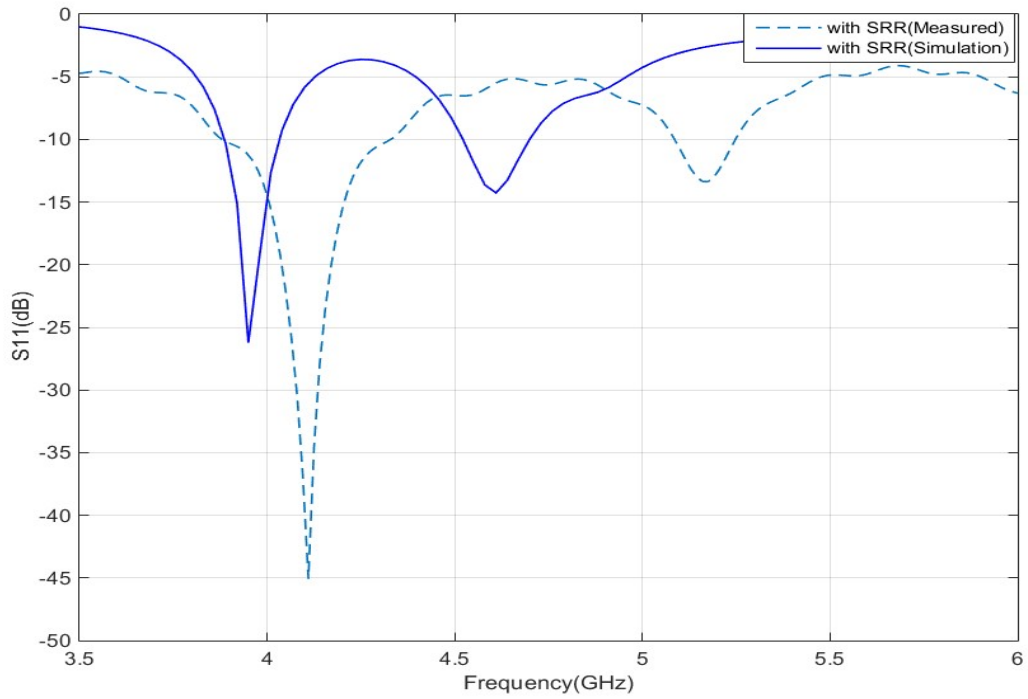

Figure 7.16 Reflection response of fabricated antenna with integrated SRR at Hdc=0.

Figures 7.17 and 7.18 superimpose the E-plane and H-plane radiation patterns of the antenna at the first measured resonance compared with simulated ones at the first resonance. Figure 7.19 and 7.20 show the measured and simulated E-plane radiation pattern of the second resonance in both gain and absolute scale, respectively. Note that the pattern shows a tilting to 10^{o} compared with 15^{o} in the simulation, which builds a good match between the measured and simulation data. Figure 2.21 shows the H-plane of the second resonance of the antenna.

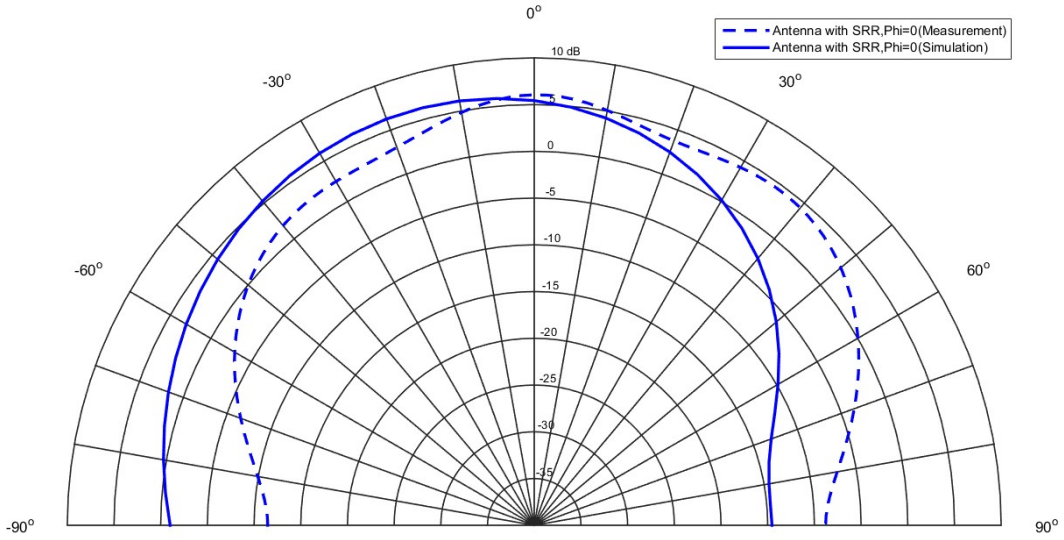

Figure 7.17 Radiation pattern of first resonance at Phi=0 (E-plane) with Hdc=0.

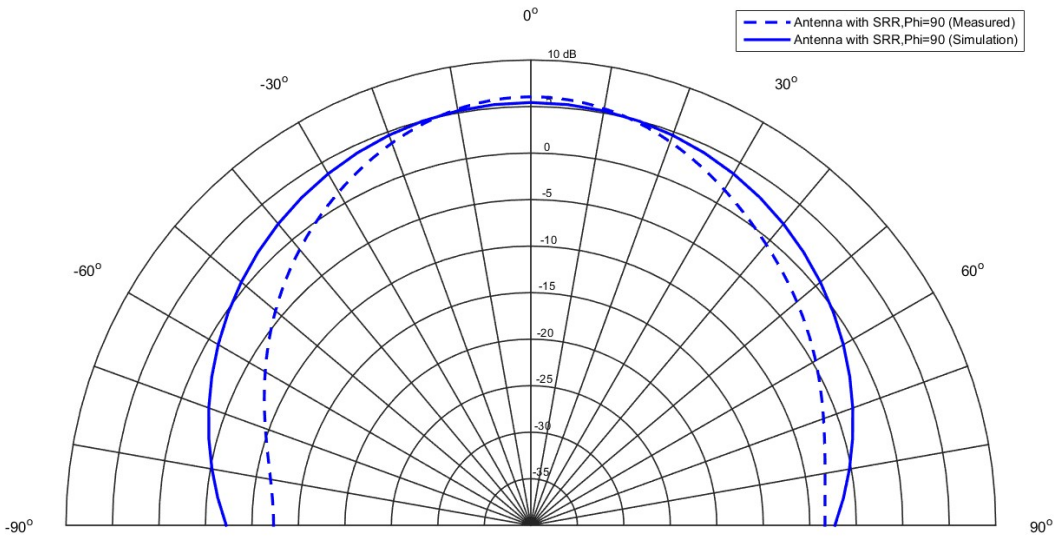

Figure 7.18 Radiation pattern of first resonance at Phi=90 (H-plane) with Hdc=0.

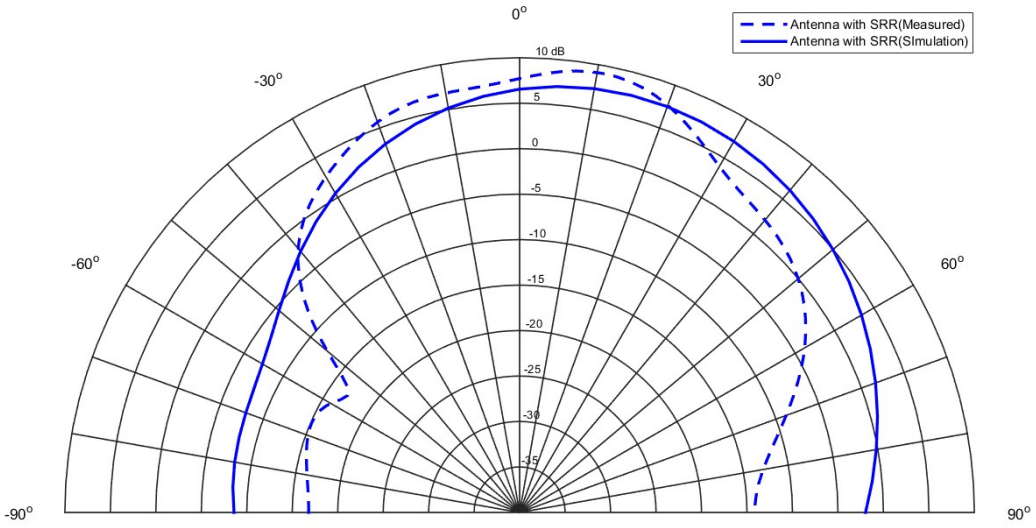

Figure 7.19 Radiation pattern of the antenna for the second resonance at Phi=0 (E-Plane) with Hdc=0.

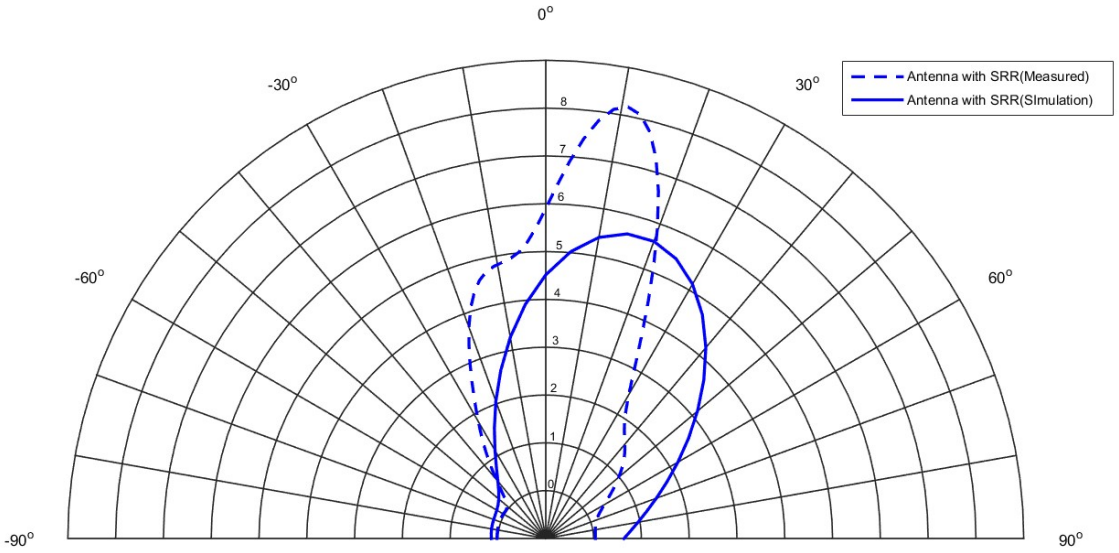

Figure 7.20 Absolute radiation pattern of the antenna for the second resonance at Phi=0 with Hdc=0.

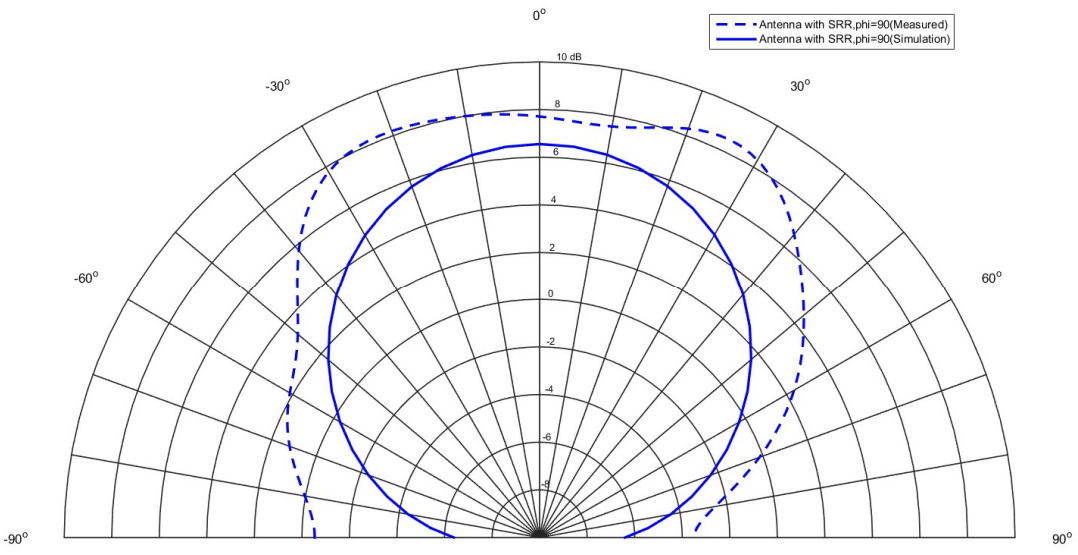

Figure 7.21 Radiation pattern of the antenna for the second resonance at Phi=90 (H-Plane) with Hdc=0.

7.5 Conclusions

In this chapter, the fabrication of antenna with ferrite slabs embedded has been verified. It was shown that the frequency tuning range of the antenna achieved is 750 MHz compared with 850 MHz of simulated results with 13.7% of error. The radiation pattern agreed well with simulated ones.

In addition, an antenna with SRR embedded in ferrite slabs has been fabricated and measured. The reflection coefficient showed some variation due to human error and possible air gap, introduced by SRR shapes, in-between the two components of the ferrite slab, where the trend stayed the same. Radiation pattern at the first resonance showed good agreement and the measured tilting in radiation pattern at the second resonance was 10° compared with 15° for the simulated results.

CHAPTER 8

CONCLUSIONS

8.1 Contributions

In this research work, novel magnetic-metamaterial based patch antenna is designed and optimized to achieve frequency, pattern and polarization reconfigurable coverage

A design of patch antenna with ferrite slabs embedded has been introduced. By optimally choosing the proper magnetization on the ferrite, tuning range of 870 MHz of a simple patch was achieved by applying 0.1T field, which constructs a broader tuning range than the introduced range in the literature with small ferrite slabs and same magnetization field. Moreover, split ring resonators (SRR's) were integrated within the ferrite material to constructively couple and enhance the frequency tuning range compared with typical ferrite based tuning of 570 MHz with an average gain 5dB and by applying the same magnetization field.

This structure has also introduced beam steering reconfigurability to the simple patch. The radiation pattern of the antenna showed 25^{o} of beam scanning for the external magnetic biasing field of 0.062T. A simple 2x1 array is also designed to demonstrate three-dimensional (3D) scan capabilities, with 15^{o} in the E-plane and 10^{o} in the H-plane. The designed antenna also demonstrates polarization reconfigurability when magnetized ferrite disks and slabs are integrated within the center of the substrate. It was demonstrated that by changing magnetic biasing (H_{DC}), the polarization was tuned between left-hand (LHCP)

and right-handed (RHCP) circular or elliptical polarizations. The antenna was fabricated using available facilities in KFUPM labs. This introduced human errors, particularly while integrating the tiny SRR rings within the ferrite slab. The simulated results agreed well with the experimentally obtained data. Minor disagreements were due to errors resulted from fabrication and magnetization of the ferrite slabs.

8.2 Future work

1. Design and implement an integrated active controlled biasing networks within ferrite materials to reduce the magnetization field required using low temperature co-fired ceramics (LTCC) technique. Moreover, the effect of the field on magnetization of the ferrite will be theoretically and experimentally studied and calculated.
2. Design an active controlled tunable ferrite-metamaterials structures that are suitable for microwave circuit integration to provide reconfigurability for microwave devices and antennas.

References

[1] G. M. Rebeiz and J. B. Muldavin, "RF-MEMS Switches and Switch Circuits", IEEE Microw. Mag., vol. 2, no. 4, pp. 59–71, Dec. 2001.

[2] U. L. Rohde and D. P. Newkirk, RF/Microwave Circuit Design for Wireless Applications. New York: Wiley, 2000.

[3] I. Gutierrez, E. Hernandez, and E. Melendez, “Design and Characterization of Integrated Varactors for RF Applications”. New York: Wiley, 2006.

[4] C. Kittel, “Introduction to Solid State Physics”, 7th ed. New York: Wiley, 1996.

[5] G. Christodoulou, Y. Tawk, Steven A. Lane, and Scott R. Erwin, "Reconfigurable Antennas for Wireless and Space Applications”, Proceedings of the IEEE, Vol. 100, Iss. 7 , July 2012.

[6] Haupt, R.L., Lanagan, M., “Reconfigurable Antennas”, Antennas and Propagation Magazine, IEEE ,Vol.55-1, pp. 49–61, 2013.

[7] C. A. Balanis, “Antenna Theory: Analysis and Design”, 3rd ed., Hoboken, NJ: Wiley, 2005.

[8] Liu, S., M.-J. Lee, C. Jung, G.-P. Li, and F. De Flaviis, "A frequency-reconfigurable circularly polarized patch antenna by integrating MEMS switches," Proc. Antennas and Propagation Society International Symposium, Vol. 2, pp. 413-416, 2005.

[9] C.Won,M. Lee, G. P.Li, and F.De Flaviis, “Reconfigurable beam scan single-arm spiral antenna with integrated with RF-MEMS switches”, IEEE Trans. Antennas Propagation, Vol. 54-2, pp. 455–463, Feb. 2006.

[10] C. J. Panagamuwa, A. Chauraya, and J. C. Vardaxoglou, “Frequency and beam reconfigurable antenna using photo-conducting switches,” IEEE Trans. Antennas Propagation, Vol. 54, no. 2, pp. 449–454, Feb. 2006.

[11] S. S. I. Mitu etal. "Analogue/Digital Ferrite Phase Shifter for Phased Array Antennas", IEEE Antenna and Wireless Propagation Letters (IEEE-AWPL), ISSN: 1536-1225, Vol. 9, pp.319-321, April, 2010

[12] Kompa G. , R Janson ,” Planar waveguide model for calculating Microstrip components” Electron letters, Vol. 11, pp.459-460, 1975.

[13] A. J. Baden-Fuller, Ferrites at Microwave Frequency. London: Peter Peregrines, Ltd., 1987.

[14] D. K. Cheng, Field and Wave Electromagnetics, 2nd ed. New York: Addison Wisely Publishing Com. Inc., 1989.

[15] Pozar, David M., Microwave Engineering, 4th ed. John Wiley & Sons, Inc., 2012.

[16] Online reference material on "Ferrite data sheet", http://www.temex-ceramics.com/.

[17] D. Jiles, Introduction to Magnetism and Magnetic Materials, 2nd ed. London: Peter Peregrines, Ltd., 1987.

[18] Antar Y, Guha D, Microstrip and printed antennas: new trends, techniques, and applications. 1st ed. Hoboken, N.J: Wiley, 2011.

[19] H. How and C. Vittoria, "Radiation frequencies of magnetic patch antennas", Electronic Letters, Vol. 28, no.15, pp.1405–1406,1992.

[20] D.M. Pozar, "Radiation and scattering characteristics of microstrip antennas on normally biased ferrite substrates," IEEE Trans. Antennas Propagation, Vol. 40, no. 9, pp. 1084–1092, Sep. 1992.

[21] D. M. Pozar and V. Sanchez, "Magnetic tuning of a microstrip antenna on a ferrite substrate," Electron. Letters, vol. 24, no. 12, pp. 729–731, Jun. 1988.

[22] R. K. Mishra, S. S. Pattnaik, and N. Das, "Tuning of microstrip antenna on ferrite substrate," IEEE Trans. Antennas Propag., vol. 41, no. 2, pp. 230–233, Feb. 1993.

[23] Ramesh Garg, "Microstrip antenna design handbook", Artech House, 2001.

[24] Constantine A. Balanis, "Modern antenna handbook", 2011.

[25] R. A. Waldron, "Ferrites an Introduction for Microwave Engineers". London: D.Van Nostrand Company, Ltd., 1961.

[26] R. F. Soohoo, "Theory and Application of Ferrites". New Jersey: Prentice Hall, Inc., 1960.

[27] A. J. Baden-Fuller, "Ferrites at Microwave Frequencies". London: Peter Peregrinus, Ltd., 1987.

[28] M. S. Sodha and N. C. Srivastava, "Microwave Propagation in Ferrimagnetics". New York: Plenum Press, 1981.

[29] Guo-Min Yang, X. Xing, A. Daigle, M. Liu, O. Obi, S. Stoute, K. Naishadham, and Nian X. Sun , “Tunable Miniaturized Patch Antennas With Self-Biased Multilayer Magnetic Films”, IEEE Trans. Antennas Propagation, vol. 50, no. 7, July 2009.

[30] Hanin, Fatima Zahra; Setti, Larbi , “Performance of Patch Antenna loaded of ferrites films”, Proceedings of 2014 Mediterranean Microwave Symposium (MMS2014), pp 1–3, 2014.

[31] Alix Rivera Albino, Member, IEEE, and Constantine A. Balanis, “Gain Enhancement in Microstrip Patch Antennas Using Hybrid Substrates”, IEEE Trans. Antennas Propagation, vol. 12, no. 12, 2013.

[32] M. A. Amiri, C. A. Balanis and C. R. Birtcher, “Gain and bandwidth enhancement of ferrite-loaded CBS antenna using material shaping and positioning,” IEEE Antennas and Wireless Propag. Letters, Vol. 12, 2013.

[33] B. Lee and F. J. Harackiewicz, “The RCS of a microstrip antenna on an in-plane biased magnetic substrate,” IEEE Trans. Antennas Propag., vol. 44, pp. 208–211, Feb. 1996.

[34] H. Y. Yang, J. A. Castaneda, and N. G. Alexopoulos, “The RCS of a microstrip patch on an arbitrarily biased magnetic substrate,” IEEE Trans. Antennas Propag., vol. 41, pp. 1610–1614, Dec. 1993.

[35] Sheikh, S.I.M.; Gibson, A.A.P.; Basorrah, M.; Alhulwah, G.; Alanizi, K.; Alfarsi, M.; Zafar, J., "Analog/Digital Ferrite Phase Shifter for Phased Array Antennas",Antennas and Wireless Propagation Letters, IEEE , Volume: 9 , ,Pages: 319 - 321, 2010.

[36] Hui, W.W.G.; Bell, J.M.; Iskander, M.F.; Lee, J.J., " Low-Cost Microstrip-Line-Based Ferrite Phase Shifter Design for Phased Array Antenna Applications", Antennas and Wireless Propagation Letters, IEEE, Volume: 6, Pages: 86 - 89, 2007.

[37] Sultan, F.; Iqbal, S.S., “Beam Scannable Microstrip Patch Antenna”, Antenna Technology: "Small Antennas, Novel EM Structures and Materials, and Applications" Int. Workshop on iWAT 2014, pp. 76 – 79, 2014.

[38] H. Attia, O. Siddiqui, and O. M. Ramahi, “Theoretical and experimental demonstration of beam steering of patch antenna with superstrate.” Proc. of IEEE Antennas and PropagIntl. Symposium, Chicago, IL, 2012.

[39] T. Zervos1 A.A. Alexandridis1 F. Lazarakis1 M. Pissas2 D. Stamopoulos2 E.S. Angelopoulos1 K. Dangakis1, “Design of a polarisation reconfigurable patch

antenna using ferrimagnetic materials", Microwaves, Antennas & Propagation, IET, Volume: 6, Pages: 158 - 164, 2012.

[40] M. Sigalov, R. Shavit, R. Joffe, and E. O. Kamenetskii, "Manipulation of the Radiation Characteristics of a Patch Antenna by Small Magnetic Disks Inserted in Its Cavity Domain", Antennas and Propagation, IEEE Transactions on, V: 61, Ps: 2371 – 2379, 2013.

[41] Li-Rong Tan, Rui-Xin Wu, and Yin Poo, "Magnetically Reconfigurable SIW Antenna with Tunable Frequencies and Polarizations", Antennas and Propagation, IEEE Transactions on, Vol: 63, pp. 2772 – 2776, 2015.

[42] Eleftheriades, George V.; Keith G. Balmain (2005). Negative-refraction metamaterials: fundamental principles and applications. Wiley, John & Sons. p. 340. ISBN 978-0-471-60146-3.

[43] Engheta, Nader; Richard W. Ziolkowski, Metamaterials: Physics and Engineering Explorations. Wiley & Sons, June 2006.

[44] Mavridis, A. A., G. A. Kyriacou, and J. N. Sahalos "On the design of patch antennas tuned by transversely magnetized lossy ferrite including a novel resonating mode," Progress in Electromagnetics Research, Vol. PIER 62, pp. 165-192, 2006.

[45] Weiglhofer, W.S., Lakhtakia, A.: Introduction to complex mediums for optics and electromagnetics. SPIE Press, Bellingham, WA, USA (2003).

[46] Tie Jun Cui, David Smith and Ruopeng Liu, Metamaterials Theory, Design, and Applications, Springer , 2010

[47] V. Veselago. "The electrodynamics of substances with simultaneously negative values of epsilon and mu", Sov. Phys. Usp., vol.10, pp. 509-514, 1968.

[48] D.R. Smith, W.J. Padilla, D. Vier, S. Nemat-Nasser, and S. Schultz. Composite medium with simultaneously negative permeability and permittivity. Phys. Rev. Letter, 84(18), pp.4184-4187, May 2000.

[49] J. Pendry, A.J. Holden, W.J. Stewart, and I. Youngs. Extremely low frequency plasmons in metallic mesostructures. Phys. Rev. Letter, 76(25), pp-4773-4776, June 1996.

[50] J.B. Pendry, A.J. Holden, D.J. Robbins, and W.J. Stewart. Magnetism from conductors and enhanced nonlinear phenomena. IEEE Transactions on Microwave Theory and Techniques, 47(11), pp.2075-2084, 1999.

[51] R. W. Ziolkowski and E. Heyman, “Wave propagation in media having negative permittivity and permeability,” Phys. Rev. E, Stat. Phys. Plasmas Fluids Relat. Interdiscip. Top., vol. 64, pp.056, October 2001.

[52] Cui TJ, Liu R, Smith DR. Introduction to Metamaterials. In: Boston, MA: Springer US, 2010.

[53] http://www.emagtech.com/content/modeling-dispersive-materials-using-fdtd (online)

[54] Ben-Xin Wang, Ling-Ling Wang, Gui-Zhen Wang, Wei-Qing Huang, Xiao-Fei Li, and Xiang Zhai, “Theoretical Investigation of Broadband and Wide-Angle Terahertz Metamaterial Absorber”, IEEE Photonics Technology Letters, Vol 26, 2014

[55] Ayop, O.; Rahim, M.K.A.; Murad, N.A.; Samsuri, N.A., “Polarization Insensitive and Wide Operating Angle Metamaterial Absorber at X-band “, Applied Electromagnetics (APACE), 2014 IEEE Asia-Pacific Conference on, pp. 245 – 249, 2014.

[56] Antoniades, M.A.; Eleftheriades, G.V., “A Broadband Series Power Divider Using Zero-Degree Metamaterial Phase-Shifting Lines”, Microwave and Wireless Comp Letters, IEEE, Vol: 15, Issue: 11, pp. 808 – 810 , 2005.

[57] Antoniades, M.A.; Eleftheriades, G.V., “A broadband 1:4 series power divider using metamaterial phase-shifting lines “,Microwave Conference, 2005 European, Vol. 2, pp. 4, 2005.

[58] Jae-Gon Lee and Jeong-Hae Lee, “Suppression of Spurious Radiations of Patch Antenna Using Split Ring Resonators (SRRs)”, Antennas and Propagation Society International Symposium, 2005 IEEE, Vol:. 2B, pp. 242 – 245, 2005.

[59] Hung-Hsuan Lin; Chun-Yih Wu; Shih-Huang Yeh, “Metamaterial enhanced high gain antenna for WiMAX application”, TENCON 2007 - 2007 IEEE Region 10 Conference, pp. 1 – 3, 2007.

[60] Jain, S.K.; Shrivastava, A.; Shrivas, G., “Miniaturization of Microstrip Patch Antenna using Metamaterial loaded with SRR”, Electromagnetics in Advanced Applications (ICEAA), 2015 Int. Conf. on , pp. 1224 – 1227, 2015.

[61] Ouedraogo, R.O.; Rothwell, E.J., “Metamaterial Inspired Patch Antenna Miniaturization Technique, Antennas and Propagation Society International Symposium (APSURSI), 2010 IEEE, pp. 1-4, 2010.

[62] A. Harfianto, M0 Suprayogi; Munir, Achmad, “Incorporation of square patch and SRR metamaterials for dual-band printed antenna”, APS,URSI, 2015 IEEE International Symposium on, pp. 826 – 827, 2015.

[63] Rosaline, S.I.; Raghavan, S.. “Compact dual band antenna for GSM/WiMAX applications”, ICSCN, 2015 3rd International Conference on 2015, pp.1-3, 2015.

[64] Wenquan; Yang; Bangning; Aijun ; Tongbin; Daosheng, “A Low-Cost Compact Patch Antenna With Beam Steering Based on CSRR Loaded Ground”, IEEE ANTENNAS AND WIRELESS PROPAGATION LETTERS, VOL. 10, pp. 1520 – 1523, 2011.

[65] Sultan,F.; Iqbal,S.S.,“SRR embedded ferrite superstrate based beam scanning of 10 GHz single microstrip patch antenna, Microwave Conference (APMC), 2014 Asia-Pacific, pp. 384 – 386, 2014.

[66] A. Shamim, J. R. Bray, N. Hojjat and L. Roy, "Ferrite LTCC-based antennas for tunable SoP applications," IEEE Tranactions on Components, Packaging and Manufacturing, vol. 1, no. 7, 2011.

[67] http://www.cisco.com/

[68] Zhao, Xing, Lee, Youngki, Choi, Jaehoon, “Design of a compact patch antenna using split-ring resonator embedded substrate”, Microwave and Optical Technology Letters, vol.53.

[69] J. Zhou, T. Koschny and C. M. Soukoulis, “Magnetic and electric excitations in split-ring resonators,” Optics Express, Vol. 15, No. 26, 2007.

[70] D. R. Smith, D. C. Vier, Th. Koschny and C. M. Soukoulis, “Electromagnetic Parameter Retrieval from Inho mogeneous Metamaterials,” Physics Review E, 71, 3, 2005, 036617.

[71] Keysight Agilent E5071C manual, http://www.keysight.com.

[72] RFxpert manual, http://www.emscan.com.

[73] G.A. Deschamps, “Microstrip Microwave Antennas,” Presented at the third USAF Symposium on Antennas, 1953.

[74] J. Q. Howell, “Microstrip antennas,” Dig. IEEE Int. Symp. Antennas Propagat., pp. 177–180, Dec. 1972.

[75] R. E. Munson, “Conformal microstrip antennas and microstrip phased arrays,” IEEE Trans. Antennas Propagat., vol. 22, pp. 74–78, 1974.

Vitae

Name	:Mousa Ahmad Al-Omari
Nationality	:Jordanian
Date of Birth	:8/11/1988
Email	:momari@outlook.com
Address	:KSA - Riyadh
Academic Background	:BSc of Telecommunication Engineering
	Yarmouk University - Jordan
Professional Background	:Telecom Enigneer
	Uminah - Jordan
	Network Operation Center Engineer
	Aspire Services - Jordan
	Telecom Engineer
	Saudi Telecom Company (STC) - KSA